

## 4. SITE 613<sup>1</sup>

### Shipboard Scientific Party<sup>2</sup>

#### HOLE 613

**Date occupied:** 17 September 1983  
**Date departed:** 22 September 1983  
**Time on hole:** 119.9 hr.  
**Position:** 38°46.26'N, 72°30.43'W  
**Water depth (sea level; corrected m, echo-sounding):** 2309  
**Water depth (rig floor; corrected m, echo-sounding):** 2319  
**Bottom felt (m, drill pipe):** 2333.2  
**Penetration (m):** 581.9  
**Number of cores:** 52 (incl. 4 wash cores)  
**Total length of cored section (m):** 456.3  
**Total core recovered (m):** 357.97  
**Core recovery (%):** 78.3  
**Oldest sediment cored:**  
Depth sub-bottom (m): 581.9  
Nature: Nannofossil porcellanite and porcellaneous limestone  
Age: early Eocene  
Measured velocity (km/s): 2.05  
**Basement:** Not attempted

#### GEOLOGIC SETTING AND OBJECTIVES

Site 613 is near the toe of the upper-rise wedge (2323 m water depth), about 6 km seaward of the middle Eocene outcrop belt. The seafloor in this region is smooth compared to that near Site 612, but the downslope end of Toms Canyon incises the upper rise about 6 km northwest of Site 613. A series of gentle ridges and valleys occupies the immediate vicinity of Site 613, and the site itself is located on top of a low ridge.

The structural position of Site 613 is near the lower (seaward) slope of a buried, gently dipping, Upper Cre-

taceous continental slope, above which are stacked a series of sediment-filled Cenozoic erosional channels. The marked physiographic relief of these buried canyons is seen especially well in strike sections, such as U.S.G.S. Line 35. Several previous authors have noted these channels (e.g., Schlee and Grow, 1980) and concluded that the main channelling event(s) probably took place during the Oligocene, when relative sea level was believed to have dropped markedly (Vail et al., 1977). However, the subsequent drilling of Site 605 provided evidence for a new interpretation. At Site 605, middle Eocene strata underlie a thin Pliocene section and then dip to the southeast beneath the Site 613 location. Tracing the stratigraphy at Site 605 along line 25 to 35 reveals that a major (and perhaps the most severe) channelling event took place not in the Oligocene, but between the early and middle Eocene. The contact of the lower and middle Eocene units appears to be unconformable and marked in places by a high-amplitude reflector that might represent the porcellanite zone seen at Site 612.

Site 604 was originally intended to test this section on Line 35, and the site was positioned over the center of one of the shallowly buried channels. However, when Site 604 was drilled (Leg 93), it was found that upper Miocene conglomeratic sands fill the uppermost channel, and this sand was too thick and loosely compacted to penetrate with *Glomar Challenger's* coring system. As the importance of identifying the underlying stratigraphic section had increased with the drilling of Site 605, we searched for a position between two of the buried channels, updip from Line 35, where the Miocene sand might be thinner and fine-grained enough to be completely penetrated. A pre-site water-gun seismic reflection survey revealed a promising section about 1.8 km northeast of the originally proposed Site NJ-12, and this was chosen for Site 613.

In addition to the objectives cited above, we hoped to improve our understanding of submarine unconformities as boundaries of depositional sequences and to document the biofacies and lithofacies relationships between this upper rise site and those of adjacent slope and shelf. The other general objectives of the New Jersey Transect (see Background and Objectives chapter, this volume) also apply to Site 613.

#### SITE APPROACH AND OPERATIONS

##### Site 612 to Site 613

Upon completion of operations at Site 612 *Glomar Challenger* undertook an extensive, 47.3 n. mi. (6 hr.) water-gun survey in order to tie together Site 612, ASP-

<sup>1</sup> Poag, C. W., Watts, A. B., et al., *Init. Repts. DSDP*, 95: Washington (U.S. Govt. Printing Office).

<sup>2</sup> Addresses: C. Wylie Poag (Co-Chief Scientist), U.S. Geological Survey, Woods Hole, MA 02543; Anthony B. Watts (Co-Chief Scientist), Lamont-Doherty Geological Observatory, Palisades, NY 10964; Michel Cousin, Laboratoire de Géodynamique Sous-Marine, Université Pierre et Marie Curie VI, B. P. 48, 06230 Villefranche-sur-Mer, France; David Goldberg, Lamont-Doherty Geological Observatory, Palisades NY 10964; Malcolm B. Hart, Department of Geological Sciences, Plymouth Polytechnic, Plymouth PL4 8AA, Devon, United Kingdom; Kenneth G. Miller, Lamont-Doherty Geological Observatory, Palisades, NY 10964; Gregory S. Mountain, Lamont-Doherty Geological Observatory, Palisades, NY 10964; Yuji Nakamura, Laboratory for Earthquake Chemistry, University of Tokyo, Tokyo 113, Japan; Amanda Palmer, Department of Geology and Geophysical Sciences, Princeton University, Princeton, NJ 08544 (present address: Ocean Drilling Program, 1000 Discovery Drive, Texas A&M University, College Station, TX 77840); Paul A. Schiffelbein, Deep Sea Drilling Project, Scripps Institution of Oceanography, La Jolla, California 92093 (present address: E. I. duPont de Nemours, Louviers Bldg., Wilmington, DE 19898); B. Charlotte Schreiber, Department of Earth and Environmental Sciences, Queens College (CUNY), Flushing, NY 11367; Martha Tarafa, Chemistry Department, Woods Hole Oceanographic Institution, Woods Hole, MA 02543; Jean E. Thein, Geologisches Institut, Universität Bonn, D-53 Bonn 1, Federal Republic of Germany (present address: Fachrichtung 15.5, Angewandte Geochemie, Universität des Saarlandes, D6600 Saarbrücken, Federal Republic of Germany); Page C. Valentine, U.S. Geological Survey, Woods Hole, MA 02543; Roy H. Wilkins, Department of Earth and Planetary Sciences, Massachusetts Institute of Technology, Cambridge, MA 02139.

15, COST B-3, DSDP 108, and proposed Site NJ-12 (Fig. 1). Seismic profile recording began as the vessel passed southwestward over the ASP-15 site. The track continued to the southwest for 1.2 n. mi. before turning back to the northeast on a subparallel track, then crossing Site 612 heading almost due north. The track continued northward diagonally across the continental slope to the COST B-3 site, then turned northwestward to parallel very closely Line 79-218 (BGR). At the shelf edge (177 m depth), course was changed southwestward to parallel the shelf break for 4.5 n. mi. The ship then turned southeastward, moving in a downslope direction on a track subparallel to and between Lines 25 and 79-218, crossing Line 34, DSDP Site 108, and Line 35. At the latter crossing point was the proposed Site NJ-12. The post-site survey was terminated at 1152 hr. on 31 August. Following termination of the postsite survey, *Glomar Challenger* moved to Site 603 to attempt to complete the objectives previously set out by Leg 93, by coring the remaining 200 m to basement. All aspects of site approach, operations, and drilling carried out by Leg 95 at Site 603 are reported in *Initial Reports Volume 93* (van Hinte, Wise, et al., in press).

The rig was made secure for sea and the vessel was underway from Site 603 to Site 613 (NJ-12) at 2355 hr., 15 September. Approaching the site from the southeast, a 3.7 hr. pre-site survey was run in order to pick a loca-

tion that would avoid the loose upper Miocene sand that had plagued Leg 93 at Site 604. A series of three water-gun seismic reflection profiles (CP3a, CP3b, CP3c) were run parallel to U.S.G.S. Line 35. The profiling track crossed Lines 35, 25, and 79-218 and also the two previous *Glomar Challenger* Lines (CP1 and CP2) in the area (surveyed during approach and departure from Site 612), giving 12 crossing tie points for refined seismic correlation (Fig. 1). After completing the planned profiling, the position of the thinnest Miocene section was determined (about 10 m thick) and the beacon was dropped there at 0445 hr., September 17 (at 38°46.17'N, 72°30.18'W).

The vessel was then offset about 0.35 n. mi. to the northwest to position the site on one of the *Glomar Challenger* profiles just completed (CP3b). This location is about 1 n. mi. updip and 0.75 n. mi. northeast (along strike) from the originally proposed location of Site NJ-12. Averaged locations from satellite navigation fixes place Site 613 at 38°46.26'N, 72°30.43'W, about 0.1 n. mi. southeast of Line CP3b.

### Site 613

The vessel returned to the offset position and began running in the hole. The bottom-hole assembly was made up identically to the configuration used at Site 612 for combination piston coring and rotary coring with the

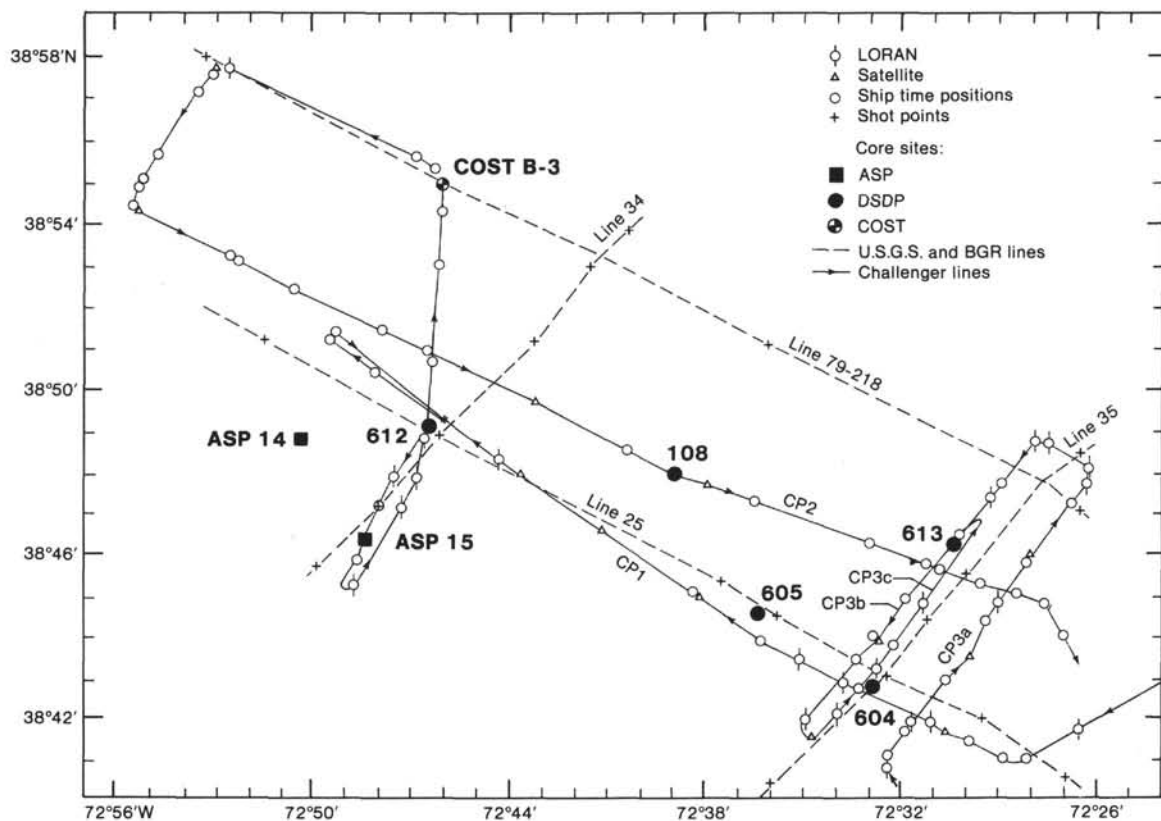


Figure 1. Location of holes and seismic reflection profiles in the vicinity of Site 612. ASP = Atlantic Slope Project (Poag, 1978). COST = Continental Offshore Stratigraphic Test (Poag, 1978). The CP lines are single-channel water-gun profiles surveyed by *Glomar Challenger* during Leg 95. Other lines are multichannel common-depth-point profiles surveyed by the U.S.G.S. and BGR.

extended core barrel (XCB) as desired. Since the big question of success at the site rested on whether or not the Miocene sand interval could be penetrated, it was decided to wash to about 250 m BSF as quickly as possible and tackle the big problem with a minimum investment of time. Failure to penetrate the sand, as had occurred at Holes 604 and 604A, would be cause to abandon the site altogether and proceed without further delay to the next alternate site.

With the XCB in use, getting through the sand would allow the desired penetration below the sand interval to be accomplished, followed by through-the-bit logging. This would leave open the option of pulling the bit to the mudline and starting a new hole to continuously core the previously washed interval, if time and scientific objectives so dictated.

DSDP in La Jolla was contacted to assure the plan to wash without continuous coring was acceptable to the JOIDES Safety Panel and did not violate the hydrocarbon monitoring and safety policies of the Project. The approval to proceed was based on the fact that the site was located only about 4.5 mi. from Site 604, which had been carefully monitored for hydrocarbons and found to be safe for *Challenger*-type drilling.

The recent experiences at nearby Sites 604 and 605 indicated that the seafloor would probably be too firm for piston coring, so spud-in was done with the extended core barrel in place. The Heave Compensator was used to mitigate the problem of applying weight to the bit so close to the surface without proper stabilization for the BHA.

The bottom was detected clearly at 2333.2 m and the hole was officially spudded at 1331 hr., 17 September. PDR depth had been a little misleading at 2319 m. An initial surface punch core was carefully taken to a sub-bottom depth of 9.7 m to establish an accurate mudline. The core barrel was then retrieved but contained only traces of clay inside the liner. This, plus the firmness and drilling characteristics observed at the mudline, suggested that the seafloor was predominately loose sand, which is commonly not recovered by the core catchers. The first core was discounted and the hole was again spudded, this time being washed to 19.8 m before pulling the wash barrel. The wash core contained only 1.39 m of clay with traces of sand.

A sequence of alternating XCB and wash cores using the XCB were then taken to a depth of 116.0 m BSF, where continuous coring was carried out for four cores in order to locate the Pleistocene/Pliocene boundary (see coring summary in Table 1). This having been accomplished, the bit was washed directly to 182.9 BSF, where continuous coring began.

Core 613-19 at 260 m BSF contained a significant proportion of sand mixed with dark mudstone. The site turned out to have been well selected, as this was the only evidence of the troublesome Miocene sand interval. Core 613-20 contained only 20 cm of Eocene chalk lodged in the core catcher. The Miocene/Eocene contact had been lost because of core catcher failure and/or jamming.

From that point to the total depth of the hole at 581.9 BSF, the formation remained Eocene chalk. Recovery

Table 1. Coring summary, Hole 613.

Core <sup>a</sup>	Date (1983)	Time	Depth from drill floor (m)	Depth below seafloor (m)	Length cored (m)	Length recovered (m)	Amount recovered (%)
1W	17 Sept.	1545	2333.2-2353.0	0.0-19.8	19.80	1.39	
2X	17 Sept.	1700	2353.0-2362.6	19.8-29.4	9.60	9.53	99
3W	17 Sept.	1805	2362.6-2391.4	29.4-58.2	28.80	0.00	
4X	17 Sept.	1910	2391.4-2401.0	58.2-67.8	9.60	3.80	40
5W	17 Sept.	2255	2401.0-2449.2	67.8-116.0	48.02	6.55	
6X	17 Sept.	2315	2449.2-2458.8	116.0-125.6	9.60	9.58	100
7X	18 Sept.	0045	2458.8-2468.3	125.6-135.1	9.50	9.58	114
8X	18 Sept.	0155	2468.2-2477.8	135.1-144.6	9.50	9.20	97
9X	18 Sept.	0430	2477.8-2487.3	144.6-154.1	9.50	9.21	97
10W	18 Sept.	0800	2487.3-2516.1	154.1-182.9	28.80	9.53	
11X	18 Sept.	0945	2516.1-2525.8	182.9-192.6	9.70	5.40	56
12X	18 Sept.	1115	2525.8-2535.5	192.6-202.3	9.70	8.80	91
13X	18 Sept.	1225	2535.5-2545.2	202.3-212.0	9.70	9.12	94
14X	18 Sept.	1400	2545.2-2554.7	212.0-221.5	9.50	8.30	87
15X	18 Sept.	1510	2554.7-2564.2	221.5-231.0	9.50	9.37	99
16X	18 Sept.	1630	2564.2-2573.7	231.0-240.5	9.50	9.37	99
17X	18 Sept.	1815	2573.7-2583.2	240.5-250.0	9.50	4.53	48
18X	18 Sept.	1940	2583.2-2592.7	250.0-259.5	9.50	8.74	92
19X	18 Sept.	2050	2592.7-2602.2	259.5-269.0	9.50	8.83	93
20X	18 Sept.	2150	2602.2-2611.8	269.0-278.6	9.60	0.20	2
21X	18 Sept.	2250	2611.8-2621.4	278.6-288.2	9.60	9.43	98
22X	19 Sept.	0005	2621.4-2631.0	288.2-297.8	9.60	9.61	100
23X	19 Sept.	0120	2631.0-2640.6	297.8-307.4	9.60	9.49	99
24X	19 Sept.	0250	2640.6-2650.2	307.4-317.0	9.60	7.74	81
25X	19 Sept.	0355	2650.2-2659.8	317.0-326.6	9.60	9.48	99
26X	19 Sept.	0505	2659.8-2669.4	326.6-336.2	9.60	9.62	100
27X	19 Sept.	0615	2669.4-2679.0	336.2-345.8	9.60	9.30	97
28X	19 Sept.	0720	2679.0-2688.6	345.8-355.4	9.60	9.19	96
29X	19 Sept.	0845	2688.6-2697.9	355.4-364.7	9.30	9.17	99
30X	19 Sept.	0955	2697.9-2707.2	364.7-374.0	9.30	0.10	1
31X	19 Sept.	1120	2707.2-2716.5	374.0-383.3	9.30	9.61	103
32X	19 Sept.	1215	2716.5-2725.9	383.3-392.7	9.40	9.25	98
33X	19 Sept.	1320	2725.9-2735.3	392.7-402.1	9.40	9.54	101
34X	19 Sept.	1445	2735.3-2744.7	402.1-411.5	9.40	9.04	96
35X	19 Sept.	1545	2744.7-2754.2	411.5-421.0	9.50	9.71	102
36X	19 Sept.	1650	2754.2-2763.7	421.0-430.5	9.50	9.62	101
37X	19 Sept.	1805	2763.7-2773.2	430.5-440.0	9.50	9.20	97
38X	19 Sept.	1930	2773.2-2782.7	440.0-449.5	9.50	5.52	58
39X	19 Sept.	2110	2782.7-2792.2	449.5-459.0	9.50	8.01	84
40X	19 Sept.	2320	2792.2-2801.7	459.0-468.5	9.50	0.55	6
41X	20 Sept.	0120	2801.7-2811.0	468.5-477.8	9.30	9.68	104
42X	20 Sept.	0345	2811.0-2820.3	477.8-487.1	9.30	0.62	7
43X	20 Sept.	0535	2820.3-2829.6	487.1-496.4	9.30	7.73	83
44X	20 Sept.	0810	2829.6-2839.1	496.4-505.9	9.50	9.60	101
45X	20 Sept.	1105	2839.1-2848.6	505.9-515.4	9.50	8.43	89
46X	20 Sept.	1310	2848.6-2858.1	515.4-524.9	9.50	9.59	101
47X	20 Sept.	1520	2858.1-2867.6	524.9-534.4	9.50	0.44	5
48X	20 Sept.	1750	2867.6-2877.1	534.4-543.9	9.50	1.54	16
49X	20 Sept.	2020	2877.1-2886.6	543.9-553.4	9.50	0.20	2
50X	21 Sept.	0055	2886.6-2896.1	553.4-562.9	9.50	8.14	86
51X	21 Sept.	0300	2896.1-2905.6	562.9-572.4	9.50	9.68	101
52X	21 Sept.	0600	2905.6-2915.1	572.4-581.9	9.50	5.66	60

<sup>a</sup> W indicates wash core, X indicates extended core barrel.

was generally high and penetration rapid until near the end of the hole. The final three cores were taken using tight throat XCB cutting shoes, which decreased core jamming. Penetration rate fell from an average 7.1 m/hr. to as low as 3.5 m/hr. at Core 613-50 and the bit exhibited many of the common signs of impending bit failure, despite the fact that the Eocene chalk being recovered appeared to be routinely drillable material. No adequate explanation for these difficulties came to light when the bit was examined later.

With available operating hours running out and the next major scientific objective, the Paleocene boundary, still many meters and hours away, the coring was terminated to leave time for logging. The hole was filled with barite-weighted mud and the bit was pulled to the logging depth of 2436.6 m (103.4 m BSF) for logging. As had been done at Site 612, the pipe was pulled using the air spinner to avoid rotating the bit and unnecessarily disturbing the hole.

The sheaves were rigged for logging and the Schlumberger tools were assembled and run down the pipe. The tool combination was the same as the first run at Site 612: dual induction, sonic, gamma ray, and caliper. The hole was found to be tight in spots, probably because of

swelling of fresh-water-sensitive clays, but the sonde was worked to total depth in less than 2 hr. Within 5½ hr. the run was complete, including a repeat for sonic waveforms, and the tools were retrieved.

The Multichannel Sonic (MCS) logging tool from Lamont was then rigged and run down the pipe. Although the hole had been "swabbed" by the Schlumberger tools, it proved to be too tight for the MCS tool, which was much lighter (about 450 lb. compared to the Schlumberger tool weight of 20,000 lb.) and was further hampered by its flexible, rubberized receiver string. Continuous working of the tool managed to get it down to a depth of 2519 m (82 m below the bit) but no further penetration could be achieved without risking severe damage to the tool. One of the 12 acoustic receivers was rendered inoperative before the exercise was completed. The 82 m of open hole was logged twice and a third run was attempted before the tool was retrieved. Both the Schlumberger and Lamont logging tools passed into and out of the pipe through the unreleased XCB/HPC bit with no trouble.

The pipe was then pulled out of the hole and the BHA components were given the routine end-of-leg Magnaflux inspection before the vessel departed the site bound for Port Everglades at 0436 hr., 22 September.

#### Site 613 to Ft. Lauderdale

The transit to Ft. Lauderdale's Port Everglades was uneventful, the vessel making good time in pleasant autumn weather, helped out by following seas. The seismic gear was streamed until the ship entered the Florida Straits near the Bahamas. The trip was completed in 98.1 hr., the average speed having been 9.1 knots. Leg 95 terminated at 0645 hr., 26 September, when the first line was secured at Berth Two at Port Everglades, Ft. Lauderdale, Florida.

### LITHOLOGY

DSDP Site 613 is located on the uppermost portion of the continental rise, 30 km and 11.5 km downslope of Sites 612 and 605, respectively. In order to avoid the unstable Miocene sand that had curtailed drilling at Site 604, 7 km along strike to the southwest, Site 613 was located where the buried sand appears to feather out to less than 10 m thickness. Determining the age and the origin of sediments beneath the Miocene sand was a primary objective of drilling at Site 613. Seismic profiles oriented parallel to bathymetric contours suggested that an undulating erosional surface representing a pronounced hiatus would be found beneath the Miocene sand and that beneath that unconformity would lie deeply incised channels filled with displaced sediment. Furthermore, a high-amplitude reflector within these displaced strata was also targeted as a drilling objective in the presite survey (see Mountain et al., "Underway Geophysics," this volume). From seismic and lithologic correlations with Sites 605 and 612, this reflector appeared to represent a zone of diagenetic porcellanite within Eocene biogenic sediments. As the following lithologic descriptions show, we successfully met our objectives.

The sedimentary sequence has been divided into three lithologic units (Fig. 2; see also Site 613 Superlog in back pocket). Lithologic Unit I is further divided into three subunits (IA, IB, and IC) which parallel the facies division made at Site 612. Lithologic Unit I, of Pliocene-Pleistocene plus Miocene(?) ages, extends from the seafloor to approximately 268.3 m, and is composed of a complex sequence of mud, calcareous mud, and nannofossiliferous mud, intercalated with glauconitic, or pyritic, silty sands. To minimize time in getting to our deeper objectives, the upper 116 m were spot cored (Fig. 3), and consequently knowledge of this part of the section is incomplete. However, at both Sites 604 and 605 (Leg 93) the equivalent section was continuously cored. Lithologic Unit II is composed of middle to lower Eocene siliceous nannofossil chalk (269.0–442.1 m BSF). Lithologic Unit III is entirely lower Eocene and is porcellanitic nannofossil chalk, limestone, and nannofossil porcellanite (442.1–577.7 m BSF). Logging characteristics suggest that this lithologic unit includes the unrecovered section down to 581.9 m.

#### Lithologic Unit I

Interbedded greenish gray to dark greenish gray mud and calcareous mud, variably diatomaceous with glauconitic or pyritic silty sand and sandy mud (Fig. 2). Top of Core 613-1 to bottom of 613-19, 0 to 268.3 m BSF. Pleistocene, Pliocene, and Miocene (?). Thickness: 268.3 m.

##### Subunit IA (top of Core 613-1 to 613-6-3, 76 cm; 0 to 119.8 m)

This subunit was poorly cored and recovered; consequently the lithologic succession is uncertain. Two sedimentologic subfacies of Subunit IA are recognized on the basis of their mineralogic components.

The first subfacies (Core 613-1 and Sections 613-2-3 to 613-4-3) consists of interlayered, glauconitic, quartzose sand, silty sand, sandy mud, and mud of greenish gray (5G 6/1) to dark greenish gray color (5G 4/1). On the basis of smear slides, the terrigenous components are quartz, sand, or silt (50–70%), feldspar (5–10%), mica (10%), heavy minerals (5–10%), clay (5–20%) and glauconite (as much as 15%).

The second subfacies (Sections 1 and 2 of Core 613-2 and Sections 613-4, CC to 613-6-3) is composed of mud, marly nannofossil ooze, and nannofossil diatomaceous ooze and mud, of greenish gray (5G 6/1), dusky gray (5YR 2/2), and dark gray (5Y 4/1) colors. Sporadic reworked middle Eocene clasts of yellowish gray color (5Y 8/1) occur in Sections 1 and 2 of Core 613-2 and in Sections 1 to 4 of 613-5, suggesting that much of this subfacies may be debris flow deposits. The variable carbonate content measured by the carbonate "bomb" method ranges from 1 to 20% and agrees with the observed interlayering of mud and calcareous mud.

Lithologic Subunit IA unconformably overlies Subunit IB. A conglomeratic mud, with 3-cm pebbles of quartz sandstone and calcareous sandstone, marks an erosion surface at the basal contact in 613-6-3, 76 cm at 119.8 m BSF.

**Subunit IB (613-6-3, 76 cm to 613-11-3, 73 cm;  
119.8–187.6 m BSF)**

Below the thin conglomerate at the base of Subunit IA, the dominant lithology consists of unbedded homogeneous mud and calcareous mud of greenish gray (5G 6/1) or grayish green color (5G 5/2). There is sporadic, glauconitic, silty sand of grayish green color (5G 4/2), and dusky green (5G 3/2) sand grains as large as 3 mm are common within large mottles and thin layers in Core 613-7 and especially in Core 613-8. Small shell fragments are disseminated throughout Cores 613-6, 613-7, and 613-8 and a well-preserved *Cardium* shell was noted in Sample 613-8-2, 25 cm.

The glauconite content decreases in Cores 613-9 and 613-10 and pyrite increases (up to 50%). Silty, pyritic mud occurs as pervasive mottles and diffuse, thin, dark gray (2.5Y 3/1) layers. This mud is seen principally in Core 613-10, where the pyritic muds alternate with homogeneous, deformed, dark gray, calcareous mud (5Y 4/1). The sediments in Cores 613-9 and 613-10 show two contrasting types of deformation. In Core 613-10, convolute disturbance is tied to possible sediment slumping; deformation in Core 613-9 is the result of coring disturbance. Below the zone of silty, pyritic mud and calcareous mud, more nearly homogenous calcareous mud (greenish gray, 5G 5/1, and olive gray, 5Y 4/2) reappears and is interlayered with coarse, sandy, glauconitic mud in Core 613-10 and in Sections 1 and 2 of Core 613-11.

Throughout Subunit IB, a good correlation exists between the boundaries of the silty, pyrite-rich zones and the especially large changes in the gamma ray log. Glauconitic layers typically yield erratic gamma ray signals. The use of the logs has aided in the reconstruction of this incompletely cored lithologic unit (Fig. 4).

The basal contact of Subunit IB is a sharp erosional break at 613-11-3, 73 cm, (Fig. 5), which coincides with the Pliocene/Pleistocene contact.

**Subunit IC (613-11-3, 73 cm to the bottom of Core  
613-19, 187.6–268.3 m BSF)**

This subunit is a predominantly structureless, nannofossiliferous, siliceous mud of dusky yellow green color (5GY 5/2 to 10GY 3/2), containing sporadic, silty, glauconitic-quartzose laminae. From smear slide estimates, nannofossil content is low, generally ranging from 2 to 10%, averaging 7%; foraminifers are generally sparse, at most constituting 5% of the sediment. Siliceous microfossils, the dominant biogenic component, are much more variable. Radiolarians generally comprise 1 to 5%, whereas diatom content is especially variable and reaches abundances as high as 20%. Total biogenic silica ranges from 1 to 35%, with an average of 12%.

Glauconite is found throughout this subunit in concentrations as much as 15% (4% is average), but in contrast to the overlying lithologic Subunit IB, glauconite rarely occurs in laminae and never is found in beds thicker than 1 cm. However, drilling disturbance varies from moderate (in Cores 613-11 through 613-13) to severe ("biscuit" artifacts) for the remainder of Subunit IC. Sand to granule sized glauconite grains, quartz sand, pyrite nod-

ules, gastropod fragments, and pebbles are consistently found in the slurry between biscuits. Furthermore, a clear increase in the glauconite component of this slurry is observed toward the bottom of several cores. This suggests that thin, poorly-lithified, coarse-grained beds may be far more common in this interval than core recovery indicates, and that most were completely destroyed and washed into the barrel during coring, where they settled during the 2500 m trip to the rig floor. The highly variable gamma-ray values measured by wireline logging further suggest that there is more heterogeneity in this subunit than is visible in the cores.

Silt-sized quartz grains are significant components within the sediment biscuits. However, on the basis of smear slides estimates, the quartz decreases from 20 to 30% in Cores 613-12 and 613-13 to 5–15% in Cores 613-15 and 613-16; below this level, values increase again to 20 to 30%. Estimates of clay content vary in the opposite sense: from as low as 25% in Cores 613-13, values increase to 60–80% in Cores 613-15 and 613-16, and then decrease again below this level. These especially fine-grained, clay-rich cores (613-15 and 613-16) are notably more uniform than others in lithologic Subunit IC, and they show the lowest glauconite contents and the smallest amounts of coarse-grained drilling slurry. Not surprisingly, part of this interval (ca. 220–230 m) shows up on the wireline log as a zone that swelled considerably because of the freshwater barite mud introduced before logging. This also corresponds to a marked gamma-ray increase. All of these observations indicate an especially clay-rich zone.

Bioturbation was detected in only one 75 cm interval of lithologic Subunit IC, beginning at 613-17-3, 50 cm. The burrows are flattened, irregular, and slightly deformed. Smear slide analysis of this interval reveals a slightly higher nannofossil content (15%) than the average for this entire unit (7%), and this is the only interval completely lacking detrital quartz (which averages 18% in the unit as a whole). On this basis, the 75 cm interval in Section 613-17-3 is interpreted to be reworked sediment and is possibly a slump deposit.

Displaced sediment is also found at the base of lithologic Subunit IC. Glauconitic conglomeratic sand mixed with a 10- to 20-cm-thick interval of nonfossiliferous mud is found below 613-19-2, 70 cm. Granule sized quartz pebbles overlie a scoured surface at 95 cm in Section 613-19-5. Although the Miocene/Pliocene contact occurs in Core 613-19, the similarity of lithologic character across this biostratigraphic boundary does not warrant any lithologic subdivision. The bottom of Core 613-19 constitutes the base of lithologic Unit IC, seen at 268.3 m BSF. However, the actual bottom of this unit may be at about 278 m (unrecovered in cores) on the basis of the downhole core logs.

**Lithologic Unit II**

Siliceous nannofossil chalk (Fig. 6) of light greenish gray (5G 8/1) color with burrows of light olive gray (5Y 6/1) and olive gray (5Y 4/1). 613-20, CC to 613-38-2, 60 cm (278.0 m to 442.1 m BSF). Middle to lower Eocene. Thickness: 164.1 m.

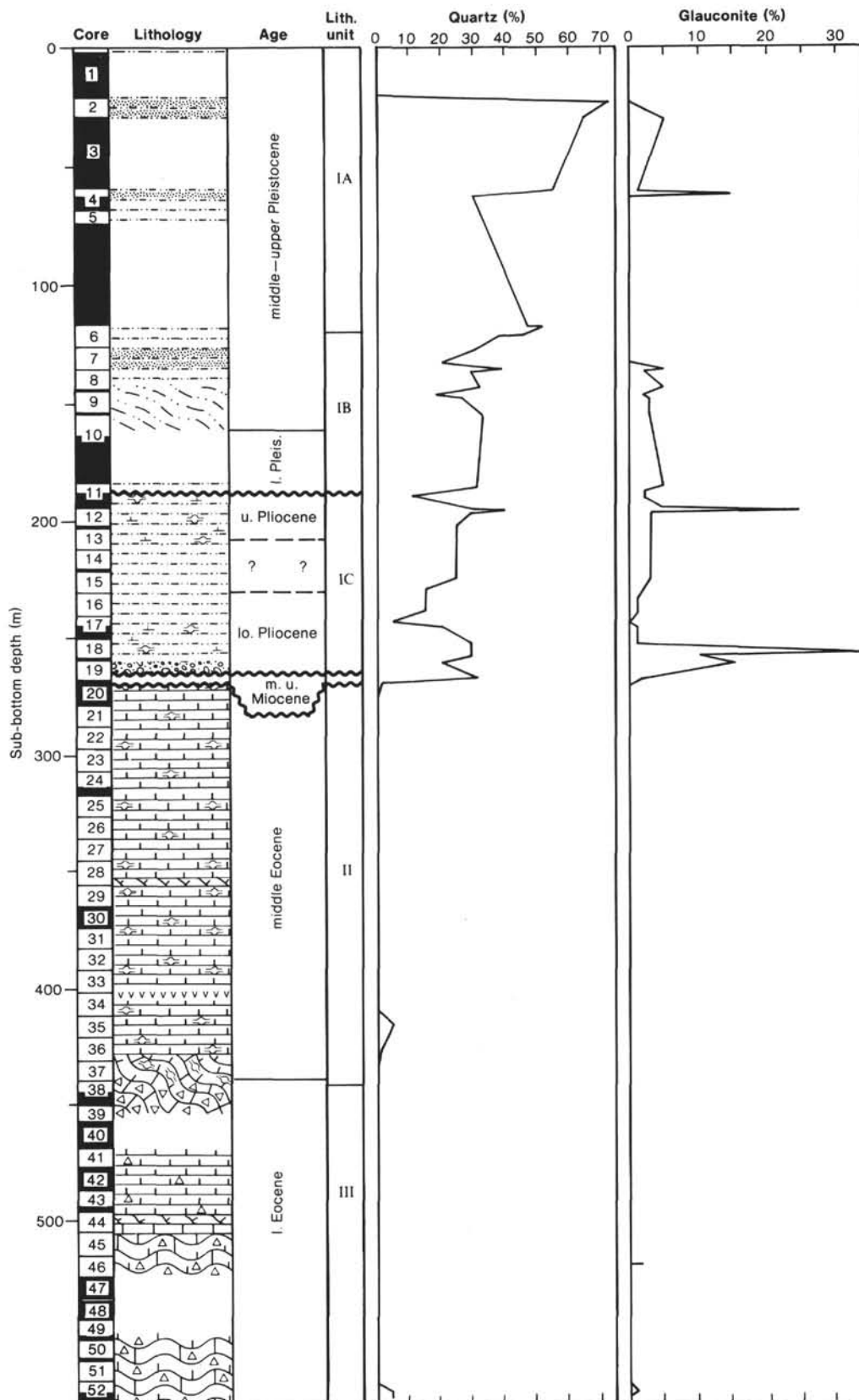


Figure 2. Lithostratigraphic column for Site 613.

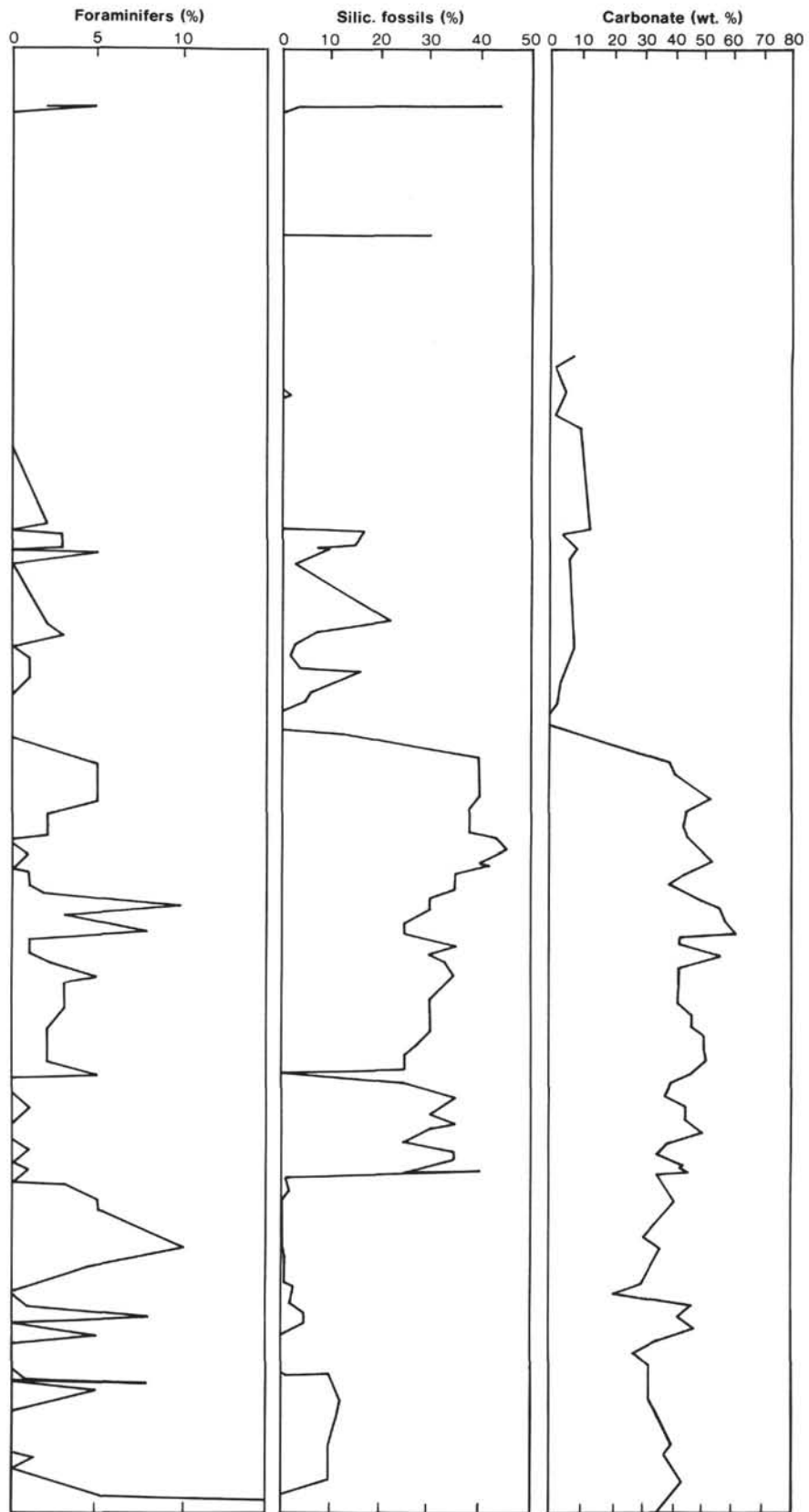


Figure 2 (continued).

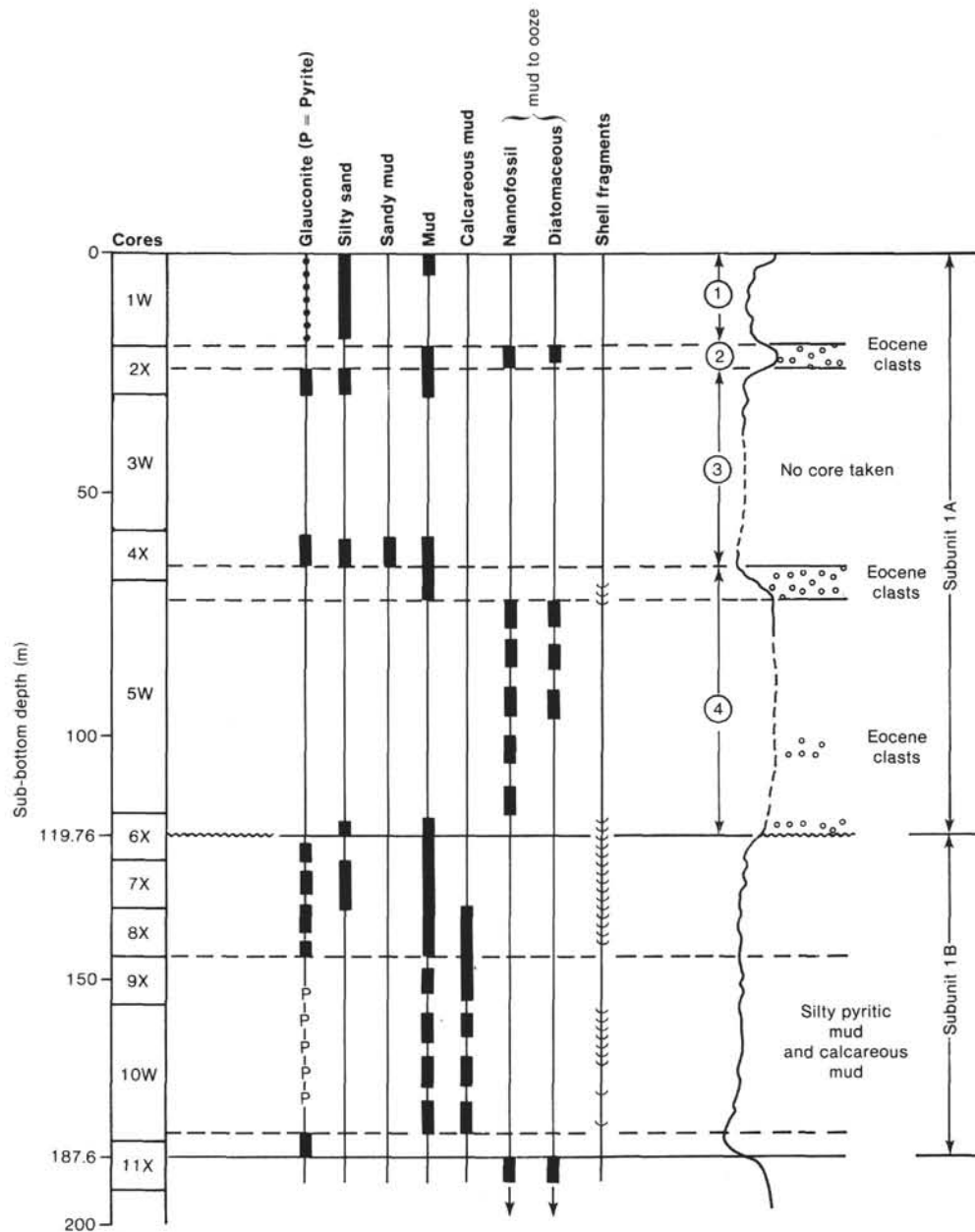


Figure 3. Criteria employed in the lithologic reconstruction of lithologic Subunits 1A and 1B. (W = wash core, X = extended core barrel.) Data taken from smear slide estimates. Wash cores are "stretched" through the entire interval they represent. ① to ④ indicate 4 mineralogically distinct zones.

The exact location of the upper boundary of Unit II is uncertain because of the poor recovery in Core 613-20. Based on the gamma ray log, the unrecovered boundary is placed at 278.0 m BSF. The lower boundary of Unit II is defined as the top of the first firmly lithified porcelanitic bed in 613-38-2, 60 cm and lies approximately 2 m below the middle/lower Eocene biostratigraphic contact.

Lithologic Unit II consists of intensely burrowed, bio-siliceous nannofossil chalks. The color ranges from mostly light greenish gray (5G 8/1) to grayish yellow green (5GY 7/2); the burrows vary from light olive gray (5Y 6/1), greenish gray (5GY 6/1), grayish brown (10YR 5/2), to light gray (N7).

Total carbonate contents measured by "bomb" analysis vary from a high of 61% to a low of 34%, with a mean content of 46%. Siliceous organisms, mainly diatoms with minor amounts of radiolarians and sponge spicules, are as abundant as 45% and vary about a mean value of 30%. Nannofossil content in these sediments is about 35%, with a peak of 66% at the top of the unit.

Some of the burrows are surrounded by oval-shaped diagenetic halos, marked with a thin, dark, pyritic outer rim. The entire unit is intensely bioturbated except in sporadic thin laminated zones. Burrows are similar to those in Unit II at Site 612: horizontal and diagonal spreiten, Planolites-type smooth round tubes, large irregular diagonal to vertical root-shaped dwellings, and rare bur-

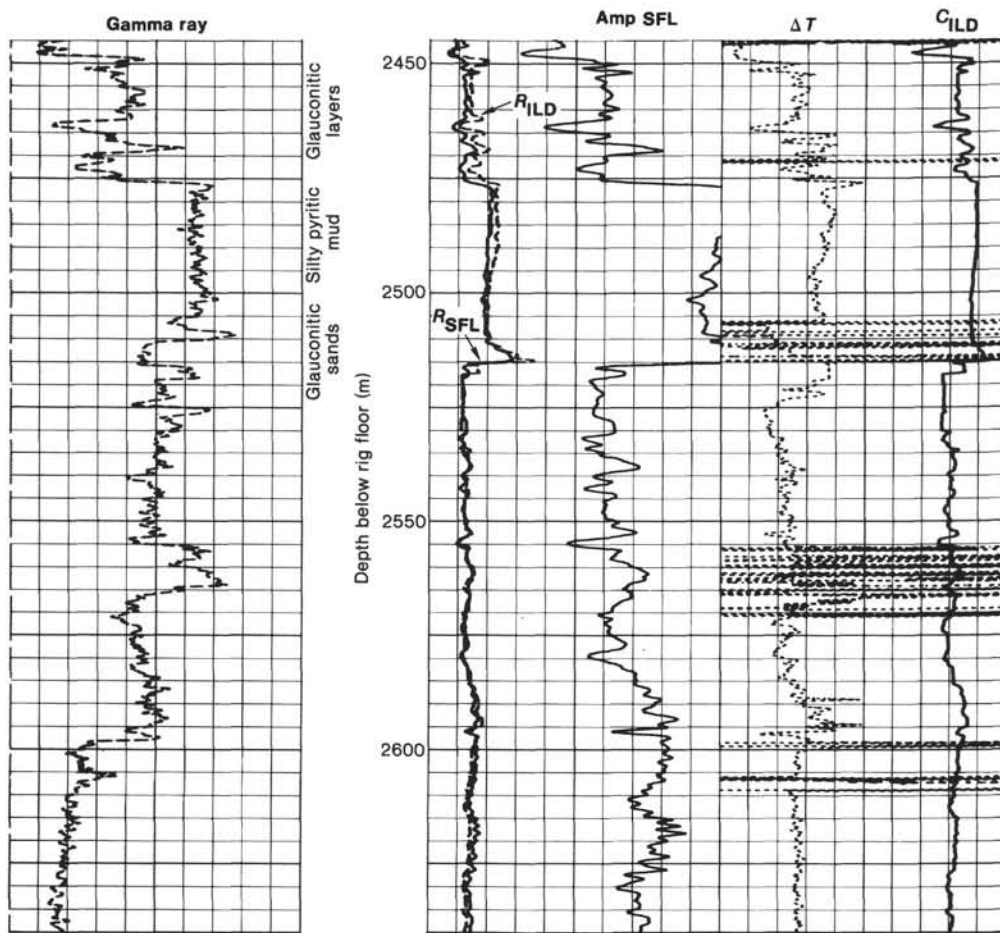


Figure 4. Schlumberger logs used in the reconstruction of the stratigraphic positions of the diverse lithologies found in wash Core 10.

rows of Zoophycos and Chondrites. Thin sections reveal that many burrows are filled with foraminifers. Most burrows are flattened (compacted).

The uniform lithology of lithologic Unit II is interrupted by several slumps. The shallowest of these is in 613-29-1, 1–130 cm and clearly shows small horizontal and overturned folds and no bioturbation. Slumping is also common in Cores 613-36 and 613-37. 613-36-3, 10–55 cm, is evenly parallel bedded, with bedding surfaces dipping at various angles. Slump features include folds, contorted beds, and small-scale faulting, best seen in Cores 613-36 and 613-37 (Fig. 7). Core 613-37 consists of a series of slumps, which nannofossil dating shows to be the repeated imbrication of middle and lower Eocene sediment.

In 613-34-1, 107 cm, a 5-cm-thick layer of volcanic ash interrupts the otherwise monotonous biogenic sediments. It consists of sand-sized glass shards. A similar layer is reported at Site 605 of Leg 93.

Well-preserved siliceous organisms continue to be found in abundances of 25–35% in the lowermost meters of Unit II; they decrease markedly in the top few meters of lithologic Unit III. They vanish in Section 613-38-3, beginning first with the dissolution of diatoms, followed within 40 cm by the dissolution of radiolarian and sponge spicules. In thin sections, it appears that both foraminif-

ers and radiolarians are replaced by sparry calcite and opal C-T. The first traces of opal C-T, as determined by X-ray diffraction (see also Thein and von Rad, this volume) occur in Core 613-37. Large amounts of opal C-T first appear in Core 613-38 and numerous occurrences throughout the underlying sediment distinguishes this unit from lithologic Unit III.

### Lithologic Unit III

Greenish gray to gray porcellanitic nannofossil chalk and limestone and nannofossil porcellanite (Fig. 8, Plate 1). Samples 613-38-2, 50 cm to 613-52-4, 85 cm (bottom of section at Hole 613); 442.1 m to 577.7 m BSF. Lower Eocene. Thickness: 135.6 m.

This unit includes porcellanitic nannofossil chalk and limestone as well as nannofossil porcellanite ranging in color from pale green (5G 7/2), light greenish gray (5G 8/1) to light gray (N7). As in Unit II, burrow mottles of brown (10YR 5/3), light brown (10YR 6/3), and gray colors (N4, N5, and N6) are found throughout Unit III. Many of the burrows exhibit diagenetic halos.

There is extensive slumping throughout Unit III as seen in Cores 613-38, 613-39, 613-44, and 613-52. In some zones chevron folds and small faults are evident, as in the overlying Unit II, but we also note a variant on slumped structure style in Core 613-52 where a massive,

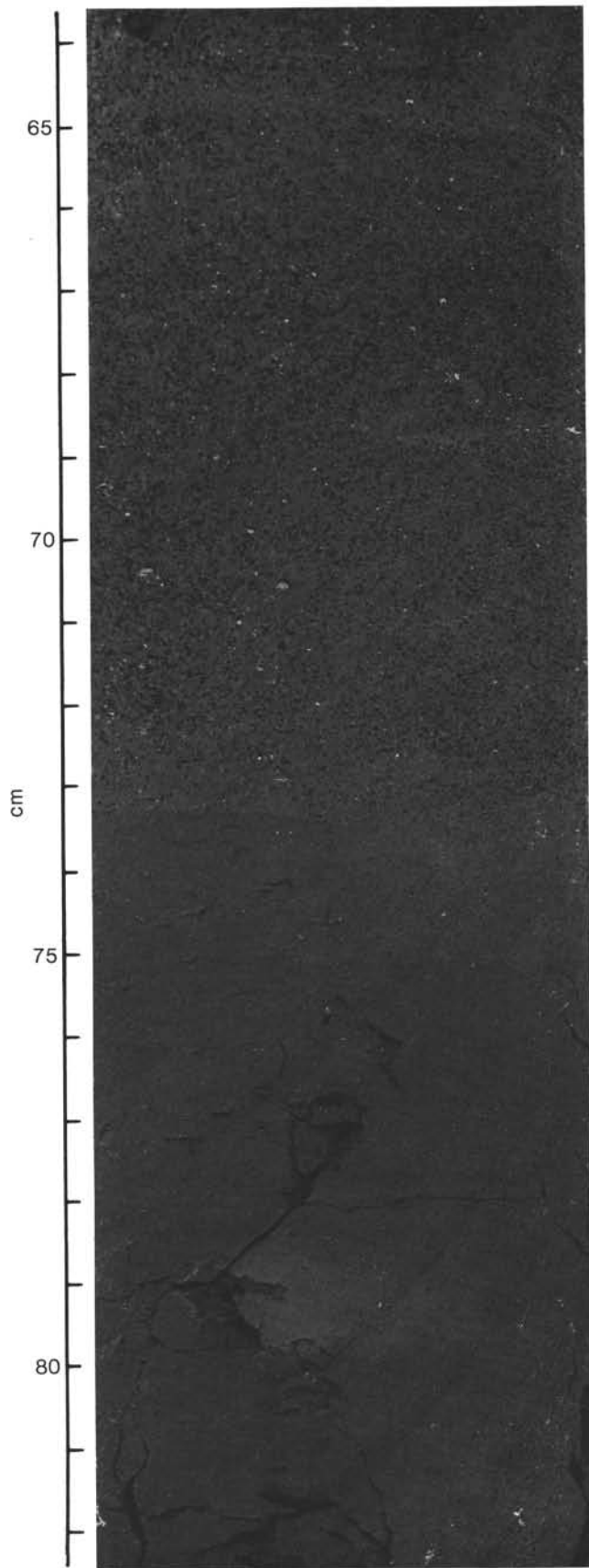


Figure 5. Erosional contact between Subunits IB and IC; also Pliocene/Pleistocene contact. (613-11-3, 64-82 cm).

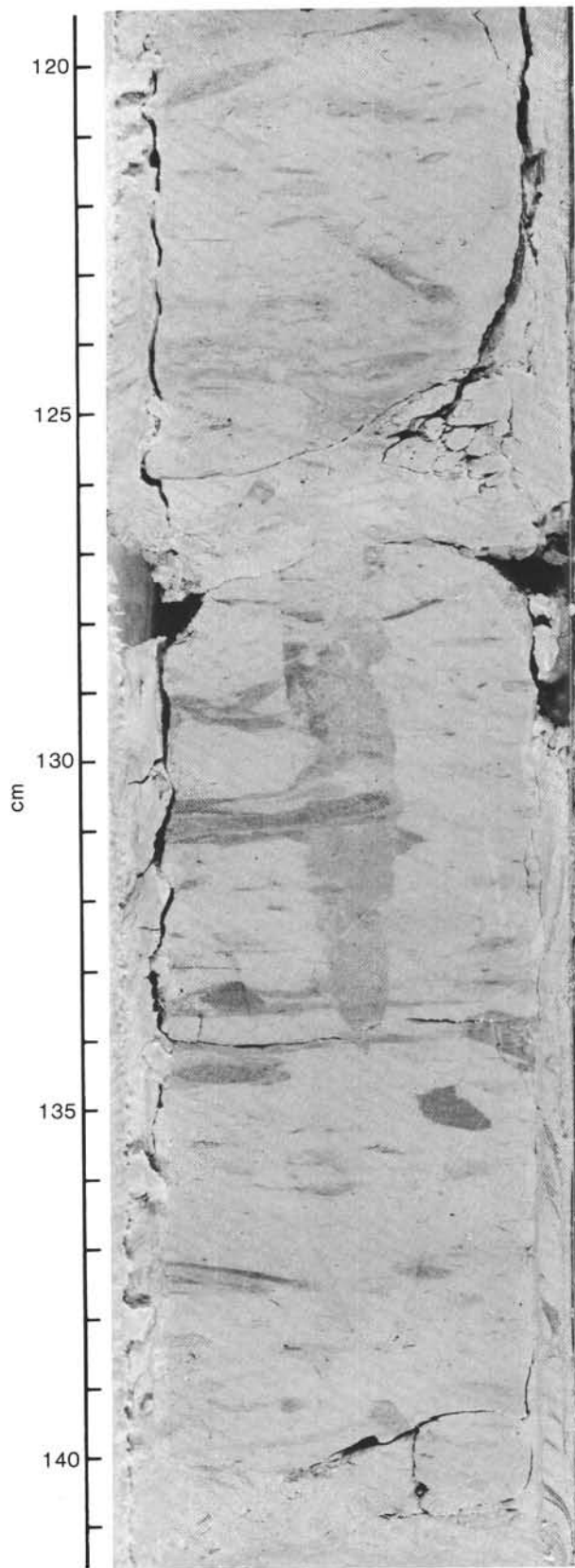


Figure 6. Lithologic Unit II; siliceous nannofossil chalk with diverse burrow types (613-28-4, 119-141 cm). At center is a root shaped dwelling structure crossed by a younger horizontal burrow. Both are surrounded by a bleached diagenetic halo fringed by a thin rim of pyrite framboids (at arrow).

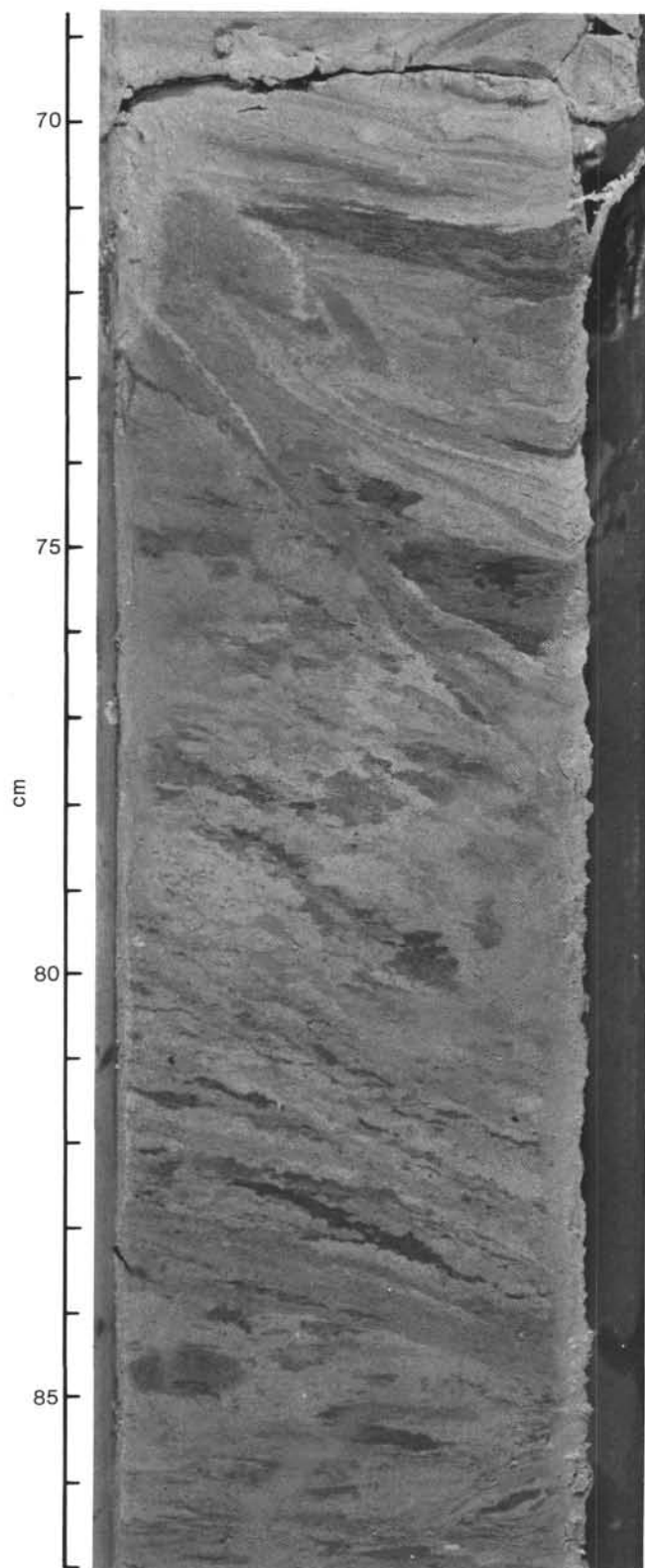


Figure 7. Lithologic Unit II; siliceous nannofossil chalk containing small scale chevron folds formed by slump movement over a limited distance (613-37-2, 69-87 cm).

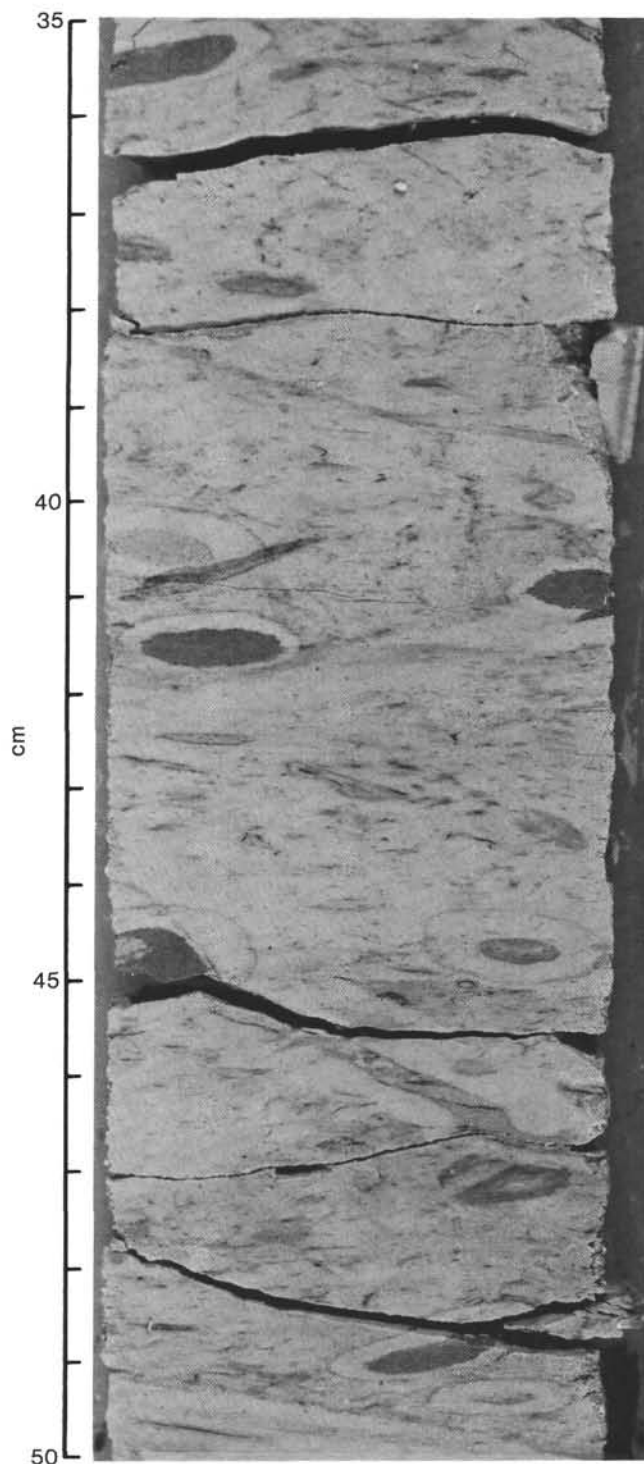


Figure 8. Lithologic Unit III; porcellanitic nannofossil limestone with oval, flattened, horizontal burrows filled with organic-rich sediment, and surrounded by bleached diagenetic halos (613-41-2, 35-50 cm).

almost featureless zone contains just a few slump structures and some stretched burrows. Large quantities of calcareous nannofossils (20-35%) are noted in smear slides throughout Unit III, but only a few percent of poorly preserved foraminifers are noted. Diatoms and radiolarians, which are plentiful in the overlying lithologic Unit

II, show evidence of etching and dissolution toward the bottom of Unit II. Poorly preserved biota continue down into Unit III below the uppermost layer of well-developed porcellanite, for about 2.3 m to 613-38-3, 130 cm. Below this level they are completely replaced by either sparry calcite or opal C-T throughout the rest of the cored section.

The diagenesis that created this facies is uneven in both style and degree. Some layers have become hard porcellanitic limestone and nannofossil porcellanite while others, with apparently similar compositions, have remained porcellanitic nannofossil chalk. Some zones exhibited an unusual physical attribute noted while cutting the cores: the sediment of Unit III is initially dense and indurated, but when rinsed with fresh water some intervals swelled, cracked, and lost cohesion. This was not the case for sediments from the same zones that were not rinsed. Not surprisingly, shipboard velocities measured in these sediments exhibit marked anisotropy and many samples rapidly lost cohesion and became very difficult to cut and measure for their physical properties. Shore-based geochemical studies suggest increased clay content in these intervals may be responsible for their unusual behavior.

The original sediment comprising Lithologic Unit III was rich in siliceous microfossils, but as at Site 612 and many other areas of the North Atlantic, it has been modified by diagenesis. At Site 613, there is an additional large component of nannofossil carbonate, which does not change in abundance across the diagenetic front. Widespread, moderately rapidly deposited biogenic siliceous sedimentation during the lower and middle Eocene provided the background for the development of porcellanites.

Two major differences between Units II and III at Sites 612 and 613 are obvious. The first is that non-bioturbated, laminated intervals are found only up dip at Site 612. The second is that Eocene slump deposits occur only at Site 613. Seismic profiles (see Poag and Mountain, this volume) show clearly the change from undeformed Eocene margin sediments at Site 612 to well developed slumps filling base-of-slope channels in the vicinity of Site 613.

**BIOSTRATIGRAPHY**

**General Summary**

Hole 613 penetrated 581.9 m of sediment in 52 cores, ranging in age from Pleistocene to early Eocene (Fig. 9; see also Site 613 Superlog in back pocket). Sediment recovery in most rotary cores was good, although the wash cores in the Pleistocene and some drilling problems in the lower Eocene meant that recovery was only 78.3% for the hole. Throughout much of the succession, faunas and floras are abundant and preservation is moderate to good, although the radiolarians are either poorly preserved or totally recrystallized in the lower Eocene section. In the same interval, the foraminifers are also poorly preserved and some key species have not been recorded.

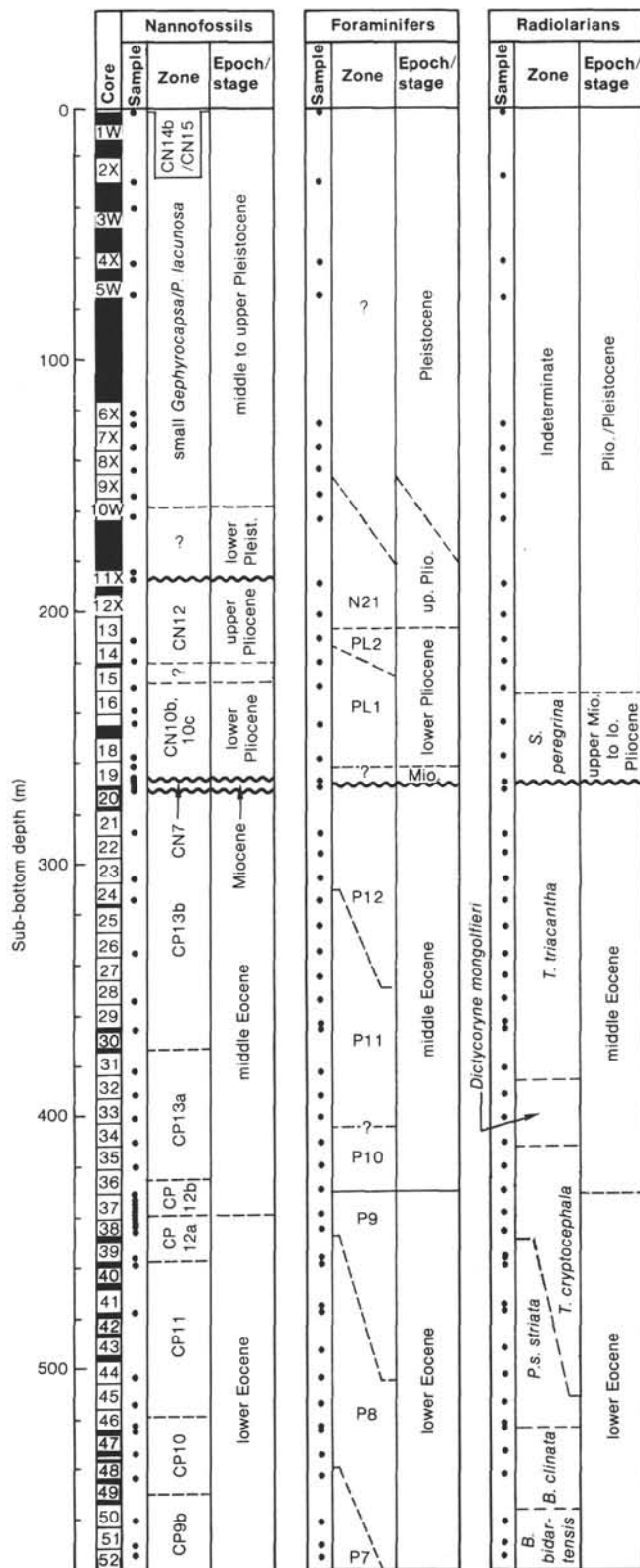


Figure 9. Biostratigraphic column for Site 613. X = extended core barrel; W = wash core.

This report is based mainly on core-catcher material from Cores 613-1 through 613-52, although some additional nannofossil samples were used to locate chronostratigraphic boundaries. Throughout the succession there was reasonable agreement between the nannofossil, radiolarian, and foraminiferal age assignments, but some detailed zonal adjustments await shore-based work.

The lowermost strata recovered have been shown to be lower Eocene (P7/P8 or CP9b) by all the fossil groups. The lower and middle Eocene succession is 304 m thick (613-52,CC to 613-20,CC) and appears to represent almost continuous deposition with no major breaks being detected, although slumping in Core 613-37 at the lower/middle Eocene contact might indicate a hiatus undetected in the shipboard work. The middle Eocene section is overlain disconformably by approximately 10 m of middle to upper Miocene sand (Core 613-19). The remainder of the section is 77 m of Pliocene sediments (Cores 613-18 to 613-11) overlain by 184 m of Pleistocene strata.

### Foraminifers

Fifty-two cores representing an Eocene to Quaternary section were recovered at Site 613. Only core catcher samples were examined for foraminifers.

#### Lower Eocene

Cores 613-52 through 613-37 represent the lower Eocene succession at this site, as recognized using planktonic foraminifers. The Paleocene/Eocene contact was not recovered, and it is difficult to assess how much lower Eocene, if any, is missing from this site. The lowermost sample recovered (Sample 613-52,CC) contains a moderately well-preserved planktonic foraminiferal assemblage that includes several species of the genus *Morozovella* (*M. aragonensis*, *M. lensiformis*, and *M. formosa gracilis*). In the overlying sample (613-51,CC), *M. marginodentata* also occurs; together these associations suggest assignment to the lower Eocene Zone P8 of Blow (1979); however, this association could be assigned to the *M. formosa formosa* Zone (Stainforth et al., 1975); which is equivalent to Blow's Zone P7 (Berggren et al., 1985; Berggren, Kent, and Flynn, in press). Therefore, we favor a shipboard assignment to undifferentiated Zones P7-P8 pending shore-based studies.

The interval from Samples 613-48,CC through 613-45,CC is assigned to Blow's (1979) Zone P8, based upon the absence of *M. marginodentata*, *M. lensiformis*, and *M. caucasica*. The interval between Samples 613-44,CC and 613-39,CC is assigned to the undifferentiated Zones P8-P9. The foraminifers in this interval are poorly preserved; they include *M. aragonensis*, *M. caucasica*, *Globigerina soldadoensis*, and *Globigerinita taroubaensis*. The appearance of *Truncorotaloides praetopilensis* and *Subbotina frontosa* in Samples 613-38,CC through 613-37,CC indicate assignment to lower Eocene Zone P9.

#### Middle Eocene

The last appearance of *Morozovella caucasica* and the first appearance of *Truncorotaloides rohri* mark the base of the middle Eocene section in Sample 613-36,CC. Convoluted bedding consisting of interbeds of lower and mid-

dle Eocene sediments (see nannofossil biostratigraphy) occurs in Cores 613-36 and 613-37; however, the mixing of middle and lower Eocene beds was not confirmed by foraminiferal studies because we restricted shipboard studies to core-catcher samples.

Low-diversity assemblages noted in Samples 613-35,CC and 613-34,CC consist of only *M. aragonensis*, *Acarinina bullbrooki*, *Subbotina frontosa*, *Truncorotaloides rohri*, and (in Sample 613-34,CC) *Globigerinatheka index*. This association probably represents at least part of Zone P10, but the boundary between Zone P10 and Zone P11 was not distinguished. The first appearance of *T. topilensis* and the last appearance of *A. broedermanni* occurs in Sample 613-27,CC. *M. aragonensis* last appears in Sample 613-26,CC. Thus, the interval between Cores 613-33 and 613-26 is assigned to Zone P11. Cores 613-25 through 613-24 are assigned to Zones P11-P12 (undifferentiated), with probable assignment to Zone P12. Sample 613-23,CC contains an association of *T. topilensis*, *Globorotalia cerroazulensis possagnoensis*, *A. bullbrooki*, *S. frontosa*, forms transitional between *M. spinulosa* and *M. lehneri*, and *G. cerroazulensis pomeroli*, indicative of Zone P12 (probably lower part). The latter form, together with forms transitional to *G. cerroazulensis cerroazulensis* and *A. bullbrooki*, occur in Samples 613-22,CC through 613-20,CC; this association is indicative of Zone P12 (probably upper part). An unconformity representing a hiatus of approximately 37 m.y. occurs between the latter sample and Sample 613-19,CC.

#### Upper Neogene

Sample 613-19,CC contains very few foraminifers; the presence of forms provisionally assigned to *Globoquadrina dehiscens* suggests that this sample may be assigned to the Miocene. Samples 613-18,CC through 613-15,CC are assigned to lower Pliocene Zone P11, based upon the presence of *Globigerina nepenthes*, *Globoquadrina altispira*, *Globorotalia margaritae*, *G. tumida*, *G. plesiotumida*, *Sphaeroidinellopsis subdehiscens*, and *G. punctulata*. *G. crassaformis* appears in Sample 613-15,CC. The zonal assignment of overlying sample (613-14,CC) is indeterminate, but Sample 613-13,CC contains *G. margaritae*, *S. subdehiscens*, and *Sphaeroidinella dehiscens* (without *G. nepenthes*), indicative of lower Pliocene Zone P12. Upper Pliocene sediments (Zone N21) occur in Sample 613-12,CC indicated by *Globorotalia tosaensis*, *G. crassula*, *G. crassaformis*, *G. inflata*, *G. punctulata*, *Neogloboquadrina atlantica*, *N. acostaensis*, *N. humerosa*, and *N. pachyderma*. Abraded specimens of *G. truncatulinoides* noted in this sample are interpreted as contaminants. Sample 613-11,CC contains *G. miocenica*, indicative of a (late) Pliocene age. Samples 613-10,CC and 613-9,CC are indeterminate. The overlying samples (613-8,CC through 613-1,CC) contain *G. truncatulinoides*, indicative of a Pleistocene age.

#### Benthic Foraminiferal Paleoecology

Poor foraminiferal preservation in the lower Eocene section limits interpretations of benthic foraminifers. Forms noted include *Lenticulina* sp., *Gravelinella capitata*, *Bulimina trinitatensis*, *B. semicostata*, *Cibicoides*

*des subspiratus*, *C. cf. C. tuxpamensis*, *C. cf. C. grimsdalei*, *Cibicidoides* spp., *Cyclammina amplexans*, *Gyroidinoides* spp., *Vulvulina spinosa*, and *Oridorsalis* sp. The section was deposited at lower bathyal (ca. 1000–2000 m) depths.

The apparent absence of *Nuttallides truempyi* (an apparently ubiquitous early Paleogene deep-water foraminifer; Tjalsma and Lohmann, 1983) probably is due to poor preservation and insufficient analysis. *Nuttallides truempyi* occurs in the overlying lower middle Eocene section (Cores 613-37 through 613-29), where preservation is improved over the lower Eocene. Initial evaluation of the greater than 250  $\mu\text{m}$  size fraction suggests that this species occurs in moderate to great abundance (ca. 20–30%). Associated common to abundant benthic foraminifers include *Gavelinella micra*, *Lenticulina* spp., *Oridorsalis* spp., and *Globocassidulina subglobosa*. The following taxa also were noted; *Bulimina trinitatensis*, *B. semicostata*, *B. tuxpamensis*, *Gavelinella semicribrata*, *G. cf. G. semicribrata*, *G. capitata*, *Gyroidinoides* spp., *Vulvulina spinosa*, *Buliminella grata*, *Osangularia mexicana*, *Cibicidoides subspiratus*, *C. cf. C. tuxpamensis*, *C. ungerianus*, *Pullenia eocenica*, *Lenticulina cf. L. decorata*, *Gaudryina cf. G. laevigata*, and *Anomalinoides* sp. This section is interpreted as having accumulated in lower bathyal (1000–2000 m) depths.

*Nuttallides truempyi* was not observed in the initial inspection of the greater than 250  $\mu\text{m}$  size fraction of the middle Eocene section (Cores 613-28 through 613-20); however, it is present in the 150–250  $\mu\text{m}$  size fraction. Most of the taxa noted above also occur in this section, accompanied by *Alabama dissonata* and *Hanzawaia cushmani*. *Cibicidoides* dominates in abundance in the greater than 250  $\mu\text{m}$  size fraction; *Bulimina trinitatensis* also is abundant. Upon initial inspection, this section might be interpreted as having been deposited at shallower depths than the underlying section, based upon the apparent lesser abundance of *N. truempyi*. However, comparison with western North Atlantic DSDP Site 390 (ca. 2700 m “backtracked” paleodepth for the middle Eocene, according to Tjalsma and Lohmann [1983]), shows that *N. truempyi* is significantly lower in abundance in the middle middle Eocene (Zones P11 and P12). At Site 390, *C. subspiratus* and buliminids are dominant middle middle Eocene constituents. We interpret the middle middle Eocene section as having been deposited at lower bathyal (perhaps upper abyssal) depths, consistent with comparisons with Site 390.

The (?)Miocene to Pliocene section (Cores 613-19 through 613-11) contains an excellent late Neogene bathyal benthic association. Although abundances fluctuate from sample to sample, *Uvigerina* spp. (including *U. peregrina*, *U. senticosa*, and *U. aculeata*), *Globobulimina* spp., *Planulina wuellerstorfi*, *Globocassidulina subglobosa*, and buliminids (including *B. alazanensis*, *B. striata mexicana*) dominate the assemblages. Also noted were *Pygromurrhina*, *Pullenia bulloides*, *Laticarinina pauperata*, *Melonis affine*, *Karriella bradyi*, *Sphaeroidina bulloides*, *Sigmoilopsis schlumbergeri*, *Cibicidoides mediocris*, *C. bradyi*, *Eggerella cf. E. bradyi*, *Oridorsalis* sp., *Stilostomella* sp., *Plectofrondicularia* sp., *Hoeglundina ele-*

*gans*, *Anomalinoides globulosus*, *Martinottiella* sp., *Lenticulina* sp., *Cassidulina* sp. (common in Sample 613-11, CC), and *Gyroidinoides* sp. Based upon comparisons with Recent assemblages in this region (Miller and Lohmann, 1982) and with data from van Morkhoven et al. (pers. comm., 1983), this assemblage is interpreted as representing deposition at lower bathyal depths.

The Pleistocene section at Site 613 (Cores 613-11 through 613-1) provides an interesting mixture of benthic foraminiferal assemblages. The lower portions of the section contain a *Quinqueloculina* assemblage containing *Elphidium* sp., *Bulimina aculeata*, *B. marginata*, and nonionellids. A *Uvigerina* assemblage occurs in Core 613-5 in which cassidulinids, globobuliminids, nonionellids, bolivinids, *Elphidium* spp., and *Bulimina aculeata* occur together. Core 613-4 contains a *Bolivina-Globobulimina* assemblage in which the specimens are thin and translucent. This assemblage is typical for the upper bathyal oxygen-minimum zone on the modern U.S. continental slope. Also noted in this sample are persistent *Elphidium* spp. The association of *Elphidium* spp., *Nonionella* spp., and *Quinqueloculina* spp. with the buliminids, uvigerinids, and globobuliminid-bolivinid assemblages may be interpreted as either: (1) mixtures of transported neritic specimens with upper-middle bathyal assemblages; or (2) autochthonous assemblages in which supposed shallower-water taxa (e.g., *Elphidium*) lived at greater (bathyal) depths.

#### Calcareous Nannofossils

Calcareous nannofossils at Site 613 are, with the exception of several intervals, abundant and well preserved. The samples studied for this preliminary report are from core catchers, except where closely-spaced samples were studied near some stratigraphic boundaries. Several biostratigraphic zones that have not been identified may be revealed with closer sampling. This study employs the zonation of Bukry (1973, 1975), Okada and Bukry (1980) and Gartner (1977) and the time scale of Berggren and others (Berggren et al., 1985).

#### Lower Eocene (581.90–439.25 m)

The oldest sediment recovered at Site 613 is early Eocene porcellaneous chalk that is approximately 143 m thick. A nannoflora assigned to the *Discoaster binodosus* Subzone (CP9b) is present from Samples 613-52, CC to 613-50, CC (581.90–562.90 m; Fig. 9). Species present include *Campylosphaera dela*, *Chiasmolithus californicus*, *C. grandis*, *Discoaster diastypus*, *D. multiradiatus*, *Discoasteroides kuepperi*, *Ellipsolithus macellus*, *Lophodolitus nascens*, *Neococcolithes dubius*, *Sphenolithus radians*, *Toweius eminens*, and *Tribrachiatus orthostylus*. The earliest Eocene subzone (CP9a), recognized by the presence of *Tribrachiatus contortus*, was not penetrated.

The *Tribrachiatus orthostylus* Zone (CP10) extends from Samples 613-49, CC to 613-46, CC (553.40–524.90 m). The base of this zone is placed at the first appearance of *Discoaster lodoensis*. Some of the associated species are *Campylosphaera dela*, *Chiasmolithus californicus*, *C. grandis*, *Cyclococcolithina formosa*, *Discoaster*

*diastypus*, *Discoasteroides kuepperi*, *Neococcolithes dubius*, *Sphenolithus radians*, *Toweius eminens*, and *Tribrachiatus orthostylus*.

The *Discoaster lodoensis* Zone (CP11) is present from Samples 613-45, CC to 613-40, CC (515.40–468.50 m), from the first appearance of *Coccolithus crassus* to the first appearance of *Discoaster sublodoensis*. Other species present include *Campylosphaera dela*, *Chiasmolithus consuetus*, *C. expansus*, *C. grandis*, *C. solitus*, *Chiphragmalithus calathus*, *Coccolithus eopelagicus*, *Cyclococcolithina formosa*, *Discoaster barbadiensis*, *D. lodoensis*, *Discoasteroides kuepperi*, *Helicosphaera lophota*, *Neococcolithes dubius*, *Sphenolithus radians*, and *Tribrachiatus orthostylus*.

The top of the lower Eocene sequence is represented by the *Discoasteroides kuepperi* Subzone (CP12a) from Samples 613-39-6, 51 cm to 613-37, CC (459.00–440.00 m). The base of this subzone is placed at the first appearance of *Discoaster sublodoensis*; in other aspects the nanoflora resembles that found in Zone CP11.

#### Middle Eocene (439.20–278.60 m)

Middle Eocene siliceous chalk is approximately 161 m thick. It appears to be biostratigraphically conformable with the lower Eocene, which contains far less biogenic silica. The middle Eocene is overlain disconformably by middle to upper Miocene sand.

The *Rhabdosphaera inflata* Subzone (CP12b) is present from Samples 613-37-6, 120 cm to 613-36, CC (439.20–259.50 m). *R. inflata* is restricted to this subzone and associated species include *Chiasmolithus expansus*, *C. grandis*, *C. solitus*, *Cyclococcolithina formosa*, *Discoaster barbadiensis*, *D. saipanensis*, *D. sublodoensis*, *Helicosphaera lophota*, *H. seminulum*, *Neococcolithes dubius*, and *Sphenolithus radians*. Within this interval, there is a slump of lower Eocene sediment (CP12a) about 80 cm thick from Samples 617-37-5, 142 cm to 613-37-6, 70 cm.

The overlying strata from Samples 613-34, CC to 613-31, CC (411.50–374.00 m) is assigned to the *Discoaster strictus* Subzone (CP13a). This subzone lies between the last occurrence of *Rhabdosphaera inflata* and the first appearance of *Chiasmolithus gigas*. Species present include *Campylosphaera dela*, *Chiasmolithus expansus*, *C. grandis*, *C. solitus*, *Coccolithus eopelagicus*, *C. staurion*, *Cyclococcolithina formosa*, *Discoaster barbadiensis*, *D. sublodoensis*, *Helicosphaera lophota*, *H. seminulum*, *Nannotetrina quadrata*, and *Neococcolithes dubius*.

The remaining middle Eocene strata in Hole 613 are assigned to the *Chiasmolithus gigas* Subzone (CP13b), and they extend for about 100 m from Samples 613-30, CC to 613-20, CC (374.00–278.60 m). *Chiasmolithus gigas* is restricted to CP13b, but the subzone is extraordinary thick in both Holes 612 and 613. Further study is required to confirm the age of this interval at both sites. Species present include *Campylosphaera dela*, *Chiasmolithus expansus*, *C. gigas*, *C. grandis*, *C. solitus*, *Cyclococcolithina formosa*, *Coccolithus eopelagicus*, *C. staurion*, *Discoaster barbadiensis*, *D. saipanensis*, *Helicosphaera lophota*, *H. seminulum*, *Nannotetrina quadrata*, *Neococcolithes dubius*, *Sphenolithus furcatolithoides*, and *S. radians*.

#### Middle to Upper Miocene (267.98 m)

Sample 613-19, CC contains reworked Eocene nanofossils and a sparse Neogene flora that is poorly preserved and cannot be dated accurately. Sample 613-19-6, 98 cm also contains a sparse flora. The presence of *Calcidiscus macintyreii*, *Discoaster bollii*, *D. brouweri*, *D. hamatus*, and *D. quinqueringus* suggest an age of middle to late Miocene (CN7) for this sample and perhaps also for the interval penetrated by Core 613-20, which was recovered empty except for 20 cm of middle Eocene chalk in the core catcher.

#### Lower Pliocene (260.71–231.00 m)

The interval from Samples 613-19-1, 121 cm to 613-15, CC (260.71–231.00 m) is provisionally assigned to the *Ceratolithus acutus* Subzone (CN10b)/*Ceratolithus rugosus* Subzone (CN10c) of the basal Pliocene. The *C. acutus* subzone is defined by the presence of *C. acutus*, and the base of the *C. rugosus* Subzone is at the first appearance of *C. rugosus*. Both species are present in this interval but not consistently in their normal stratigraphic sequence.

Species present include *Amaurolithus delicatus*, *A. tricorniculatus*, *Calcidiscus macintyreii*, *Ceratolithus armatus*, *C. rugosus*, *Cyclococcolithina leptopora*, *Discoaster asymmetricus*, *D. brouweri*, *D. calcaris*, *D. pentaradiatus*, *D. surculus*, *D. tridens*, *D. triradiatus*, *D. variabilis*, *Helicosphaera sellii*, *Reticulofenestra pseudoumbilica*, and *Sphenolithus neoabies*.

#### Upper Pliocene (221.50–193.60 m)

The *Discoaster tamalis* (CN12a) and the *Discoaster surculus* (CN12b) subzones are represented by the beds from Samples 613-14, CC to 613-13, CC (221.50–212.00 m). The flora in this interval includes *Calcidiscus macintyreii*, *Discoaster asymmetricus*, *D. brouweri*, *D. pentaradiatus*, *D. surculus*, *D. triradiatus*, *Cyclococcolithina leptopora*, and *Helicosphaera sellii*. Sample 613-11, CC (193.60 m) is provisionally assigned to the *Calcidiscus macintyreii* Subzone (CN12d) and contains only *Discoaster brouweri* among the discoasters.

#### Pleistocene (183.95–0.00 m)

Sample 613-11-1, 5 cm (183.95 m) and a 29-m wash Core 613-10, CC (182.90–154.10 m) recovered sediment that contains rare nanofossils including small *Gephyrocapsa* species. This interval is provisionally assigned an age of early Pleistocene.

The beds from Samples 613-9, CC to 613-2, CC (154.10–29.40 m) contain a flora that includes *Crenalithus doronicoides*, *C. productellus*, *Cyclococcolithina leptopora*, *Gephyrocapsa oceanica*, small *Gephyrocapsa* spp., *Helicosphaera carteri*, *Pseudoemiliana lacunosa*, and *P. ovata*. These species and the absence of *Calcidiscus macintyreii* and *Helicosphaera sellii* are the basis for assigning these beds to the combined small *Gephyrocapsa* Zone–*Pseudoemiliana lacunosa* Zone of middle to late Pleistocene age.

Core 613-1 is a wash core from the seafloor to 19.80 m. It contains a flora similar to the underlying interval ex-

cept that *Pseudoemiliana lacunosa* and *P. ovata* are absent. This interval is assigned to the combined *Ceratolithus cristatus* Subzone (CN14b)–*Emiliana huxleyi* Zone (CN15) of the upper Pleistocene.

### Radiolarians

Radiolarians at Site 613 were studied from core catchers of both rotary and wash cores. Radiolarians are diverse and well preserved only in the middle Eocene section at this site. The lower Eocene section contains only poorly preserved radiolarians. The Neogene interval has few or no Neogene radiolarians, but reworked middle Eocene specimens are frequent.

Zones assigned in this study are those of Riedel and Sanfilippo (1978); absolute age estimates are from Berggren et al., (1985).

#### Lower Eocene

The lower Eocene *Bekoma bidartensis* Zone was recognized in Samples 613-52, CC through 613-50, CC (581.9–562.9 m) based on the occurrence of *Buryella tetradica*. Radiolarians are very poorly preserved in this interval, making recognition of species difficult.

No diagnostic taxa could be identified in Samples 613-49, CC and 613-48, CC (553.4–543.9 m) because of poor silica preservation. However, in Samples 613-47, CC and 613-46, CC (534.4–524.9 m) the presence of *Phormocyrtis striata exquisita* suggests the *Buryella clinata* Zone.

Poor silica preservation hindered recognition of diagnostic species in Samples 613-45, CC and 613-44, CC (515.4–505.9 m). The presence of *Phormocyrtis striata striata* without *Dictyoprora mongolfieri* in Sample 613-43, CC (496.4 m) through Sample 613-38, CC (449.5 m) suggests the *Phormocyrtis striata striata* or *Theocotyle cryptocephala* zone, although radiolarians in Samples 613-42, CC through 613-40, CC (487.1–458.5 m) are too poorly preserved to yield biostratigraphic information.

#### Middle Eocene

Abundant, diverse, and well preserved middle Eocene radiolarians first appear in Sample 613-37, CC (440.0 m). Species found in this interval include *Dictyoprora urceolus*, *D. amphora*, *Lithocyclus ocellus*, *Lithapium anoectum*, *Lophocyrtis biaurita*, *Lamptonium obelix*, *Lithochytris vespertilio*, *Ceratospyrus articulata*, *Phormocyrtis striata striata*, *Podocyrtis sinuosa*, *Thyrsocyrtis tensa*, *Thyrsocyrtis triacantha*, *Thyrsocyrtis hirsuta*, *Periphaena tripyramis triangula*, *Periphaena tripyramis tripyramis*, *Theocotylissa ficus*, *Podocyrtis dorus*, *Podocyrtis diamesa*, and *Dictyophimus craticula*. The section is further subdivided into several zones.

A well preserved *Theocotyle cryptocephala* Zone assemblage occurs in Samples 613-37, CC through 613-35, CC (440.0 to 421.0 m), below the first occurrence of *Dictyoprora mongolfieri*. This zone contains the lower/middle Eocene boundary according to Berggren et al. (1985).

Samples 613-34, CC through 613-32, CC (411.5–392.7 m) are assigned to the *Dictyoprora mongolfieri* Zone based on the presence of *Dictyoprora mongolfieri* but not *Eusyringium lagena*.

The *Thyrsocyrtis triacantha* Zone was recognized in Samples 613-33, CC through 613-20, CC (383.3–278.6 m). The base of the zone was placed at the first morphologic appearance of *Eusyringium lagena*. The top part of this zone is evidently not present since neither the first morphologic appearance of *Eusyringium fistuligerum* nor the last appearance of *Podocyrtis diamesa* or *Podocyrtis dorus* are observed in this interval.

#### Neogene

Radiolarians are not abundant in the Neogene of Site 613. Sample 613-19, CC (269.0 m) is barren of radiolarians, and Sample 613-18, CC (259.5 m) contains only reworked Eocene radiolarians. Samples 613-17, CC and 613-16, CC (250.0–240.5 m) are tentatively assigned to the upper Miocene to lower Pliocene *Stichocorys peregrina* Zone, based on the presence of *Stichocorys peregrina*. Frequent reworked middle Eocene and early to middle Miocene radiolarians were also observed in this interval.

These results suggest that between Samples 613-20, CC and 613-17, CC there is a biostratigraphic gap of approximately 32 m.y. (from below the top of the *Thyrsocyrtis triacantha* Zone at 48.6 Ma to the bottom of the *Stichocorys peregrina* Zone at 6.2 Ma).

Few or no radiolarians were found in Samples 613-15, CC through 613-1, CC (231.0–19.8 m). The only age-diagnostic assemblages are found in Sample 613-11, CC (193.6 m) (assigned to the Pliocene–Pleistocene based on the occurrence of *Pseudocubus* sp.) and Sample 613-5, CC (115.8 m) (assigned to the Pleistocene based on the occurrence of *Theocalyptra davisiana*). The *T. davisiana*-dominated assemblage in Sample 613-5, CC is similar to that described from Sample 612-4, CC at Site 612. These occurrences suggest that a regional horizon of *T. davisiana* blooms may exist in the area, possibly associated with a Pleistocene climatic change (*T. davisiana* has been linked with glacial events by Morely and Hays, 1979).

Most of the Neogene assemblage consists of biostratigraphically nondiagnostic taxa, including litheliids, porodiscids, actinommids, spongodiscids, and dictyocorynids. The deep-dwelling taxa *Cornutella*, *Peripyramis*, and *Bathropyramis* occur consistently, indicating that bathyal to abyssal paleodepths prevailed during the Neogene at Site 613.

### SEDIMENTATION RATES AND SUBSIDENCE HISTORY

The sedimentation rates for Hole 613 have been calculated on the basis of the detailed faunal and floral examination of core catcher samples (see sections on foraminiferal, nannofossil, and radiolarian biostratigraphy). Using the Cenozoic time scale of Berggren et al. (1985) and the Cretaceous time scale of van Hinte (1976), age-depth plots have been constructed for the foraminiferal, nannofossil, and radiolarian data (Figs. 10–12). These three plots are similar in most respects, but they are presented separately here, pending further shore-based study.

The duration of the longest hiatus (middle Eocene/Miocene contact) is similar in all three figures (ca. 35 m.y.), although dating of the thin Miocene section is tentative.

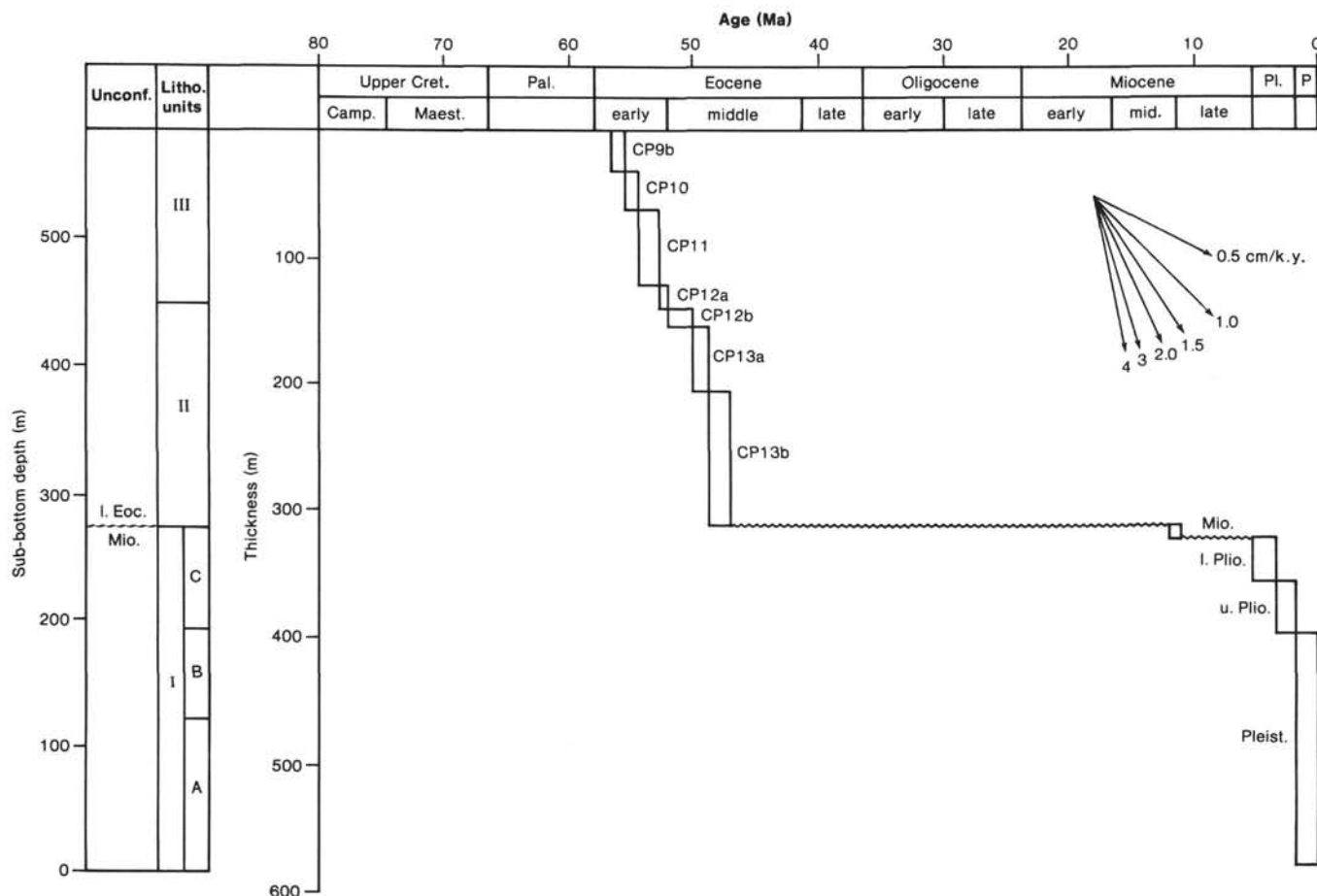


Figure 10. Sediment accumulation rates at Site 613 based on nannofossil biostratigraphy.

Eocene sedimentation rates are estimated to be about 5.5 cm/k.y. (55 m/m.y.). Middle Eocene rates are slightly lower, approximately 3.0 cm/k.y. (30 m/m.y.) to 3.5 cm/k.y. (35 m/m.y.).

Miocene sedimentation rates cannot be reliably estimated. The lower Pliocene sedimentation rate was ca. 3.0 cm/k.y. (30 m/m.y.), but decreased in the upper Pliocene to ~1.2 cm/k.y. (12 m/m.y.). This estimate is tentative because of problems identifying precisely the Pliocene/Pleistocene boundary. The sedimentation rate in the Pleistocene appears to have been about 11 cm/k.y. (109 m/m.y.), by far the highest rate of the cored section.

The sedimentation rates for Hole 613 were analyzed using the "backstripping" technique described in the Site 612 report (see Sedimentation Rates and Subsidence History). To correct for the effect of compaction we used shipboard measurements of sonic velocity to determine the variation of porosity with depth (see Physical Properties) and a constant grain density of 2.65 g/cm<sup>3</sup>. Shipboard measurements of grain density were not used because they were unavailable at the time of preparing this report. The use of a different grain density should not, however, significantly affect the results. A long-term sea-level curve was used to compute the effect of water loading, similar to that used at Hole 612.

Figure 13 shows the sedimentation rate ( $S$ ) and the depth of the basement through time corrected for sediment and water loading ( $Y'$ ). As in the case at Hole 612, the area between the two curves represents that part of the sedimentation rate curve caused by sediment and water loading, while the region above the curve, labeled  $Y'$ , compared to  $S$ , shows that backstripping successfully accounts for variations in sedimentation rates due to compaction, variable sediment supply, and local sea-floor processes. This is particularly noticeable for the Pleistocene at Site 613, which is associated with average sedimentation rates of 11 cm/k.y. Backstripping reduces their rates to a smooth curve of average slope 0.4 to 0.7 cm/k.y., similar to that expected from thermal compaction of the lithosphere. Thus, the high sedimentation rates that are observed during the Pleistocene are most probably the result of little compaction.

Like Site 612, Site 613 is probably located on oceanic crust. A comparison of the predicted thermal subsidence at Site 612 with  $Y'$  at Site 613 shows there is good general agreement between predicted and observed curves.

Backstripping suggests that thermal compaction of the lithosphere following rifting is an important factor contributing to the subsidence history at Site 612. In general, sedimentation rates exceeded subsidence rates due to thermal compaction, suggesting that sedimentary sup-

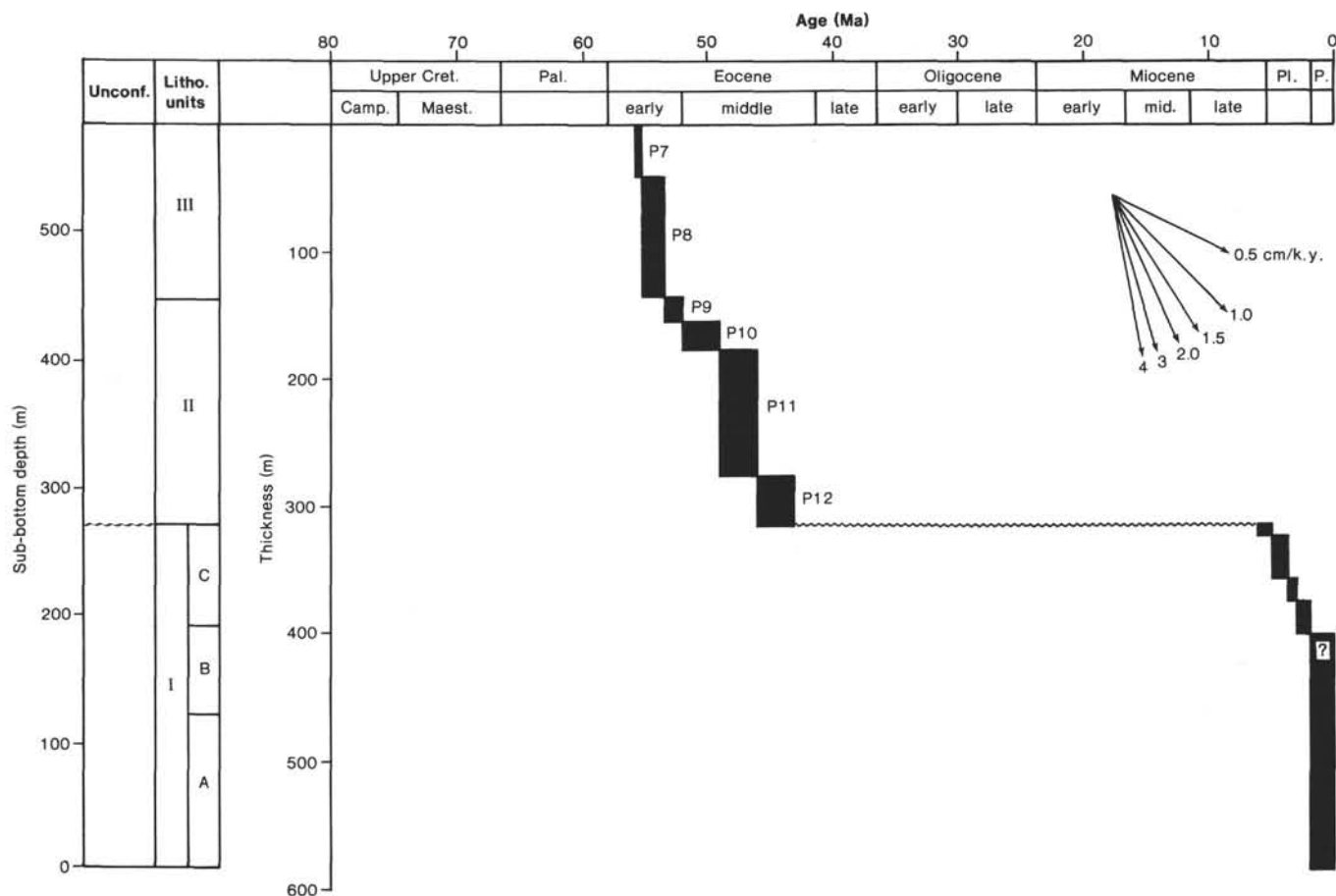


Figure 11. Sediment accumulation rates at Site 613 based on foraminiferal biostratigraphy.

ply was sufficient to keep up with subsidence. The differences between sedimentation and subsidence rates were greatest during the lower to middle Eocene and Pliocene to Pleistocene. The Pliocene to Pleistocene, however, is poorly compacted and appears to be unusually thick at Site 613. In contrast, the lower to middle Eocene is more fully compacted, suggesting that sedimentation rates during the lower to middle Eocene actually greatly exceeded those that are estimated today. The large differences between sedimentation and subsidence rates at Site 613 (Fig. 13) imply significant upbuilding and/or outbuilding of the margin during the lower to middle Eocene. Apparently, this growth of the margin during the lower to middle Eocene was accompanied by significant mass movement of material downslope (see Lithology).

#### INORGANIC GEOCHEMISTRY

Interstitial water was squeezed from 11 Site 613 sediment samples spaced approximately every 50 m down-core. Samples were analyzed for pH, salinity, alkalinity, chlorinity, calcium, and magnesium using the same methods as Site 612. Sulfate concentrations were also measured at Site 613 using the shipboard Wescan dual channel ion analyzer.

The results are listed in Table 2 and shown graphically in Figure 14. Chlorinity (14D) and salinity (14C) values recorded at Site 613 are much smaller than values recorded at Site 612 and are very similar to values recorded

for surface seawater. Salinity and chlorinity are fairly constant throughout Hole 613 except for a slight increase in salinity (33.8‰) at 342 m BSF (Core 613-27).

Sulfate concentrations (Fig. 14G) above 292 m BSF are depleted relative to surface seawater. The observed sulfate depletion and increase in alkalinity between 152.05 and 243.45 m BSF may be due to the presence of sulfate-reducing microorganisms.

Calcium (Fig. 14E) depletion relative to surface seawater occurs about 243.4 m BSF (Core 613-17). Magnesium (Fig. 14F) is also depleted relative to surface seawater throughout Hole 613.

Figure 15 is a plot of  $-\Delta\text{Mg}$  and  $\Delta\text{Ca}$  as described for Site 612. Unlike Site 612, there is a good linear correlation (gradient = 1) between  $-\Delta\text{Mg}$  and  $\Delta\text{Ca}$  below 292 m sub-bottom depth at Site 613, implying that calcium-magnesium reactions control the observed concentrations. Calcium-magnesium substitutions are commonly observed in calcareous and calcareous-siliceous sediments having sedimentation rates of a few cm/k.y. (Sayles and Manheim, 1975), such as those at Site 613 (see Sedimentation Rates and Subsidence History). Depletion of magnesium above 243 m BSF may be attributed to the formation of a magnesium-containing mineral, such as glauconite, which is abundant in these cores. pH (Fig. 14A) values are slightly basic ( $>7.0$ ) throughout Hole 613 except for 342.15 m BSF (Core 613-27), which coincides with a slight salinity maximum.

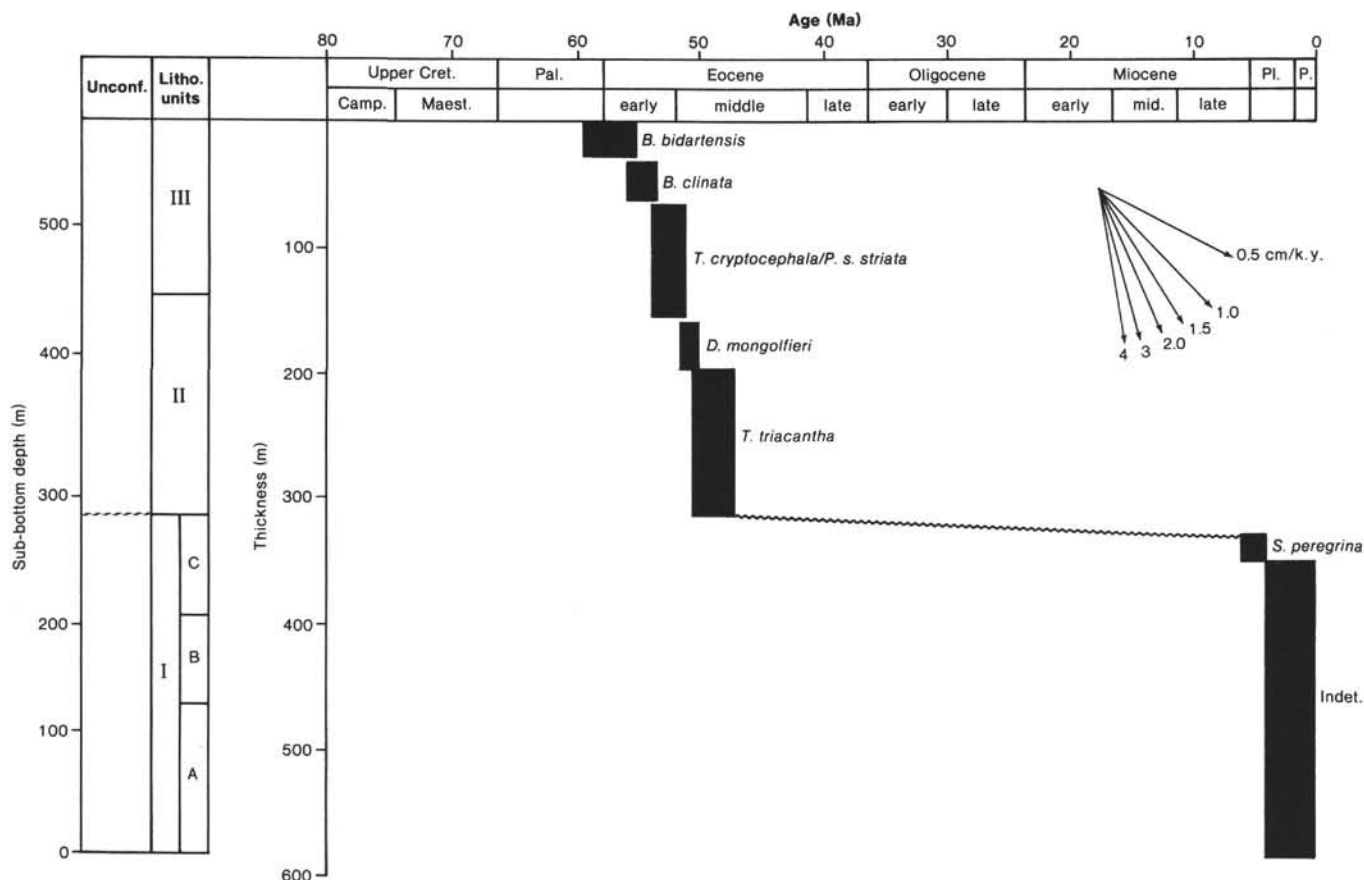


Figure 12. Sediment accumulation rates at Site 613 based on radiolarian biostratigraphy.

## ORGANIC GEOCHEMISTRY

Cores collected at Site 613 were monitored for gas, as is customary to observe the DSDP safety precautions. Most of the gases encountered in DSDP sediments are microbiological in origin (see, for example, DSDP Leg 44, the Black Sea; and DSDP Legs 56 and 57, the Japan Trench). In addition, shipboard monitoring of core gas at Site 613 provides useful information for shore-based studies of microbiological gas formation in sediments collected on Leg 95 (see Tarafa et al., this volume).

Visual evidence of gas (minor bubbling of the cores) was found in 12 of the cores recovered at Site 613. The cores were maintained at room temperature in the core lab for 1–2 hr., after which the caps of the core liners bulged slightly. Gas was collected at gas cracks (observed through the core liner) using a stopcock on/off valve equipped with a needle capable of perforating the core liner. A hypodermic needle was fitted on the sampler, allowing the gas to fill pre-evacuated Vacutainer tubes (Beckton Dickenson Corp., Rutherford, NJ).

Gas was present in Cores 613-2 (22.33 m BSF) and 613-5 through 613-19 (68.83–263.09 m BSF). Gas was not present in Cores 613-1, 613-3, and 613-4, possibly because of loss due to poor core recovery (a total of only 5.19 m was recovered from these cores). Cores 613-5W (67.8–115.8 m) and 613-10W (115.8–182.9 m) are wash cores.

Gas concentrations were monitored within several minutes after collection. Methane and CO<sub>2</sub> were measured using a Carle 8000 gas chromatograph equipped with a thermal conductivity detector. Helium was used as the carrier gas. Gas samples (0.2 ml) were directly injected into a column (QS, 1.5 m × 3.1 mm OD) heated to 50°C. Quantitative determination was carried out using the external standard method. Response factors and retention times were calculated using a Matheson Gas Standard (methane, 1000 ppm; ethane, 1000 ppm).

Ethane, propane, isobutane and *n*-butane were measured using a Hewlett Packard 5711A gas chromatograph equipped with a dual flame ionization detector. Details of this procedure have been previously described for other DSDP sites (see, e.g., Whelan, 1979.) Scotty Calibration Gas Mixture #1 (gas concentrations of C<sub>1</sub>–C<sub>6</sub> normal alkanes approximately 10–12 ppm) was used to calculate response factors and retention times. A large “blank” was present in the C<sub>5+</sub> region of the chromatogram due to contamination from the *n*-butyl rubber stoppers of the Vacutainers. Compounds which evolve in this area (i.e., pentanes, hexanes) of the chromatogram were not recorded. Small blank levels of ethane, propane, and isobutane were subtracted from the results.

Figure 16 shows concentration vs. depth in core for the gases monitored at Site 613. Figure 16A is a plot of methane concentration. Sample 613-5W-1, 103 cm (~119.7 m BSF) had the highest methane concentration observed

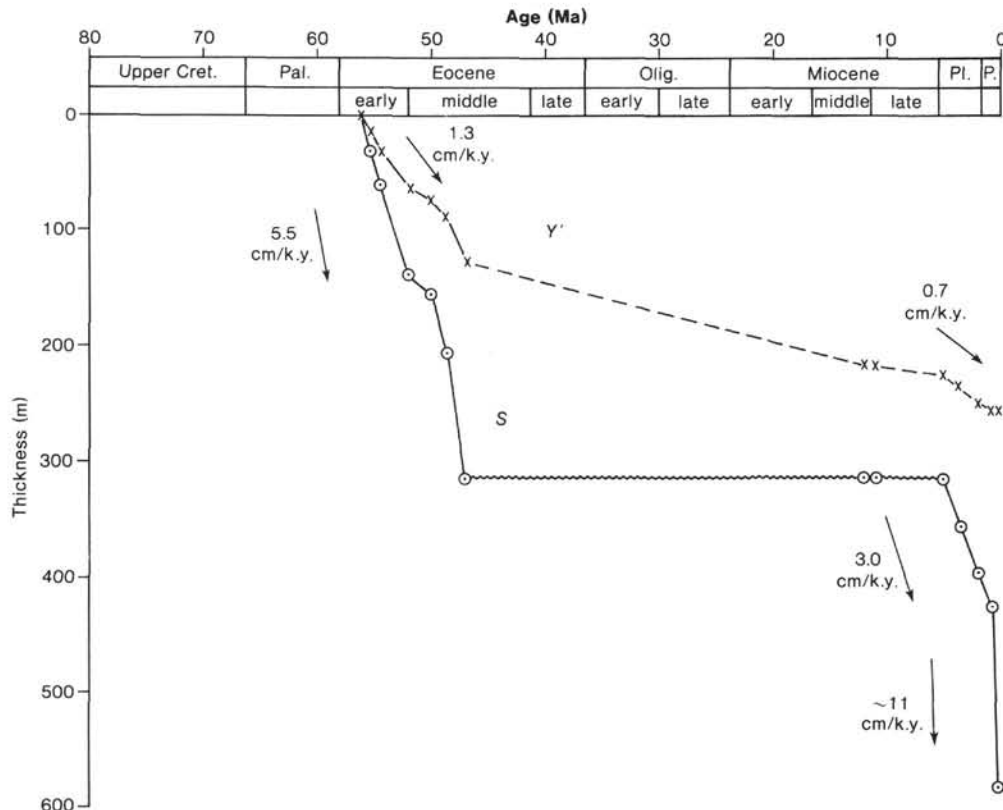


Figure 13. Sedimentation rate *S* and tectonic subsidence *Y'* at Site 613.

Table 2. Summary of shipboard inorganic geochemical data.

Core-Section (interval in cm)	Sub-bottom depth (m)	pH	Alkalinity (mEq/l)	Salinity (‰)	Calcium (mM)	Magnesium (mM)	Chlorinity (‰)	Sulfate (mM)
Surface seawater		8.23	2.32	33.8	10.37	52.39	18.75	29.1
4X-2,140	61.10	7.74	9.17	33.0	6.54	42.28	18.67	12.2
6X-5,145	123.45	7.77	7.17	31.9	6.48	32.20	19.37	1.7
9X-5,145	152.05	7.59	5.14	32.0	7.27	34.49	19.44	4.9
12X-3,145	197.05	7.66	10.20	32.0	9.97	32.35	19.24	4.3
17X-2,145	243.45	7.43	15.27	32.2	8.67	36.71	19.11	2.0
22X-3,145	292.65	7.08	10.20	32.5	10.45	37.22	19.17	8.4
27X-3,145	342.15	6.83	9.46	33.8	15.57	33.07	19.21	10.21
32X-4,145	389.25	7.04	7.82	33.0	18.64	33.32	19.27	12.2
37X-4,145	436.45	7.38	6.60	32.2	20.10	32.52	18.97	12.4
43X-3,145	491.55	NES <sup>a</sup>	NES	32.0	26.01	25.90	18.84	12.2
50X-4,145	559.35	NES	NES	32.2	22.48	26.58	NES	12.8

<sup>a</sup> NES = Not enough sample.

at this site ( $7.5 \times 10^5$  ppm). Methane minima at this site occur between 127.1 and 154.1 m and between 234.98 and 236.2 m BSF. Methane concentrations, which range between 0 and 1950 ppm and 1440 and 7500 ppm, respectively, at these minima, coincide with the presence of glauconitic sand (Cores 613-7, 125.7–135.1 m; 613-8, 135.1–144.6 m; and 613-10, 154.1–182.9 m) and possible slump deposits (Cores 613-7, 125.7–135.1 m; 613-9, 144.6–154.1 m; and 613-10, 154.1–182.9 m). There is an increase in porosity according to the sonic logs between 127 and 154 m BSF, suggesting possible diffusion of methane generated *in situ* out of these coarser-grained sediments. Below Core 613-5, methane concentration decreases almost linearly with depth, if low values (less than 1000 ppm) are ignored.

Figure 16B is a plot of ethane concentration with depth. Values range between 0 (Cores 613-16 and 613-19) and 480 ppm (Core 613-2), which is a point off-scale on the figure. Most of the values greater than zero are between 5 and 15 ppm. Ethane decreases slightly with depth and correlates well with the methane profile. Ethane values are several orders of magnitude lower than methane values, resulting in the very small  $C_2/C_1$  ratios shown graphically in Figure 16F.  $C_2/C_1$  values range from 0 (Cores 613-16 and 613-19) to  $1.13 \times 10^{-3}$  (Core 613-2). Most of the values greater than zero fall between  $2 \times 10^{-5}$  and  $5 \times 10^{-5}$ .  $C_2/C_1$  values are all well below  $2 \times 10^{-2}$ , which is the DSDP safety standard.  $C_2/C_1$  ratios greater than  $2 \times 10^{-2}$  indicate a possible hazard to the drilling operation.

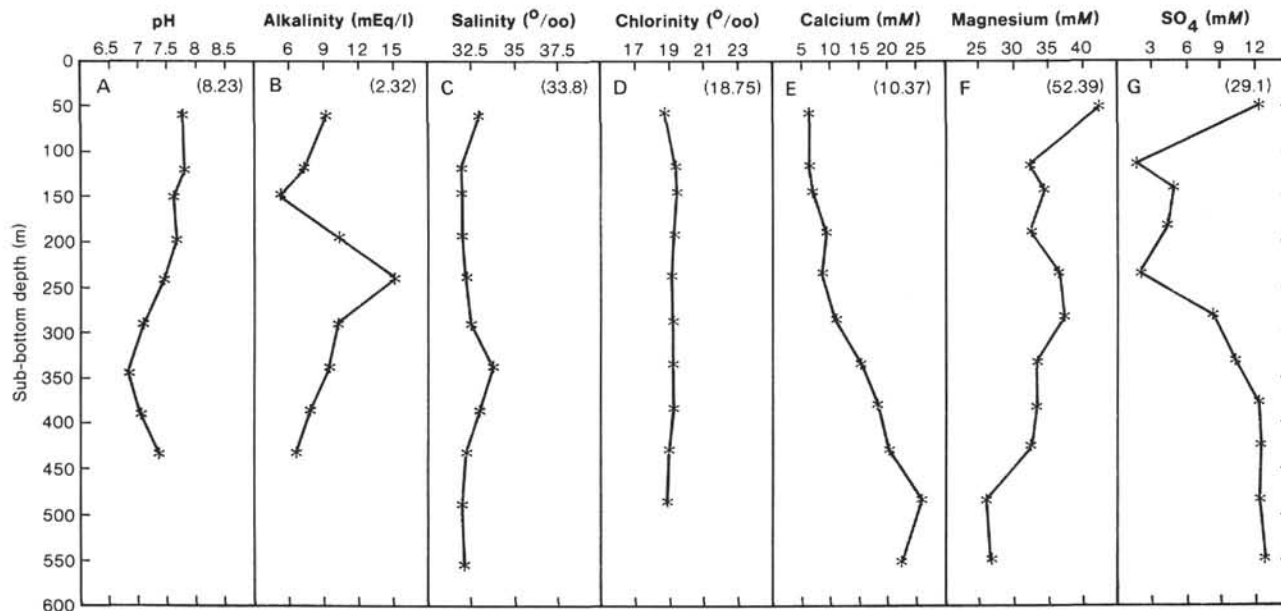


Figure 14. Interstitial pore water profiles for Hole 613. Values in parentheses on the figures are surface seawater concentrations.

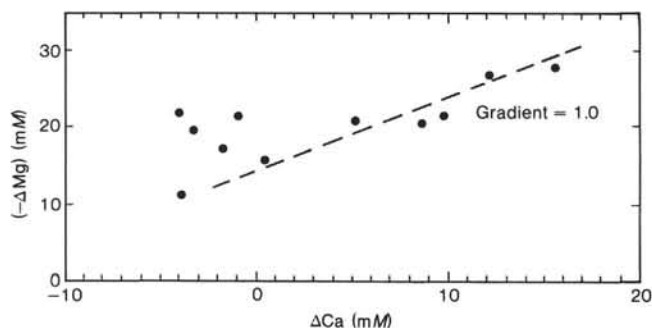


Figure 15. Plot of  $-\Delta\text{Mg}$  and  $\Delta\text{Ca}$  for Hole 613. ( $-\Delta\text{Mg}$  = Mg concentration in pore water - Mg concentration in surface seawater;  $\Delta\text{Ca}$  = Ca concentration in pore water - Ca concentration in seawater).  $-\Delta\text{Mg}$  reflects negative values due to Mg depletion.

Trace concentrations (5 ppm) of propane and isobutane were observed at Site 613, except for Section 613-2-2, in which propane and isobutane values were 260 and 29 ppm, respectively (Fig. 16C, D).

Figure 16E is a plot of carbon dioxide ( $\text{CO}_2$ ) concentration with depth for Site 613. Values range from 0 (Section 613-8-4, top) to  $5.4 \times 10^3$  ppm (Section 613-8-6, top). A plot of carbon dioxide concentration follows the methane and ethane profiles except for samples from Core 613-8 (142.6 m) and Core 613-9 (144.7 m), whose values are high and are marked by an absence of methane. It is possible that methanogenic bacteria capable of utilizing the available  $\text{CO}_2$  may not have been present at these two particular intervals.

The high levels of methane, low  $\text{C}_2/\text{C}_1$  ratio, and relatively small amounts of ethane, propane, and isobutane observed at Site 613, are typical of DSDP sediments in which a biological, rather than a petrogenic, source is responsible for gas production. Carbon-isotope studies on core gas samples indicate that the methane gas at Site 613 is microbiological (see Whiticar and Faber, this vol-

ume). There is also a strong correlation between ethane, propane, and isobutane, which supports the hypothesis that these compounds are being produced *in situ* rather than migrating from a deeper source (see, e.g., DSDP Leg 64, Site 479).

Section 613-2X-2 contains the highest levels of ethane, propane, and isobutane observed at this site. Section 613-2-2 also has the largest  $\text{C}_2/\text{C}_1$  ratio ( $1.13 \times 10^{-3}$ ), but this ratio is also below the DSDP safety standard ( $2 \times 10^{-2}$ ). In addition to these compounds, Section 613-2-2 also contains 12.4 ppm of neopentane, a gem-dimethyl compound. As observed in DSDP Legs 56 and 57, this compound probably has a microbiological origin, since it is rarely observed in petroleum.

Experiments were set up on board ship to measure the microbiological activity of these sediments. Sediment samples were collected from Cores 613-2, 613-4, 613-5, 613-6, 613-7, and 613-8 and incubated in the absence of oxygen with radiolabeled bacterial substrates. Radiolabeled methylamine ( $^{14}\text{CH}_3\text{NH}_3$ ), acetate ( $^{14}\text{CH}_3\text{COO}^-$ ) and  $^{35}\text{S}$ -labeled sulfate ( $^{35}\text{SO}_4^{2-}$ ) were added in known concentrations to sediments sealed in oxygen-free vials. Samples were incubated on board ship, allowing for a "time course" incubation in which bacteriogenic gases could be measured at 0, 3.5, and 7.5 days or 0, 4, and 8 days.  $^{14}\text{C}$ -labeled methane ( $^{14}\text{CH}_4$ ), carbon dioxide ( $^{14}\text{CO}_2\text{LS}$ ), and hydrogen sulfide ( $\text{H}^{35}\text{S}$ ) were measured using liquid scintillation techniques at shore-based laboratories.

Experimental details and results of this study are presented and discussed elsewhere (Tarafa et al. this volume). It should be noted here, however, that there is strong evidence in Cores 613-2, 613-4, 613-5, and 613-7 for anaerobic microbial oxidation of acetate to carbon dioxide. This is evident from significant amounts of radiolabeled  $^{14}\text{CO}_2$  generated in sediments from these cores incubated with  $^{14}\text{C}$ -acetate. Carbon dioxide can be sub-

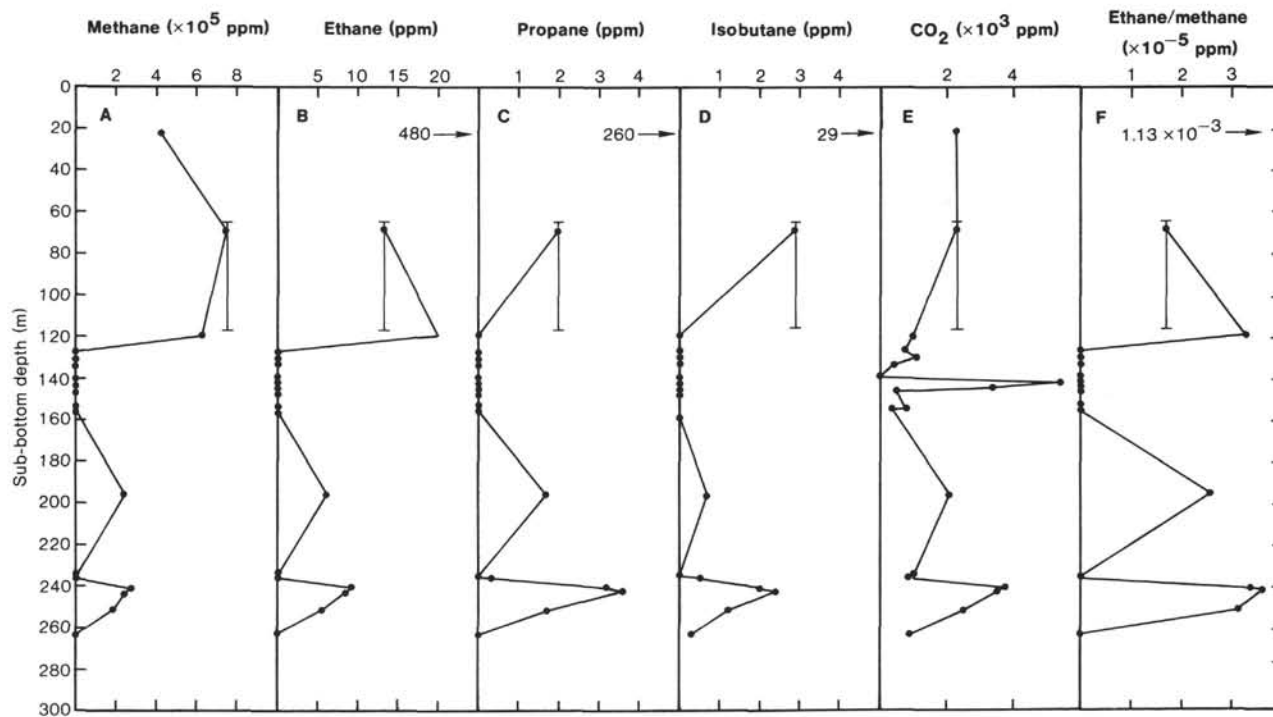
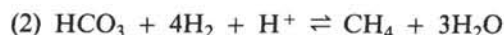


Figure 16. Core gas profiles vs. depth (m) for Hole 613. Vertical bar is for Sample 613-5W-1, 103 cm. Core 5W is a wash core.

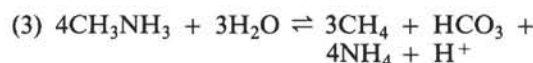
sequently converted to methane by methanogenic bacteria as in the reactions:



Acetate levels in Site 613 samples were smaller than at other DSDP sites studied (Leg 96, Sites 618 and 619), but were large enough to support bacterial populations. None of the radiolabeled incubations showed significant production of  $^{14}\text{C}$ -labeled methane from acetate. The short incubation times used in these experiments may not have allowed for microbial reduction of  $\text{CO}_2$  to methane.

The highest levels of  $^{14}\text{CO}_2$  production from acetate by microorganisms in sediment incubations were observed in samples from Cores 613-2, 613-4, and 613-7. Cores 613-5 and 613-6 also showed significant activities. Methane was found in the core gas of all of these cores except for Core 613-4, which was incompletely recovered, and gas could have been lost. Core 613-8 showed the smallest  $^{14}\text{CO}_2$  activity of any of the microbiological experiments for Site 613, although the highest levels of *in situ*  $\text{CO}_2$  gas were found in this core. Activity levels ( $^{14}\text{CO}_2$ ) for sediment samples from Core 613-8 were lower after 7.5 days of incubation than after 3.5 days of incubation, perhaps because of experimental error. No traces of methane were found in Core 613-8.

$^{14}\text{C}$ -methane production from radiolabeled methylamine was not significant in the Site 613 microbiological experiments. Microbes utilize methylamine as a methane precursor according to the reaction:



Methylamine may not be an important bacterial substrate in Site 613 sediments. Methylamine concentrations in these cores are reported elsewhere.

Interstitial pore-water sulfate levels (Fig. 14G) between 123.5 m BSF (Section 613-6-5) and 342.2 m BSF (Section 613-27-3) are lower than at the shallowest depth (sample at 61.1 m BSF). This downward decrease in sulfate levels could be the result of microorganisms utilizing available sulfate. Sulfate-reducing acetate-utilizing microorganisms can reduce sulfate according to the reaction:

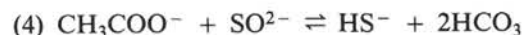


Figure 14B is a plot of interstitial water alkalinity. Above 152 m BSF, alkalinity and sulfate levels both decrease with depth. The most significant feature of this profile is an almost linear increase in alkalinity at 152 m (Core 613-7) and 243 m BSF (Core 613-17). Sulfate levels (Fig. 14G) increase slightly at the beginning of this interval and then decrease. The alkalinity maximum is at 243 m BSF which is also the interstitial pore water sulfate minimum. Below 243 m, alkalinity decreases and sulfate levels increase.

The relationship between alkalinity and sulfate could be explained by Eq. 4, wherein  $\text{HCO}_3^-$  would produce the observed increases in alkalinity. The presence of sulfate-reducing, acetate-utilizing microorganisms between 152 and 243 m BSF could account for the observed alkalinity and sulfate profiles.

Minor sulfate reduction activities in the form of  $H^{35}S$  were found in sediments when incubated with  $^{35}S$ -labeled sulfate. This activity ( $H_2^{35}S$ ) was found in Cores 613-5 (68–116 m), 613-6 (120 m) and 613-8 (140 m) only. However, if iron is available in these cores,  $^{35}S$  may have been incorporated into pyrite and not detected by the methods used in this study (Howarth and Jørgensen, in press).

Geochemical parameters observed at Site 613 can be summarized as follows:

1. Methane concentrations are highest near the surface (22–119 m BSF) and show a minimum between 127 and 155 m BSF. These sudden changes in concentration could be attributed to changes in lithology and porosity of the sediments as indicated by the presence of glauconitic sands, slumps, and changes in the geophysical logs.

2. A decrease in interstitial pore water sulfate and an increase in alkalinity suggests that sulfate reduction may be occurring between 123 and 243 m BSF.

3. Small  $C_2/C_1$  ratios, good correlation between  $C_2-C_4$  compounds and the presence of neopentane in Core 613-2 indicate that the gas in Site 613 cores was formed *in situ* by microorganisms. Evidence for microbiological methane production is provided by carbon-isotope measurements, as determined by Whiticar and Faber (this volume).

4. Preliminary data from microbiological experiments indicate that acetate metabolism by microbes may be the principal source of gas generation in these sediments. Acetate levels are sufficient to sustain microbiological growth in these sediments.

### PHYSICAL PROPERTIES

During drilling at Site 613, measurements of sediment samples were made in the laboratory to determine wet-bulk density, porosity, water content, grain density, and sonic velocity. The procedures used were those of Boyce (1976). The results are plotted versus depth below the seafloor in Figure 17A–E and summarized in relation to the lithostratigraphy in Table 3 (see also Site 613 Superlog in back pocket). Tables 4 and 5 contain complete listings of the data. Because of degassing of the samples from Unit I, sonic velocity measurements were not reliable and have not been recorded.

The sediments at Site 613 have much in common with the upper three lithostratigraphic units described at Site 612 (see Site 612 chapter, this volume). There is variation in the sediment character on a scale of centimeters which cannot be adequately described by the sampling interval (on the order of meters) that is depicted in Figure 17. However, trends in the data are observed and ranges in property values (Table 3) can be used to distinguish the various lithostratigraphic units. Some measure of the small-scale variation can be seen in the geophysical well logs. A comparison of well log and laboratory measurements is presented in Goldberg et al. (this volume).

In terms of physical properties, the major division of the sedimentary column is between the upper unlithified units (I and II) and the lower lithified Unit III. Density and velocity increase across the lithification boundary whereas porosity decreases. The variation within Units I and II is mainly a result of composition and sediment

structure. Unit I grain densities are uniformly high, reflecting the relatively minor component of biogenic silica ( $= 2.2\text{--}2.4 \text{ g/cm}^3$ ). The absence of a large component of either siliceous or calcareous microfossil tests also contributes to the generally lower porosity values seen in Unit I. In the unlithified sections the presence of microfossil tests helps to keep the sediment framework open and the porosity high, as seen in Unit II.

Sonic velocity values in Unit II are relatively uniform and show small variations, which are roughly associated with density variations. In general, the velocity behavior is consistent with typical behavior of marine chalks, and the low absolute values suggest that the sediment is very poorly consolidated.

The Unit II/Unit III boundary marks the transition from unlithified to lithified sediments and is seen in both density and sonic velocity values. Across the boundary, the siliceous tests in the sediment have been dissolved, thus removing one component of structure that would maintain open pores. In addition, some of the dissolved silica has precipitated in the form of lepispheres inside other pores created by calcareous tests. This diagenesis results in a large reduction in sediment porosity and a concomitant increase in bulk density. Grain density values also increase slightly because of the presence of silica as a somewhat denser phase in the lithified section.

### DOWNHOLE LOGGING

#### Introduction

Downhole logs produced by Schlumberger at Site 613 included induction, sonic traveltime and waveform, gamma ray, and caliper measurements (Fig. 18). The measurements made by these logging tools is discussed briefly in the Site 612 Downhole Logging section.

Logging at Site 613 was carried out from 116 to 582 m BSF. Correlations between the formation responses recorded by the logging measurements and the lithostratigraphic units described from the recovered core are generally good. These correlations promote accurate interpretations of seismic sequences and the sedimentary history of this continental margin.

#### Log/Lithologic Correlation

The spiky gamma ray response in Unit IB from 120 to 147 m BSF may be due to effects of variable compaction in high porosity oozes. A distinctive increase in gamma ray response takes place at 147 m within Unit IB and values remain relatively high to 269 m BSF, or throughout most of Unit IC. This increase corresponds to the occurrence of glauconite in the core. Several sharp increases in gamma ray response in Unit IC are probably due to expanded radioactive clays that constrict the borehole (note decrease in caliper log). The disappearance of glauconite in Units II and III corresponds to a low and slightly varying gamma ray response, except for an increase just above Unit IIIA. A sharp peak in the gamma ray log at 403 m correlates with an ash layer recognized in the core.

The resistivity log response in Unit IB is variable in the porous oozes to 147 m BSF, where an increase in resistivity correlates with the occurrence of glauconite and

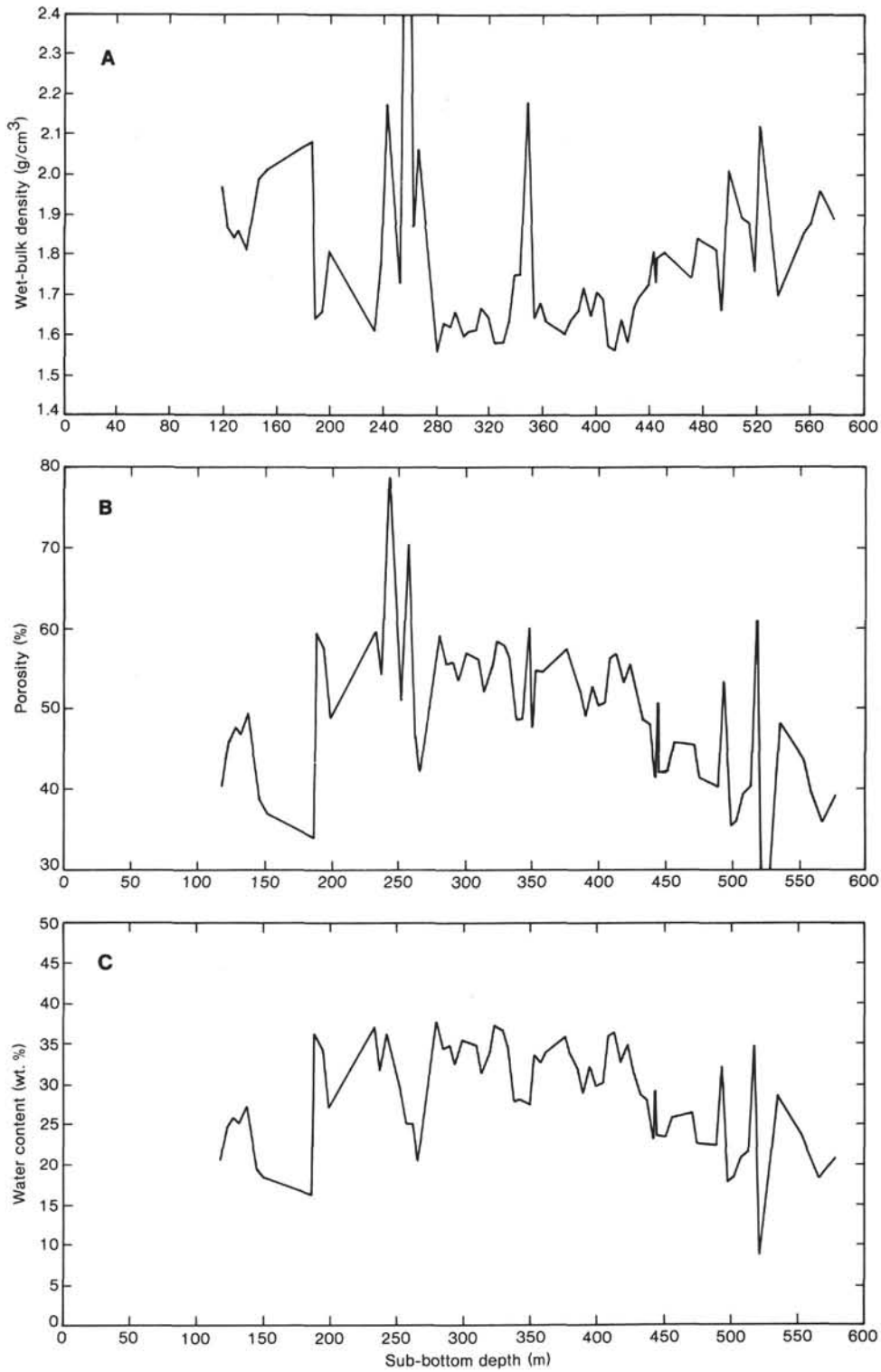


Figure 17. Physical properties values for Hole 613. (Dashed line, horizontal; solid line, vertical.)

remains constant to the Unit IB/IC boundary at 187 m. At this depth, a decrease in resistivity is expected because of the slight increase in porosity, but the competing effects of increased silica and carbonate (see Lithology, this chapter) seem to dramatically decrease the resistivity to about 200 m BSF. The resistivity response increases slowly to 582 m BSF, showing only slight vari-

ations across the other lithostratigraphic boundaries. Separation between the shallow and deep investigation resistivity tools increases at a constant rate throughout the logged interval indicating increasing mud invasion and permeability.

The upper portion of Unit IB shows spiky sonic traveltimes corresponding to nearly the compressional ve-

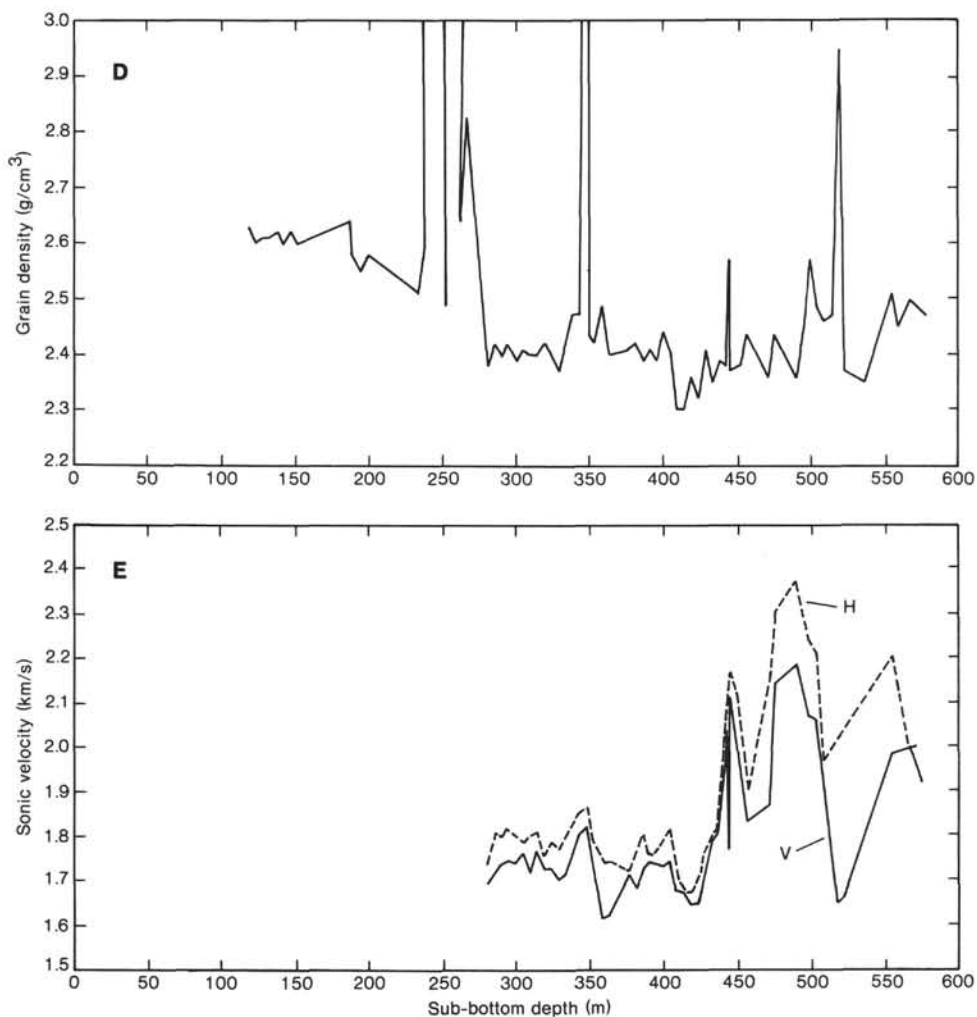


Figure 17 (continued).

Table 3. Summary of physical properties measurements, Hole 613.

Lithostrat. unit	Wet-bulk density (g/cm <sup>3</sup> )	Porosity (%)	Grain density (g/cm <sup>3</sup> )	Sonic velocity (km/s)
I	1.6-2.1	35-60	2.6	No data
II	1.6-1.8	47-60	2.3-2.5	1.6-1.8
III	1.7-2.1	35-48	2.4-2.6	1.8-2.3

locity of drilling mud and indicating a high sediment porosity. The sonic traveltime decreases sharply at the occurrence of glauconite at 147 m BSF. The appearance of biogenic silica and carbonate at 190 m BSF, just below the Unit IB/IC boundary corresponds with an increase in traveltime, an indication that the porosity increased in this section. The effects of compaction decrease the traveltime steadily through Unit IC to about 268 m BSF, where an increase of up to 40% in biogenic silica and carbonate content in Unit II increases sonic traveltime and porosity. The effects of compaction continue to decrease traveltime at a relatively constant rate throughout the remainder of Units II and III. The intervals deleted from the sonic log result from noise from

the effects of constrictions of the borehole by swollen clays (note the correlation of decreases in caliper and increases in gamma ray). The log responses in Subunit IIIA are shaded across Figure 18. By inverting the sonic traveltime for velocity, the maximum velocity can be calculated and varies between 1.5 and 3.0 km/s in this interval of the well.

#### Seismic/Lithologic Correlation

The seismic two-way traveltime is calculated in Table 6 by the average interval velocities and the approximate depth of each log-lithologic unit and subunit. Also shown in Table 6 are the average bulk density ( $\bar{\rho}$ ), the approximate interval thickness ( $\Delta Z$ ), interval two-way traveltime ( $\Delta T$ ), and cumulative two-way sub-bottom traveltime (TT). The average velocity is calculated from the sonic log. The bulk density had been inferred from nearby Site 612 logs or laboratory measurements for corresponding lithologies.

The seismic reflectors observed in the section of U.S.G.S. Line 35 (along strike of the continental slope) in Figure 18 are caused by impedance changes in sediments below the seafloor (see Downhole Logging, Site 612). The cumulative traveltimes (TT) in Table 6 are as-

Table 4. Physical properties data, Hole 613.

Sub-bottom depth (m)	Grain density (g/cm <sup>3</sup> )	Wet-bulk density (g/cm <sup>3</sup> )	Wet water content (%)	Porosity (g/cm <sup>3</sup> )
118.26	2.63	1.97	20.5	40.4
122.76	2.60	1.87	24.6	45.9
127.86	2.61	1.84	25.9	47.7
132.36	2.61	1.86	25.2	46.7
137.36	2.62	1.81	27.3	49.6
141.86	2.60	1.88	24.0	45.1
146.86	2.62	1.99	19.4	38.7
151.36	2.60	2.01	18.4	37.0
186.16	2.64	2.08	16.3	34.0
188.57	2.58	1.64	36.3	59.5
194.86	2.55	1.66	34.5	57.3
199.36	2.58	1.81	27.1	48.9
233.26	2.51	1.61	37.1	59.7
237.76	2.60	1.73	31.5	54.4
242.76	6.62	2.18	36.2	79.0
252.26	2.49	1.73	29.7	51.2
256.76	7.18	2.81	25.2	70.7
261.76	2.64	1.87	25.1	46.9
266.26	2.83	2.06	20.5	42.2
280.86	2.38	1.56	37.9	59.2
285.36	2.42	1.63	34.3	55.7
290.46	2.40	1.62	34.6	55.9
294.46	2.42	1.66	32.4	53.7
300.06	2.39	1.60	35.6	56.9
304.56	2.41	1.61	35.0	56.5
309.66	2.40	1.61	34.9	56.3
314.16	2.40	1.67	31.2	52.2
319.26	2.42	1.64	33.7	55.2
323.76	2.40	1.58	37.3	58.7
328.86	2.37	1.58	36.6	57.8
333.36	2.42	1.62	34.5	56.0
338.46	2.47	1.75	27.8	48.7
342.96	2.47	1.75	27.9	48.8
348.06	3.99	2.18	27.6	60.3
349.56	2.44	1.75	27.3	47.9
352.56	2.42	1.64	33.5	54.9
357.66	2.49	1.68	32.5	54.5
362.16	2.40	1.63	34.1	55.4
376.26	2.41	1.60	35.9	57.4
380.76	2.42	1.64	33.2	54.6
385.54	2.39	1.66	31.7	52.6
390.06	2.41	1.72	28.8	49.3
394.89	2.39	1.65	32.0	52.9
399.43	2.44	1.71	29.6	50.6
404.35	2.40	1.69	30.1	50.8
408.81	2.30	1.57	35.9	56.3
413.75	2.30	1.56	36.3	56.7
418.25	2.36	1.64	32.5	53.2
423.25	2.32	1.58	35.1	55.6
427.86	2.41	1.67	31.2	52.2
432.73	2.35	1.70	28.6	48.6
437.32	2.39	1.72	28.0	48.2
442.26	2.38	1.81	23.0	41.5
444.03	2.57	1.77	28.9	51.1
444.19	2.44	1.77	26.5	46.7
444.42	2.38	1.73	27.0	46.8
444.72	2.39	1.79	23.8	42.8
444.89	2.37	1.79	23.6	42.2
451.76	2.38	1.80	23.4	42.1
456.26	2.44	1.78	25.8	45.9
470.76	2.36	1.74	26.3	45.7
475.26	2.44	1.84	22.6	41.5
489.36	2.36	1.81	22.3	40.4
493.86	2.42	1.66	32.3	53.5
498.72	2.57	2.01	17.7	35.5
503.16	2.49	1.95	18.5	36.1
508.16	2.46	1.89	20.9	39.4
513.73	2.47	1.88	21.5	40.3
517.65	2.95	1.76	34.8	61.1
522.10	2.37	2.12	8.7	18.4
535.18	2.35	1.70	28.6	48.5
554.16	2.51	1.85	23.4	43.3
558.66	2.45	1.87	21.2	39.7
566.66	2.50	1.96	18.3	35.9
577.66	2.47	1.89	20.8	39.4

Table 5. Sonic velocity, Hole 613.

Sub-bottom depth (m)	Velocity (km/s)	H/V <sup>a</sup>	Liner (yes/no)
280.85	1.738	H	N
280.85	1.692	V	N
285.35	1.806	H	N
285.35	1.717	V	N
290.45	1.799	H	N
290.45	1.738	V	N
294.95	1.824	H	N
294.95	1.744	V	N
300.05	1.802	H	N
300.05	1.741	V	N
304.55	1.784	H	N
304.55	1.764	V	N
309.65	1.716	V	N
314.15	1.808	H	N
314.15	1.768	V	N
319.25	1.756	H	N
319.25	1.724	V	N
323.75	1.782	H	N
323.75	1.728	V	N
328.85	1.768	H	N
328.85	1.702	V	N
333.35	1.798	H	Y
333.35	1.712	V	Y
338.45	1.826	H	Y
338.45	1.765	V	Y
342.95	1.852	H	Y
342.95	1.806	V	Y
348.05	1.873	H	Y
348.05	1.823	V	Y
352.55	1.777	H	Y
352.55	1.719	V	Y
357.65	1.745	H	Y
357.65	1.614	V	Y
362.15	1.741	H	Y
362.15	1.617	V	Y
376.25	1.721	H	Y
376.25	1.714	V	Y
380.75	1.761	H	Y
380.75	1.679	V	Y
385.55	1.812	H	Y
385.55	1.725	V	Y
390.05	1.760	H	Y
390.05	1.741	V	Y
394.95	1.758	H	Y
394.95	1.738	V	Y
399.45	1.792	H	Y
399.45	1.729	V	Y
404.35	1.816	H	Y
404.35	1.743	V	Y
408.85	1.727	H	Y
408.85	1.673	V	Y
413.75	1.666	H	Y
413.75	1.671	V	Y
418.25	1.676	H	Y
418.25	1.645	V	Y
423.25	1.636	H	Y
423.25	1.642	V	Y
427.75	1.776	H	Y
427.75	1.723	V	Y
432.75	1.773	H	Y
432.75	1.788	V	Y
437.25	1.809	H	Y
437.25	1.799	V	Y
442.25	2.074	H	N
442.25	2.032	V	N
443.75	1.785	H	N
443.75	1.766	V	N
444.98	2.167	H	N
444.98	2.115	V	N
451.75	2.073	H	N
451.75	1.969	V	N
456.25	1.913	H	N
456.25	1.830	V	N
470.75	2.118	H	N
470.75	1.864	V	N

Table 5 (continued).

Sub-bottom depth (m)	Velocity (km/s)	H/V <sup>a</sup>	Liner (yes/no)
475.25	2.301	H	N
475.25	2.137	V	N
489.35	2.368	H	N
489.35	2.183	V	N
498.70	2.218	H	N
498.70	2.061	V	N
503.15	2.218	H	N
503.15	2.058	V	N
508.15	1.960	H	N
508.15	1.881	V	N
517.65	1.648	V	Y
522.15	1.662	V	Y
554.15	2.198	H	N
554.15	1.984	V	N
566.65	1.982	H	N
566.65	1.997	V	N
574.65	2.026	H	N
574.65	1.917	V	N

<sup>a</sup> H = horizontal propagation direction, V = vertical propagation direction.

Table 6. Approximate two-way traveltimes (TT) below seafloor in Hole 613.

Approx. sub-bottom depth (m)	$\bar{V}_p$ (km/s)	$\bar{\rho}$	$\Delta Z$ (km)	$\Delta T$ (s)	TT (s)	Lith.
0	1.64	1.85 <sup>a</sup>	0	0.0	0.000	SF
110	1.75	1.85 <sup>a</sup>	0.110	0.130	0.130	IA
140	1.95	1.85 <sup>a</sup>	0.030	0.034	0.164	IB
180	2.00	1.85 <sup>a</sup>	0.040	0.041	0.205	IB
200	1.70	1.65 <sup>a</sup>	0.020	0.020	0.225	IC
270	1.80	1.70 <sup>b</sup>	0.070	0.082	0.307	IC
320	1.85	1.70 <sup>b</sup>	0.050	0.056	0.363	IIA
430	2.00	1.95 <sup>b</sup>	0.110	0.119	0.482	IIA
450	2.00	1.87 <sup>b</sup>	0.020	0.020	0.502	IIB
						IIB

<sup>a</sup> From laboratory density measurements.  
<sup>b</sup> From density log in Hole 612.

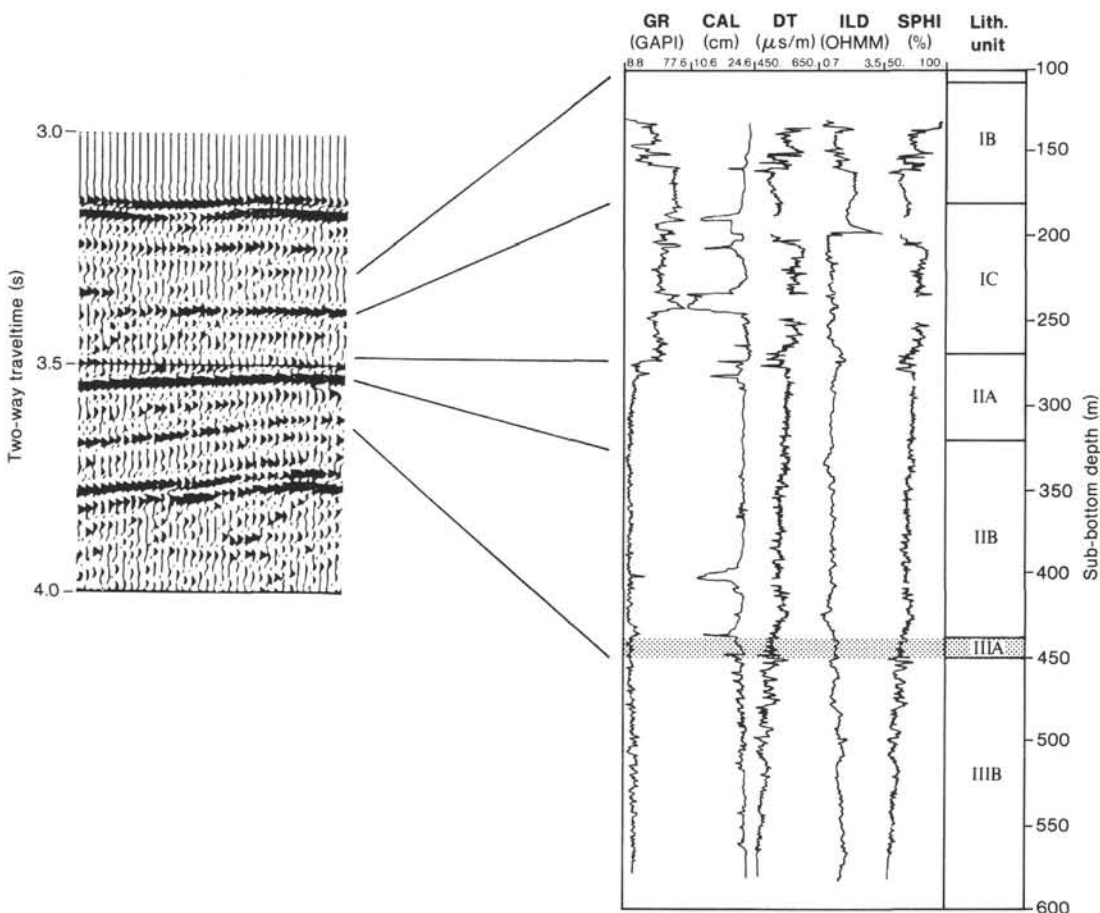


Figure 18. Geophysical logs recorded in Hole 613 and correlation to U.S.G.S. Line 35. GR = gamma ray, CAL = caliper, DT = interval transit time, ILD = deep induction log, SPHI = spherically focused resistivity.

sociated with the impedance contrasts calculated across lithologic boundaries in the logged interval. The approximate location of the reflectors in U.S.G.S. Line 35 are correlated by the two-way times calculated to the corresponding depth intervals in the logs.

Although the correlation is preliminary, we are able to constrain the approximate depths of several reflectors by the integrated sonic log response. Corrections of the interval velocities and densities in the upper 250 m of the well (Table 6) are necessary to improve the correlation of impedance contrasts to the seismic reflectors. Of particular interest for the local seismostratigraphy is the reflector associated with the top of Subunit IIIA.

### Conclusions

Three log-lithologic units have been identified between sharp features on the logs and, within the depth resolution achievable, are coincident with the lithostratigraphic units identified in the cored section. Synthetic two-way traveltimes have been calculated by the interval velocities from the sonic log and the lithostratigraphic boundaries and correlated to U.S.G.S. seismic Line 35. The preliminary correlation reasonably constrains the seismic reflectors with depth at Site 613. Further analysis of the acoustic logs and synthetic seismograms will improve the seismic depth constraints.

## SEISMOSTRATIGRAPHY

### Introduction

Site 613 is located about 0.2 km southeast of *Glomar Challenger* water-gun profile CP 3, which was run as a presite survey (Figs. 1, 19). This places the site ca. 1.8 km updip and 1.4 km northeast along strike from the proposed location of Site NJ-12. A dense network of seismic reflection profiles, including 12 intersections among Lines 35, 25, 79-218, CP1, CP2, and CP3, enhances seismic sequence interpretation and regional extrapolation of the Site 613 stratigraphic section (Fig. 1). As projected onto Line 25 (Figs. 1, 19), Site 613 is about 20 km downdip from Site 612, about 4 km downdip from Site 605, about 1.5 km updip from Hole 604, and approximately on strike with Hole 604A. Its projection onto Line 35 is about 6 km northeast of Site 604 (Figs. 19, 20).

Structurally, Site 613 is located over a buried ridge that separates two distinct sets of stacked erosional channels (Fig. 20) as seen on Line 35. Additionally, the hole penetrated near the updip pinchout of the Miocene channel-fill deposit (Figs. 20, 21), which was a critical factor in enabling us to core through the channel-fill without operational difficulty.

Beneath the upper channeled surface, Line 25 (dip section; Fig. 19) shows that the combined Paleogene and Upper Cretaceous sections thicken southeastward from the intersection with Line 35 to near shot point 3600, at which point the slope is diminished, suggesting the geometry of a slope-rise transition. Along strike (Line 35), the Paleogene–Upper Cretaceous units are seen to have been distinctly channeled by several erosional events (Fig. 20). The combined geologic data from Sites 605, 604,

and 613 allow us to more accurately interpret the causes and geohistorical implications of these channels. Especially important is the recognition that the lower to middle Eocene transition was the period of most severe submarine channeling in this region (i.e., the deepest channels are cut into the lower Eocene surface and are filled with middle Eocene sediments) (Figs. 20, 21).

### Correlation of Seismic Reflections with Downhole Geophysical Logs

This section assesses the relationships between the prominent reflections on our seismic lines, especially sequence boundaries, with the geological boundaries in the borehole. This is accomplished using acoustic velocity measurements and integrated transit time derived from the downhole sonic log. Four geologic boundaries are assessed.

The Pleistocene/Pliocene unconformable contact was noted at about 187 m in Hole 613, and corresponds to a prominent seismic sequence boundary at 3.36 s (two-way traveltime) on Line CP3B (Fig. 21). The gamma ray log indicates a clayey Pleistocene section about 3 m thick above less argillaceous Pliocene strata (Fig. 22). The sonic log is noisy in this interval and difficult to evaluate, but a distinct downhole decrease in formation resistivity is associated with the contact.

The unconformable Pliocene/upper Miocene contact occurs at about 266 m depth (Fig. 23) and is represented by a strong reflection at 3.45 s on Line CP3B (Fig. 21). The upper Miocene/middle Eocene contact was not recovered, but the gamma ray log indicates a clay-depleted (sandy) section about 12 m thick between 266 m (where Miocene strata were recovered) and 278 m (where 17 cm of middle Eocene section were recovered), which probably represents the lower part of the upper Miocene section (Fig. 23).

The clay content decreases even further below 278 m in the biosiliceous, chalky, middle Eocene unit. This level is represented by a prominent reflector at about 3.46 s on seismic Line CP3B (Fig. 21).

The middle Eocene/lower Eocene contact is not a sharp one but consists of a series of middle Eocene slump deposits that disturbed the upper surface of the lower Eocene sediments and incorporated some of them into an unconformable transition “zone” (about 438–440 m BSF). A broad peak of increased gamma-ray values indicates an increasing clay content associated with this slumped interval (Fig. 24). Shipboard velocimeter measurements show that a notable sonic velocity increase begins around 440 m, and this coincides with a slight increase in sonic log values. The prominent seismic reflector at 3.63 s appears to correspond to a marked increase in sonic velocity at 438.0 m in Hole 613 (Fig. 24).

### Seismic and Depositional Sequences

The oldest depositional sequence penetrated in the up-rise wedge is the Maestrichtian, which was cored at Site 605 (Fig. 19) which is projected on Line 25 between shot points 3200 and 3500. Its irregular upper surface is formed by a series of discontinuous, moderate- to high-amplitude reflections that are interrupted in several plac-

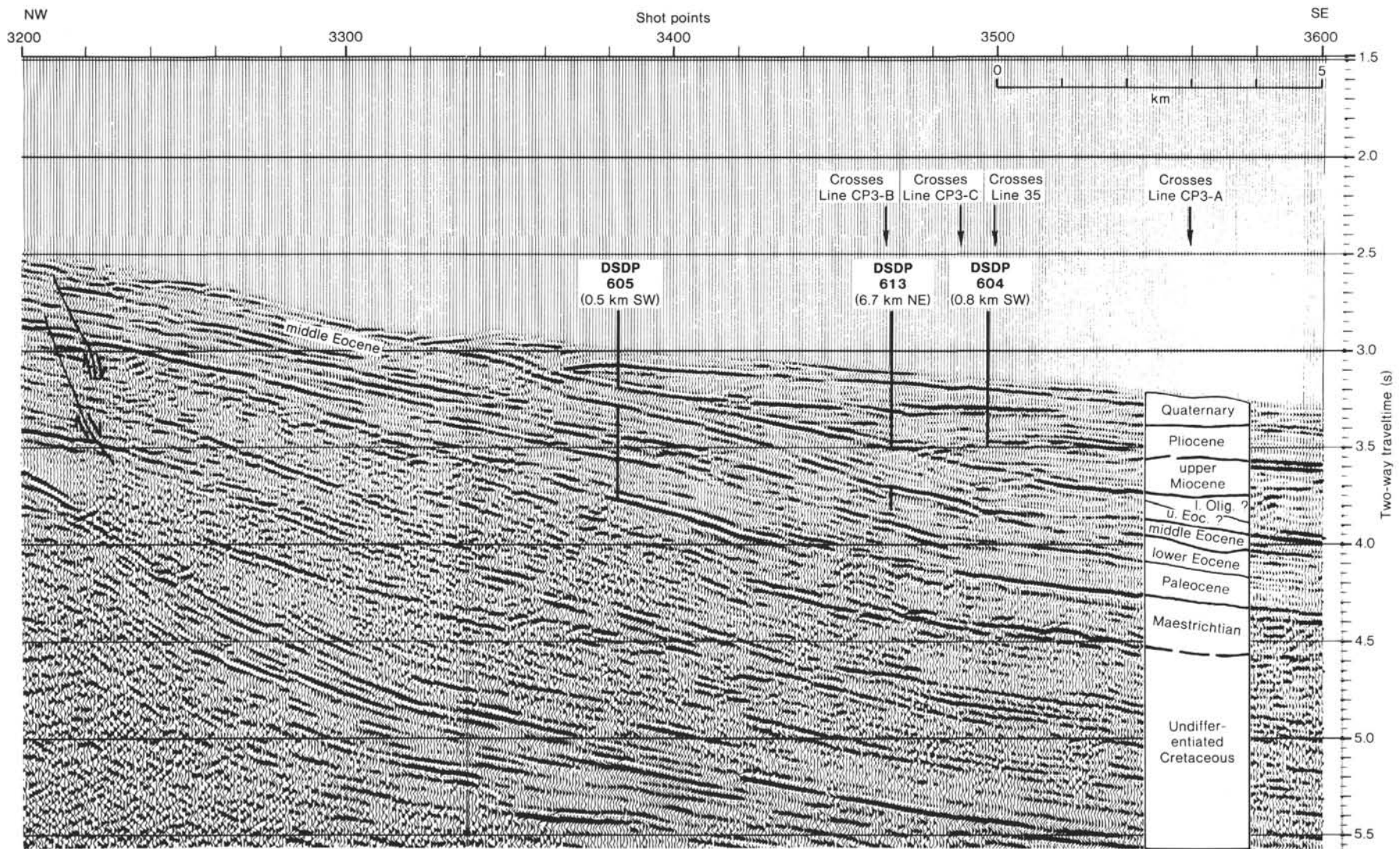


Figure 19. Multichannel seismic reflection profile (Line 25) crossing vicinity of Sites 604, 605, and 613 in a dip direction. Numbers in parentheses below site labels indicate distance and direction of actual site locations from Line 25 (see Fig. 1). Vertical heavy lines show stratigraphic section penetrated by each hole. Gaps in vertical lines indicate that the unit labeled "upper Eocene?" was not encountered at the drill sites (because they are not actually on Line 25). See Poag and Mountain (this volume) for more detailed discussion based on single-channel seismic reflection profiles.

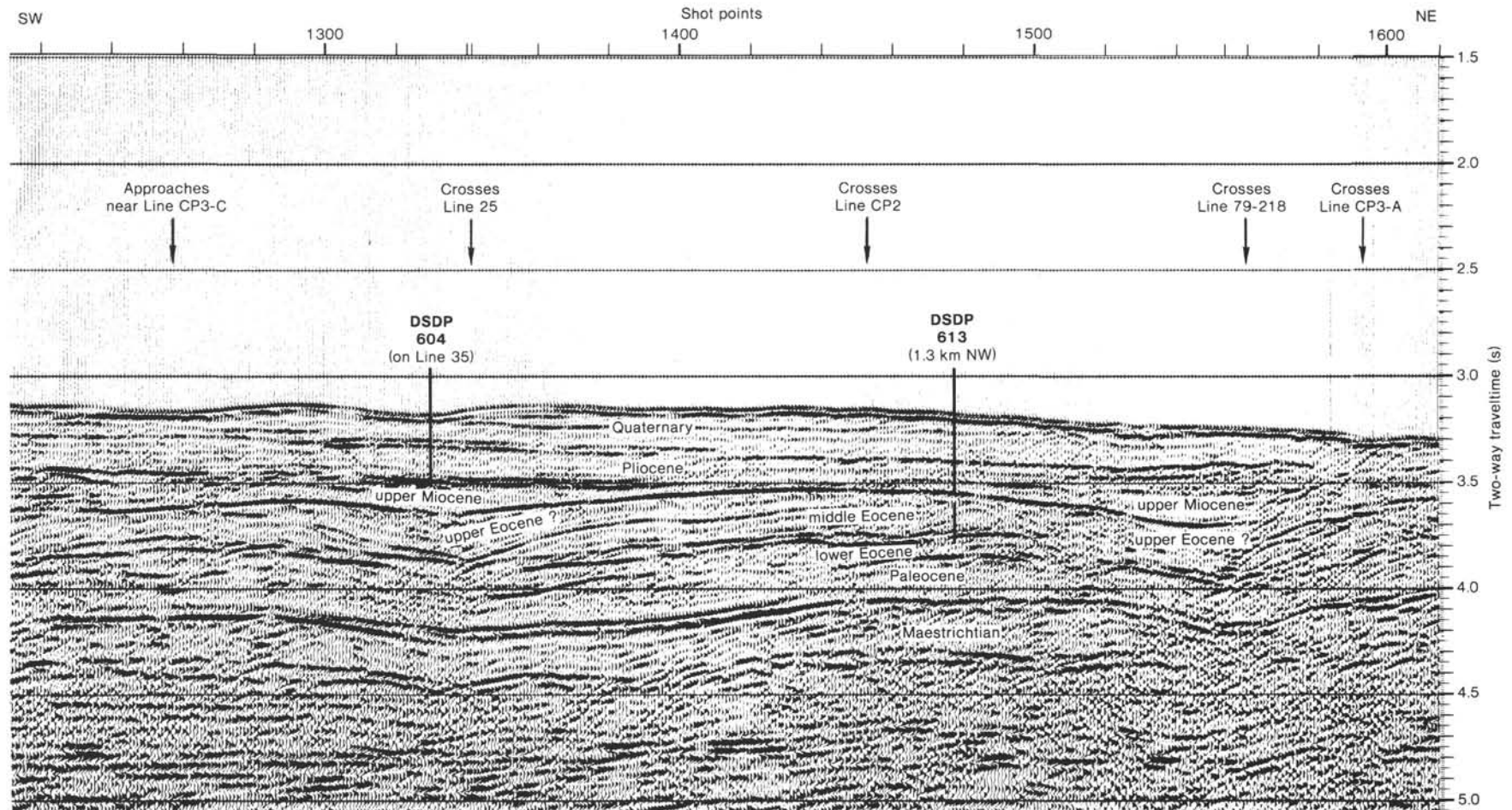


Figure 20. Multichannel seismic reflection profile (Line 35) crossing vicinity of Sites 604 and 613 in a strike direction. Numbers in parentheses below site labels indicate distance and direction of actual site locations from Line 35 (see Fig. 1). Vertical heavy lines show stratigraphic section penetrated by each hole. Gap in the vertical line at Site 613 indicates that a thin interval of upper Eocene (?) strata is not present at Site 613, which is 1.3 km northwest of Line 35.

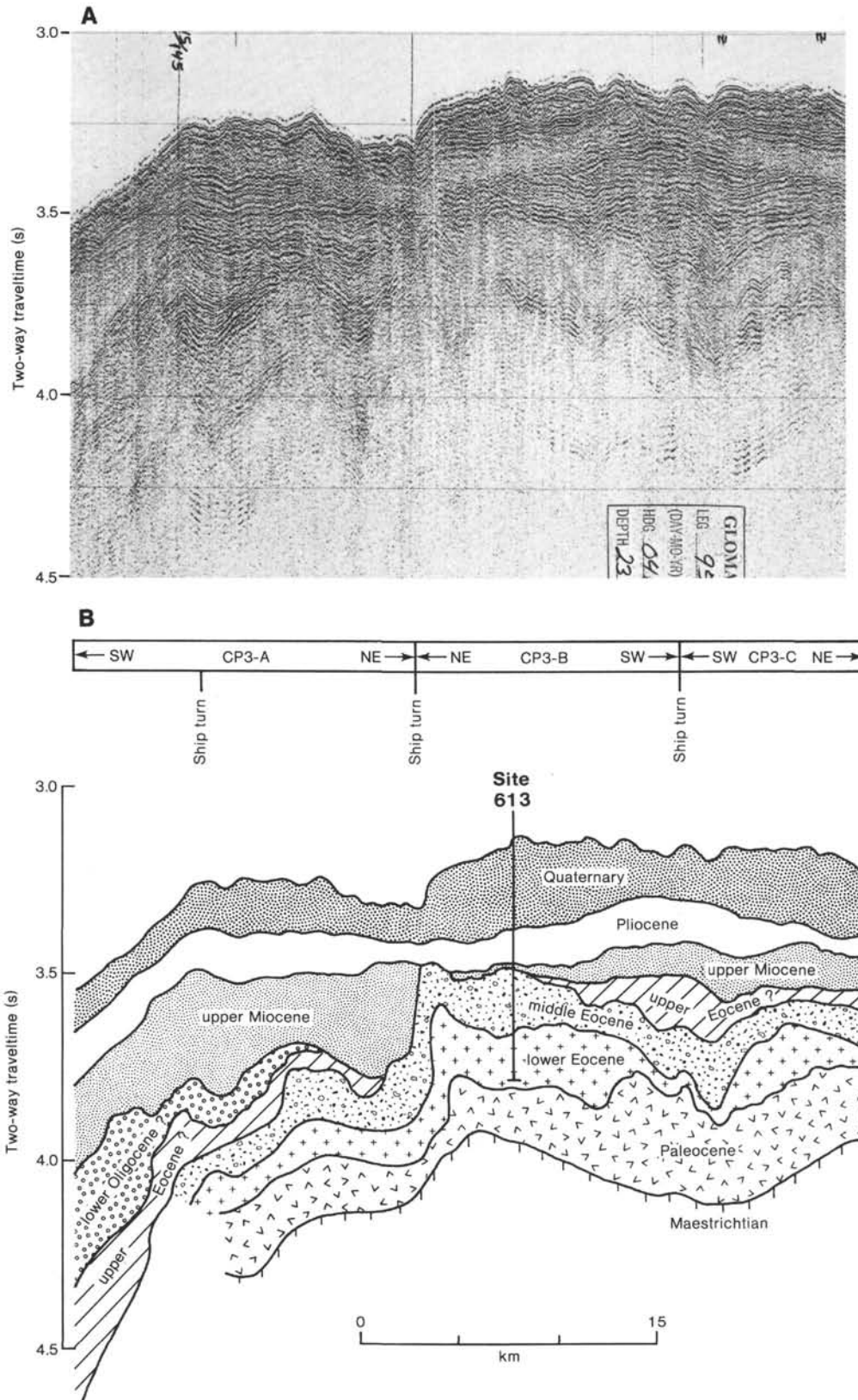


Figure 21 A. Uninterpreted single-channel seismic reflection profile CP3 obtained with shipboard water-gun seismic system prior to drilling Site 613. Notations along top of profile show intersections with seismic Lines 25, 79-218, CP1, and CP2 (see Fig. 1). B. Seismostratigraphic interpretation of Line CP3. Line CP3 consists of three parallel segments labeled CP3A-CP3C (see Fig. 1 for their relative positions in map view). Segment CP3-B was run in the opposite direction to the other two segments. The vertical heavy line on Segment CP3-B shows the location of and stratigraphic section penetrated by Hole 613.

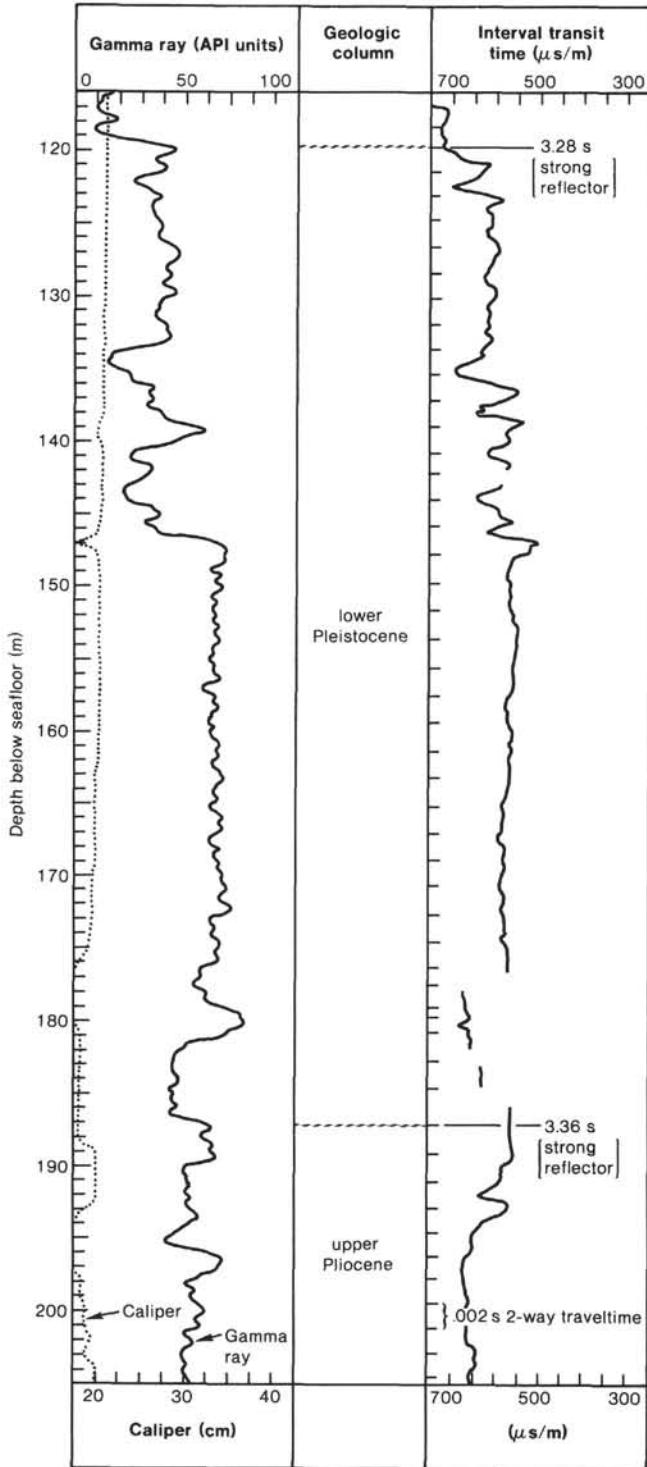


Figure 22. Segment of downhole geophysical log at Site 613. Note that sonic velocity is the reciprocal of interval transit time and increases from left to right (sonic scale is in microseconds per meter).

es by shallow channels. Underlying reflections are truncated by these channels. Similar characteristics mark the upper Maestrichtian surface along Line 35 (Fig. 20) where the channels are expressed as broad undulations.

Seaward of shot point 3500 (Line 25) the upper reflector bounding the Maestrichtian sequence becomes

continuous over broader intervals, but is broken up by small channels between shot points 3900 and 4100 (Fig. 19).

A thick (80 m) Paleocene sequence was also penetrated at Site 605, and its lower reflections can be seen to onlap the Maestrichtian surface and to fill in channels.

The upper reflector surface of the Paleocene unit is somewhat more continuous than the upper Maestrichtian reflector, and underlying truncated reflectors are more evident. In strike section (Line 35; Fig. 20), the upper reflector of the Paleocene sequence is more intermittent and of more variable amplitude. The Paleocene surface is distinctly cut by broad channels (3–5 km across), along whose margins numerous reflections are truncated.

The lower Eocene sequence is the oldest cored at Site 613 (Fig. 21). Its lowest reflections onlap the Paleocene surface and fill in the channels along seismic Line 35 (Fig. 20). Its contact with overlying sequences is variable. On Line 25, weak and strong intermittent reflections mark an undulating, channeled upper surface, as the sequence thins updip beneath the Neogene upper rise wedge (Fig. 20). Numerous underlying reflections are truncated. In strike section (Lines 35, CP3; Figs. 20, 21) the channelling is seen to constitute the most extensive erosional feature in the vicinity of Site 613. In several places, the lower Eocene has been completely removed and middle Eocene strata rest directly on Paleocene beds.

In the vicinity of Site 613 the top middle Eocene reflector is a high-amplitude, subcontinuous feature, beneath which reflections are truncated (Fig. 19). In strike section, this reflector also is of high amplitude and is nearly continuous as it undulates across the channeled middle Eocene surface (Figs. 20, 21).

Basal reflections from the upper Miocene sequence onlap the middle Eocene surface in a few places, such as at Site 613, but along most of Lines 25 and 35, two or three undrilled sedimentary sequences can be distinguished between the middle Eocene and upper Miocene sequences (Figs. 19–21). A combination of updip pinchout, strike-wise thinning across interchannel ridges, and submarine erosion caused us to miss these sequences at Site 613 (they were also missed at Sites 604 and 605). In strike section, the upper Miocene sequence forms a series of lenticular wedges, whose upper surfaces are marked by a nearly horizontal series of single and double, short, high-amplitude reflections (Fig. 20). These high-amplitude reflections are generally more prominent above the channels, and often are replaced by weak reflections over the intervening ridges. The upper Miocene surface is cut in places by small-scale channels and underlying reflections are truncated.

The cross-sectional geometry of the Pliocene sequence is strikingly different from that of the underlying units in that it is bounded by relatively horizontal surfaces (especially in dip section) except near the updip pinchout (Figs. 19, 20 and 21). Nevertheless, the basal reflections onlap the upper Miocene surface in both dip and strike sections. The reflections that form the upper Pliocene/Pleistocene contact are discontinuous and of variable amplitude (Mountain and Tucholke, 1985 refer to it as “Reflector Blue”).

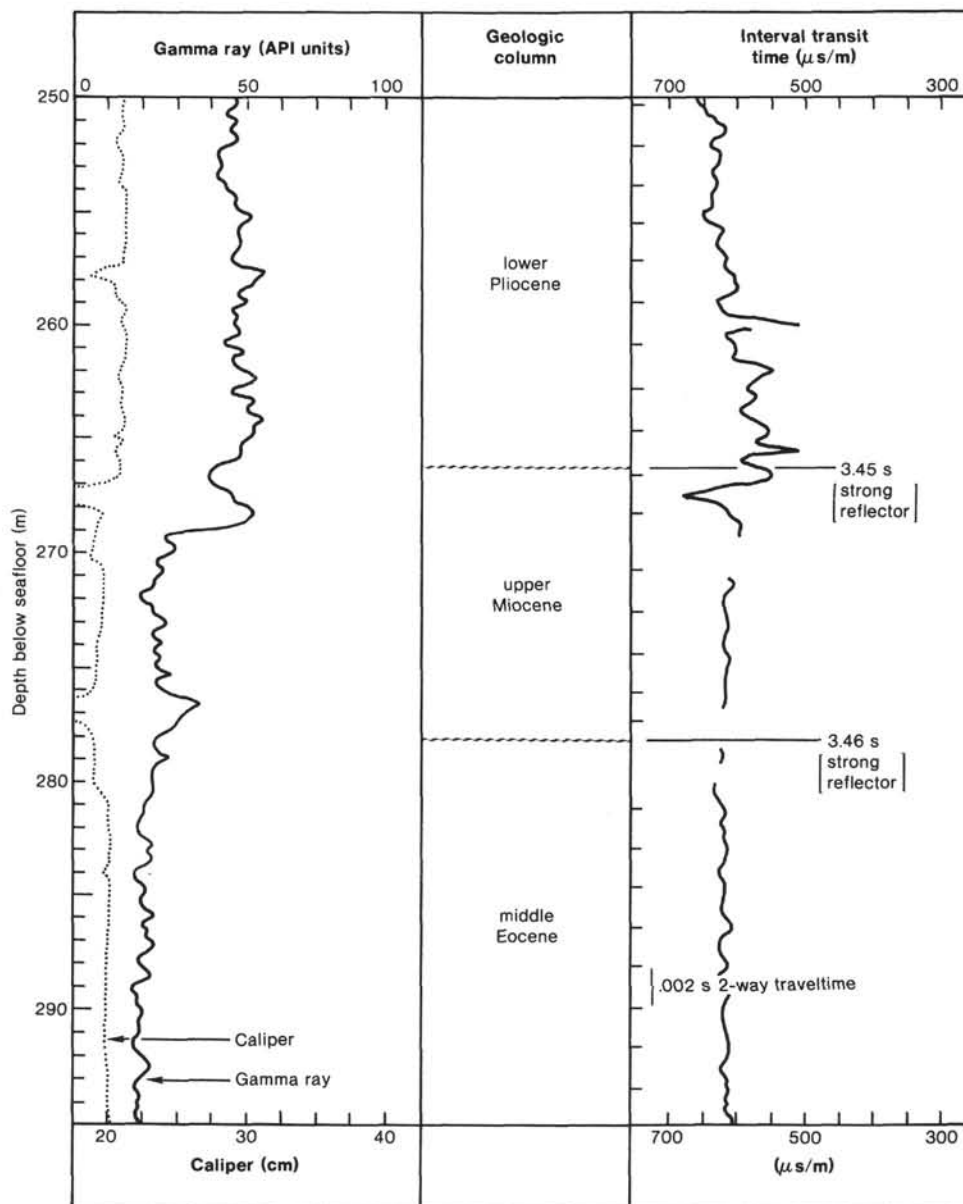


Figure 23. Segment of downhole geophysical log at Site 613 (see note on Fig. 22).

The seafloor near Site 613 is formed by a Quaternary sequence whose basal reflection overlies the Pliocene and fills in the occasional small, shallow channels in its surface (Figs. 19, 20). The thickness in strike section is quite variable, as the surface is channeled and hummocky (one channel is nearly 7 km across; Fig. 20). Numerous reflections of the upper Quaternary sequence are truncated at or near the seafloor.

#### Seismic Facies Analysis

This section describes the inferred paleoenvironments near Site 613 on the basis of seismic reflection characteristics and the cross sectional geometry of the seismic sequences.

The Maestrichtian sequence (Fig. 19) thickens down-dip from less than 100 m at Site 612 (near the presumed Maestrichtian shelf edge) to about 400 m at the Site 613

projection on Line 25. The gently sloping surface at this point markedly decreases its gradient, forming what resembles the modern slope-to-rise transition. The internal reflections of this sequence are variable between Sites 605 and 613. Two zones of arched, somewhat chaotic, short, high-amplitude reflections near shot points 2460 and 3575 (Line 25; Fig. 19) suggest slumped structures or perhaps debris flows. Intervening zones contain more uniform, subparallel, low-amplitude reflections, suggesting a more tranquil depositional style. Line 35, which crosses Line 25 near one of the chaotic zones, displays similar arched short, high-amplitude reflections (Fig. 20).

The cross-sectional geometry of the Paleocene sequence is similar to that of the Maestrichtian, thickening from about 100 m near Site 605 to 200 m near the Site 613 projection on Line 25, where the seaward sloping gradient decreases (Fig. 19). The internal reflections of this

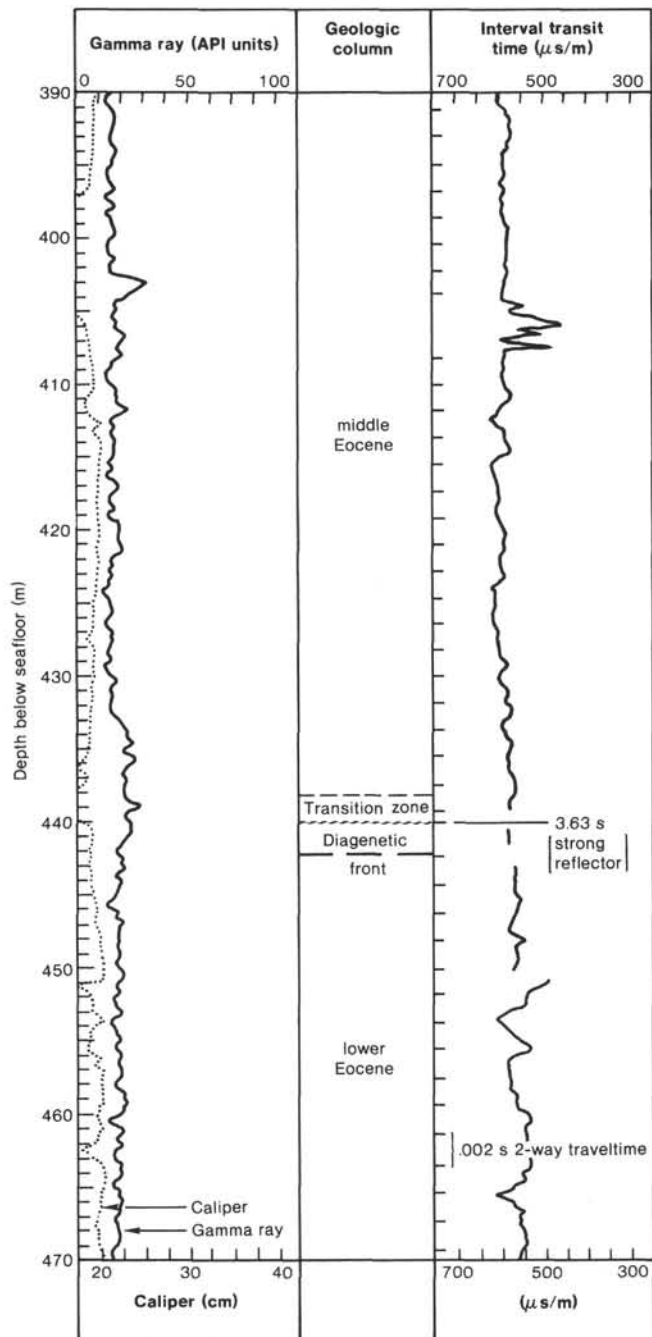


Figure 24. Segment of downhole geophysical log at Site 613 (see note on Fig. 22).

unit are subparallel in dip section (Line 25) and more regular than those of the Maestrichtian, suggesting the absence of slump and debris-flow deposits. These characteristics are generally true of Line 35 (Fig. 20) as well, but some zones of somewhat chaotic reflections are present there.

The lower Eocene sequence varies generally between 150 to 200 m in thickness across the Site 605 to 613 region depending upon the positions of channels (Fig. 20, 21). The downslope gradient decreases below the Site 613 projection like that of underlying units.

The internal reflections are of high amplitude and are parallel and distinct as they cross the slope and pass Site 605, but from there seaward they become weak and more erratic. This suggests a change from uniform slope deposition to a variable, more disrupted depositional style (Fig. 19). On Line 35, the lower Eocene sequence contains some short, high-amplitude reflections that are sometimes diagonal to the sequence boundaries, interspersed with weaker, more continuous and subparallel reflections (Fig. 20). These characteristics suggest the presence of slumps or debris flow deposits interspersed with stratified slope-front fill deposits.

On Line 25, the middle Eocene section thins from about 150 m near Site 605 to about 100 m at the Site 613 projection, and the downslope gradient decreases like that of the previous units (Fig. 19). The reflections are parallel, continuous, and of variable amplitude down to about the Site 613 projection, where they become diagonal and divergent, and of higher amplitude, suggesting a chaotically emplaced deposit. On Line 35, the internal reflections of the middle Eocene unit are highly complex and variable (Fig. 20). The undrilled depositional sequence that fills the middle Eocene channels contains variable amplitude, discontinuous, diagonal to chaotic reflections, suggesting slumps or debris flow deposits (Figs. 19, 20, 21).

The upper Miocene sequence contains a generally simpler series of reflections. They tend to be of variable amplitude, discontinuous, gently undulating, and subparallel. However, there are occasional interruptions (e.g., Line 25 at shot point 3600) by short, diagonal, or arched, high-amplitude reflections that suggest chaotic deposition (Fig. 19). The cored intervals at Sites 604 and 613 reveal that poorly sorted terrigenous sands, gravels, and conglomerates are contained in the upper part of this sequence.

The Pliocene sequence comprises generally parallel weak, sporadic reflections. High-amplitude, short, somewhat arched reflections are present near the base of the sequence, especially at the southwest end of Line 35 (Fig. 20). Coring reveals a dense clay in the upper Pliocene section, below which are coarse glauconitic sands.

The Quaternary sequence contains broad reflectorless bands punctuated by very high-amplitude, moderately continuous, horizontal to arched reflections suggesting turbidite deposition. Coring revealed an abundance of coarse sands and gravels in the Quaternary section.

### Summary and Conclusions

The seismic and depositional sequences in the vicinity of Sites 605, 604, and 613 have a quite different character from those at Site 612, although the Paleogene and Upper Cretaceous sequence boundaries are the downslope extensions of the unconformable contacts seen at Site 612. Whereas the depositional style was chiefly relatively quiet hemipelagic accumulation at Site 612, the sequences at Site 613 are heavily channeled and comprise abundant chaotic depositional units (debris flows deposits and slumps). The presite survey Line CP3 makes three perpendicular crossings of the channeled region, showing clearly the updip shallowing and narrowing of

the channels (Fig. 21), especially those cutting the middle Eocene surface. What appear to be exposed incipient channels have been reported updip at the shoreward edge of the middle Eocene outcrop belt by Robb et al. (1983).

Several major channeling events have been documented by the current drilling and seismic surveying. The most severe channeling took place between the early and middle Eocene ("A" of some authors). Further seismic sequence analysis and coring of the continental rise are needed to document confidently the areal distribution of the units documented at Site 613 and those not yet sampled by the drill. (See Poag and Mountain, this volume, for further documentation and analysis of seismostratigraphic sequences.)

## SUMMARY AND CONCLUSIONS

### Introduction

Site 604 was originally intended to be the seaward-most (downdip) coring location of Leg 95. Here the depositional sequences, unconformities, and biofacies of the upper continental rise could be analyzed and compared with those of the updip sites (612 and 605). It was thought that a fairly complete upper rise stratigraphic sequence could be cored at Site 604. However, after the drilling of Site 604 was reassigned to Leg 93, it was found that caving sands of upper Miocene age were impossible to penetrate at that location. Thus, Site 613 (2333 m water depth) was chosen for a second attempt to penetrate the upper rise strata. It was considered especially important to achieve this penetration, as extrapolation of sequences cored updip at Site 605 indicated that original (prior to Leg 93) seismostratigraphic interpretations of the pre-upper Miocene section at Site 604 were probably in error. That is, a major period of channeling thought to represent an early late Oligocene sea-level fall, appeared more likely to be an intra-Eocene event.

Several different site locations were considered before a presite seismic reflection survey by *Glomar Challenger* showed a spot where the Miocene sand unit was only about 10 m thick as it crossed the top of an interchannel ridge. The careful survey for the best location proved fully warranted as we experienced no trouble penetrating the Miocene sand which indeed, is only 12 m thick at Site 613.

In view of the short period of time left for coring at this final site of Leg 95, the upper 116 m section was washed and spot cored. Below 116 m BSF, continuous coring with the XCB was maintained to a depth of 581.9 m BSF, except for one additional 29-m washed interval (154.1–182.9 m BSF).

The principal scientific objectives were

1. To establish the composition, stratigraphic framework, and depositional environments of sediments constituting the upper continental rise.
2. To establish detailed biostratigraphic zonations and to accurately date the unconformities and major seismic reflections in the section.
3. To establish the timing of several major episodes of seafloor channeling that were indicated on seismic reflection profiles.

4. To document the lateral relationships of lithofacies and biofacies between Site 605 and Site 613, especially with regard to silica diagenesis.

5. To identify depositional sequences and evaluate their relationships with seismic sequences, relative sea level changes, oceanic current patterns, water mass composition, sediment provenance, and subsidence history.

### Results

Three distinct lithologic units were documented at Site 613. The lowermost unit penetrated, lithologic Unit III, comprises 135.6 m of porcellaneous nannofossil chalks and limestones and nannofossil porcellanites of early Eocene age. The light greenish gray to light gray sediments are generally densely burrowed, except in some slumped intervals. Slumping is extensive in this unit as opposed to the virtual lack of slumps in its counterpart (lithologic Unit III) at Site 612.

Diagenesis of the porcellaneous strata is not uniform throughout Unit III. Some layers have become hard porcellaneous limestones or nannofossil porcellanites, while others with similar compositions remain poorly lithified chalks. Swelling and cracking when rinsed with fresh water is characteristic of some intervals although very little clay content was detected by X-ray diffraction.

Increased sonic velocity resulting from the silica diagenesis is notable on the downhole geophysical log and in shipboard measurements. Shipboard values show a downward increase from 1.799 to 2.074 km/s at the top of the unit and peak values of 2.301 and 2.368 km/s between 475 and 490 m. Log values also climb to 2 km/s or more near the top of Unit III and peak to as much as 2.379 in the 484 to 511 m interval. Low gamma ray values reflect the minor clay content.

Microfossil assemblages in Unit III are partly dissolved and moderately to poorly preserved. Etched and dissolved diatoms and radiolarians are present at the very top of Unit III, but the diatoms are absent throughout most of the section. Benthic foraminifers, although poorly preserved, form an association tentatively interpreted as having accumulated in lower bathyal depths. A lower slope paleogeographic position for Site 613 during the early Eocene is supported by the geometry of Unit III as seen on a seismic depth section (Line 25). The unit slopes seaward to the southeast from Site 612, where its gradient flattens, resembling a slope-rise transition, approximately beneath Site 613.

The minimum average sediment accumulation rate for lithologic Unit III is approximately 2.0 cm/k.y., but the presence of numerous slumped intervals indicate that frequently the emplacement of sediment was much more rapid.

The contact between Unit III and overlying Unit II appears on seismic profiles as a deeply scoured erosional surface approximating the middle/lower Eocene contact, but which in places cuts down into Paleocene strata, entirely removing Unit III. However, Site 613 was chosen to avoid such channels and is located where Unit III forms part of a sedimentary ridge. The contact at Site 613 is a highly disturbed zone of slumping in which lower Eocene beds belonging to Unit III have been in-

incorporated into slump blocks of Unit II (middle Eocene). No distinct biostratigraphic gap was noted, however, during shipboard analysis. The separation of Unit III from Unit II is based upon the highest appearance of porcellanite, approximately 2 m below the middle/lower Eocene contact.

Lithologic Unit II (278.4–442.1 m BSF) comprises 164.1 m of intensely burrowed, light greenish gray to grayish yellow green siliceous nannofossil chalk. Carbonate from bomb measurements varies from 34 to 61%; bio-silica constitutes as much as 45%. Several slumps are present in this unit, displaying overturned folds and variably dipping bedding surfaces that are not burrowed. A single 5-cm-thick volcanic ash layer was noted at 403 m, showing up on the gamma ray log as a distinct peak. This ash bed may prove to be a useful correlation horizon in this region, as a similar bed was also noted in approximately the same stratigraphic position at Site 605.

The general uniformity of lithologic Unit II is reflected in the gamma ray and sonic velocity logs whose traces display little variation. Sonic velocity gradually increases from about 1.9 km/s at the top of the unit to about 2.1 km/s near the base. Shipboard velocity measurements yielded somewhat lower values ranging from ca. 1.6 to 1.8 km/s. The zone of slumping across the Unit II/III transition displays a series of gamma ray peaks. A small hole diameter in this interval suggests the presence of swelling clays.

Both calcareous and siliceous microfossils are abundant and well preserved in Unit II, and clearly establish the bulk of the unit as being of middle Eocene age. However, the last 7 m.y. of middle Eocene time are not represented by deposition here. The precise nature of the disturbed lower–middle Eocene biostratigraphic transition remains to be established by post cruise studies.

Benthic foraminiferal assemblages of Unit II are again of the lower bathyal type, but faunas that are generally thought to have preferred abyssal depths are present in moderate to large numbers. The geometry of the unit as seen on the Line 25 depth section is similar to that of the lower Eocene, suggesting that the slope–rise transition was near Site 613. Conditions similar to those of the lower Eocene are also indicated by the similar average sedimentation rate of 3.3 cm/k.y.

Lithologic Unit I comprises the upper 268.3 m at Site 613 and is a complex sequence of interbedded greenish gray to dark greenish gray mud or calcareous mud (containing variable amounts of diatoms), glauconitic or pyritic silty sand, and sandy mud. The section was not continuously cored, which along with poor recovery of certain intervals, complicates the lithologic interpretation.

Three subunits were recognized, as in Unit I of Site 612:

Subunit IA (0.0–119.8 m) was only partly cored and recovery was poor. Four mineralogically distinct zones were recognized. Zones 1 and 3 contain interlayered glauconitic quartzose sand, silty sand, sandy mud, and mud; Zones 2 and 4 are comprised of mud, marly nannofossil ooze, and nannofossil diatomaceous ooze. Middle Eocene lithoclasts are also incorporated into Zones 2 and 4. A conglomeratic mud, containing 3 cm pebbles

of quartz sandstone and calcareous sandstone marks an erosion surface at the basal contact with Subunit IB.

The upper part of Subunit IB (total interval 119.8–187.6 m) is chiefly greenish gray unbedded homogeneous mud to calcareous mud with sporadic glauconitic silty sand. The glauconite decreases downward between ca. 145 to 154 m and silty, pyritic, and calcareous mud becomes prominent. A significant downward increase of ca. 30 API units on the gamma ray log corresponds to the glauconite decrease. Evidence of slumping is seen in this section.

Within wash Core 10X (154.0–183.9 m) the calcareous, greenish gray mud interlayered with coarse sandy glauconitic mud similar to the upper part of Subunit IB reappears. A major decrease of gamma ray values near 181.5 m suggests that this is the top of the lower interval of greenish gray mud and glauconitic mud.

The basal contact of Subunit IB is a sharp erosional break at 186.6 m that is coincident with the Pliocene/Pleistocene contact.

Lithologic Unit IC (188.6–268.3 m) is chiefly structureless dusky yellow green nannofossiliferous siliceous mud containing sporadic silty, glauconitic-quartzose laminae. Glauconite rarely occurs in laminae and is never found in beds thicker than 1 cm. A zone of especially fine-grained clay-rich sediments between 227 and 236 m shows up as a significant bridge on the caliper log and an increase in gamma ray values. The base of Subunit IC contains a glauconitic, conglomeratic sand mixed with nannofossiliferous mud. Granule-sized pebbles overlie a scoured surface at 266.45 m that approximates the Pliocene/upper(?) to middle(?) Miocene contact. Subunit IC extends to the bottom of Core 19 at 268.3 m. A coring gap of about 9.4 m follows, at the bottom of which 20 cm of middle Eocene Unit II was recovered. The gamma ray characteristics suggest that the unconformable contact between Units I and II is near 278 m BSF.

The microfossils of Unit I are variably abundant and preservation is good to poor, depending upon the sediment type (sands generally have poorer assemblages). Shipboard identification of biozones and chronostratigraphic boundaries is approximate and needs to be refined by further studies onshore. Benthic foraminifers of the Neogene–Quaternary section are generally bathyal assemblages, but mixtures of displaced shallower water associations are typical in the Pleistocene strata.

Average sedimentation rates within Unit I range from ca. 1 cm/k.y. in the Miocene, to 2.4 cm/k.y. in the Pliocene, to 11.7 cm/k.y. in the Pleistocene.

Seismostratigraphic analysis shows that the Miocene unit is chiefly a series of chaotic channel-fill deposits that smoothed the deeply channeled middle Eocene surface, following a period (or several periods) of erosion and nondeposition. Prior to Leg 95, some authors had attributed the erosion to a mid-Oligocene sea level fall, but we found no evidence of Oligocene sediments at Site 613, and thus, cannot support that idea.

Reflections in the top of the Miocene unit are truncated and overlapped by Pliocene reflections. More uniform deposition took place in the region during the Pliocene and Pleistocene than during the pre-Pliocene in-

terval, but slumping and downslope displacement of strata appear to have been still common.

### Conclusions

The sediments recovered at Site 613 accumulated in a deeper water regime that those at Site 612, encompassing a series of microfossil associations having lower bathyal to abyssal affinities.

The general composition of the lithologic units at Site 613 varies only slightly from those at Site 612, but the style of deposition is significantly different. Whereas even-bedded hemipelagic deposition prevailed most of the time at Site 612, the section at Site 613 is characterized by the frequent occurrence of slump deposits and conglomeratic, sandy, channel-fill deposits.

Whereas unconformable contacts at Site 612 could easily be distinguished by their sharply scoured surfaces, contacts are often obscured at Site 613 by the churned, folded, and faulted slump units that straddle some boundaries. Thus, some of the strata being removed from the middle slope at Site 612 accumulated at the base of the slope near Site 613.

The seismic and cored record at Site 613 demonstrates that this part of the New Jersey margin has had a long history of intense channeling that began at least as far back as the middle-lower Eocene transition and was repeated during the middle Eocene-Miocene interval, and again during the Pleistocene. The channels on the lower and middle Eocene surfaces are restricted to the lower slope and deeper as shown by their lack of expression on Line 34, which runs along depositional strike through Site 612. Smaller channels noted on the surface of the middle Eocene seafloor outcrop (Robb et al., 1983) may be related to these larger buried channel systems down-dip.

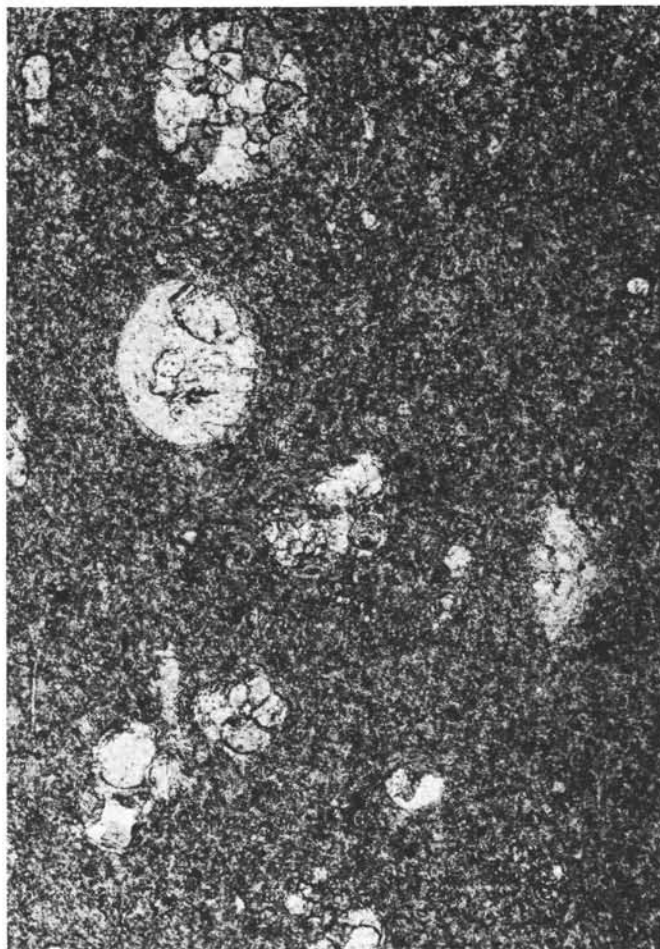
The diagenesis of silica-rich nannofossil chalk near the lower-middle Eocene transition is a phenomenon recognized throughout the Atlantic basin and its continental margins, and was documented thoroughly at Sites 612, 605, and 613. However, shipboard analyses are necessarily limited, and we expect to learn a great deal more about the processes and their causes from more intensive onshore studies.

Four apparently unconformable sequence boundaries were penetrated at Site 613, but only two were recovered in undisturbed condition (Pleistocene/Pliocene and Pliocene/Miocene). The Miocene/middle Eocene contact occurred in an unrecovered interval, and the middle Eocene/lower Eocene contact was marked by a transitional zone of intense slumping. The evidence gathered at Site 613 supports the recognition of unconformable seismic-stratigraphic sequence boundaries, but emphasizes the critical need to take additional cores. For example, the virtual absence of upper Eocene through middle Miocene deposits was not expected when the New Jersey transect was planned. We now realize that the combined features of updip pinchout and strike-wise thinning across the interchannel ridges has precluded our encountering the sediments of several seismic sequences. A deeper hole at Site 604, or to the southwest along Line 35, or down-dip along Line 25, would have sampled these additional sequences.

The results of Legs 93 and 95 provide further impetus for additional deeper coring along the New Jersey Transect in order to sort out the complex history of the overlapping, irregularly eroded sequences that constitute the continental slope and upper rise.

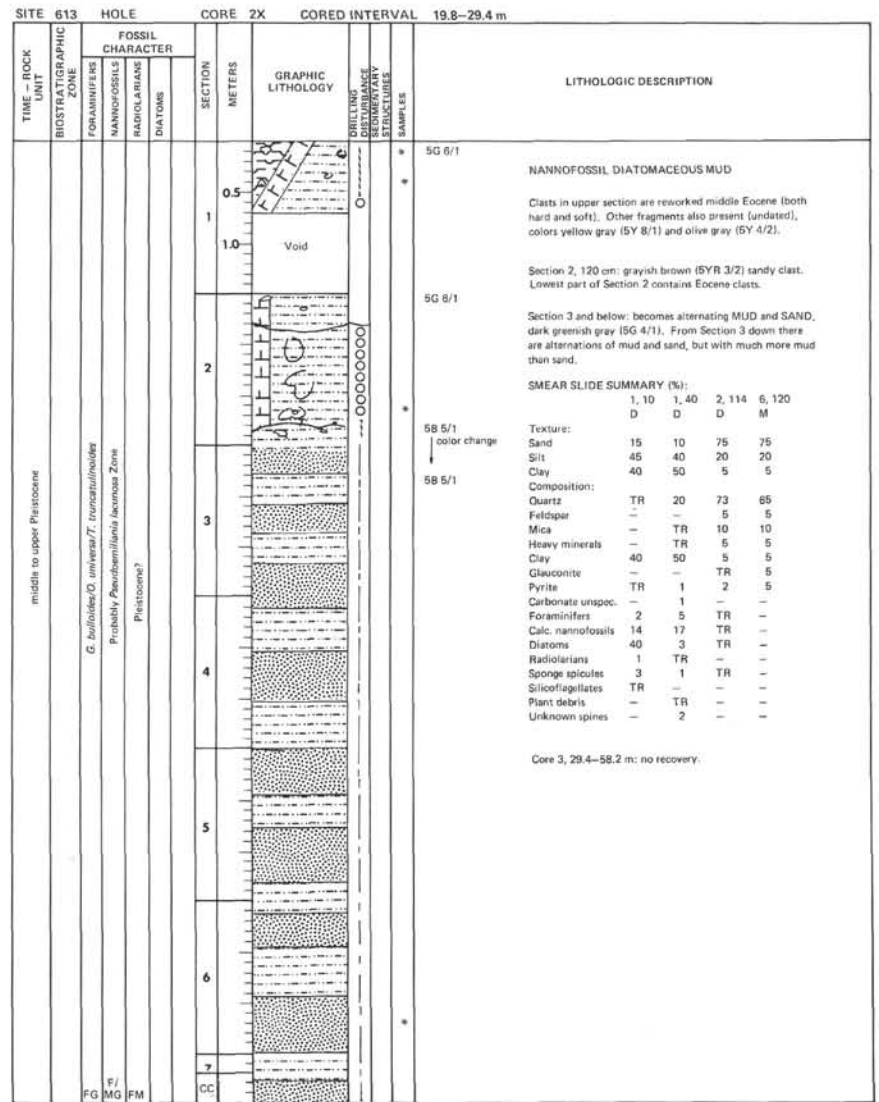
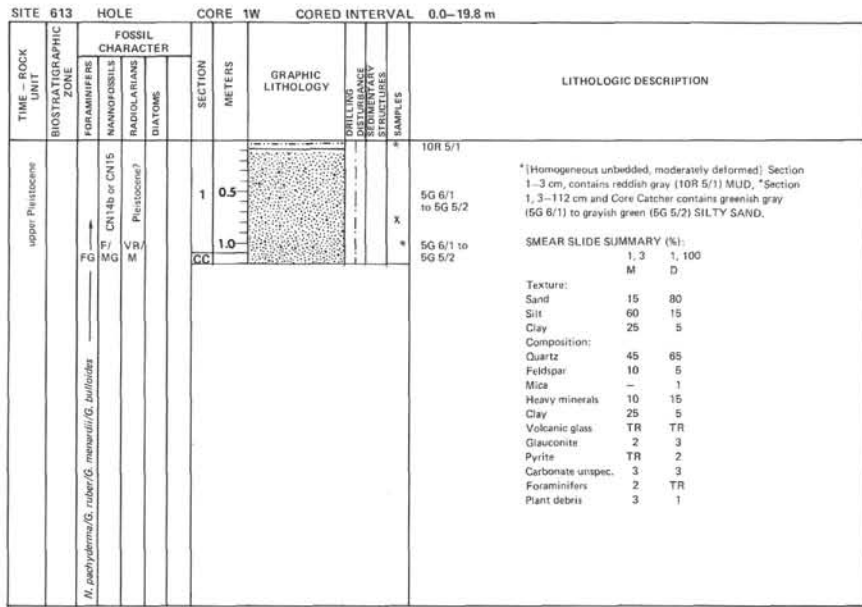
### REFERENCES

- Berggren, W. A., Kent, D. V., Flynn, J. J., and Van Couvering, J., 1985. Cenozoic geochronology. *Geol. Soc. Amer. Bull.*, 96:1407-1418.
- Blow, W. H., 1979. *The Cainozoic Globigerinida*: Leiden (E. J. Brill).
- Boyce, R. E., 1976. I. Definitions and laboratory techniques of compressional sound velocity parameters and wet-water content, wet-bulk density, and porosity parameters by gravimetric and gamma ray attenuation techniques. In Schlanger, S. O., Jackson, E. D., et al., *Init. Repts. DSDP*, 33: Washington (U.S. Govt. Printing Office), 931-958.
- Bukry, D., 1973. Low-latitude coccolith biostratigraphic zonation. In Edgar, N. T., Saunders, J. B., et al., *Init. Repts. DSDP*, 15: Washington (U.S. Govt. Printing Office), 685-703.
- , 1975. Coccolith and silicoflagellate stratigraphy, northwestern Pacific Ocean. In Larson, R. L., Moberly, R., et al., *Init. Repts. DSDP*, 32: Washington (U.S. Govt. Printing Office), 677-701.
- Gartner, S., 1977. Calcareous nannofossil biostratigraphy and revised zonation of the Pleistocene. *Mar. Micropaleontol.*, 2:1-25.
- Howarth, R. W. and Jørgensen, B. B., in press. Formation of  $^{35}\text{S}$ -labeled elemental sulfur and pyrite in coastal marine sediments (Limfjorden and Kysing Fjord, Denmark) during short-term  $^{35}\text{SO}_4^{2-}$  reduction measurements. *Geochim. Cosmochim. Acta*.
- Miller, K. G., and Lohmann, G. P., 1982. Environmental distribution of recent benthic foraminifera on the northeast U.S. continental slope. *Geol. Soc. Am. Bull.*, 93:200-206.
- Morley, J. J., and Hays, J. D., 1979. *Cycladophora davisiana*: a stratigraphic tool for Pleistocene North Atlantic and interhemispherical correlation. *Earth Planet. Sci. Lett.*, 44:383-389.
- Mountain, G. S., and Tucholke, B. E., 1985. Mesozoic and Cenozoic stratigraphy of the U.S. Atlantic continental slope and rise. In Poag, C. W. (Ed.), *Geological Evolution of the United States Atlantic Margin*: New York (Van Nostrand Reinhold), pp. 293-341.
- Okada, H., and Bukry, D., 1980. Supplementary modification and introduction of code numbers to the low-latitude coccolith biostratigraphic zonation (Bukry, 1973; 1975). *Mar. Micropaleontol.*, 5:321-325.
- Poag, C. W., 1978. Stratigraphy of the Atlantic continental shelf and slope of the United States. *Ann. Rev. Earth Planet. Sci.*, 6:251-280.
- Riedel, W. R., and Sanfilippo, A., 1978. Stratigraphy and evolution of tropical Cenozoic radiolarians. *Micropaleontology*, 24:61-96.
- Robb, J. M., Kirby, J. C., Hampson, J. R., Jr., Gibson, P. R., and Hecker, B., 1983. Furrowed outcrops of Eocene chalk on the lower continental slope offshore New Jersey. *Geology*, 11:182-186.
- Sayles, F. L., and Manheim, F. T., 1975. Interstitial solutions and diagenesis in deeply buried sediments: results from the Deep Sea Drilling Project. *Geochim. Cosmochim. Acta*, 39:103-127.
- Schlee, J. S., and Grow, J. A., 1980. Seismic stratigraphy in the vicinity of the COST No. B-3 well, United States Mid-Atlantic Continental Slope area. *U.S. Geol. Surv. Circ.*, 833:111-116.
- Stainforth, R. M., Lamb, J. L., Luterbacher, H., Beard, J. H., and Jeffords, R. M., 1975. Cenozoic planktonic foraminiferal zonation and characteristics of index fossils. *Univ. Kansas Paleontol. Contrib.*, 62:1-425.
- Tjalsma, R. C., and Lohmann, G. P., 1983. Paleocene-Eocene bathyal benthic foraminifera from the Atlantic Ocean. *Micropaleontol., Spec. Publ.*, 4:1-90.
- Vail, P. R., Mitchum, R. M., Jr., and Thompson, S., III, 1977. Seismic stratigraphy and global changes of sea level: Part IV: global cycles of relative changes of sea level. In Payton, C. E. (Ed.), *Seismic Stratigraphy—Applications to Hydrocarbon Exploration*. Am. Assoc. Pet. Geol. Mem., 26:83-98.
- van Hinte, J. E., 1976. A Cretaceous time scale. *Am. Assoc. Pet. Geol. Bull.*, 60:498-516.
- Whelan, J. K., 1976.  $\text{C}_1$  to  $\text{C}_7$  hydrocarbons from IPOD Holes 397 and 397A. In von Rad, U., Ryan, W. B. F., et al., *Init. Repts. DSDP*, 47, Pt. 1: Washington (U.S. Govt. Printing Office), 531-540.

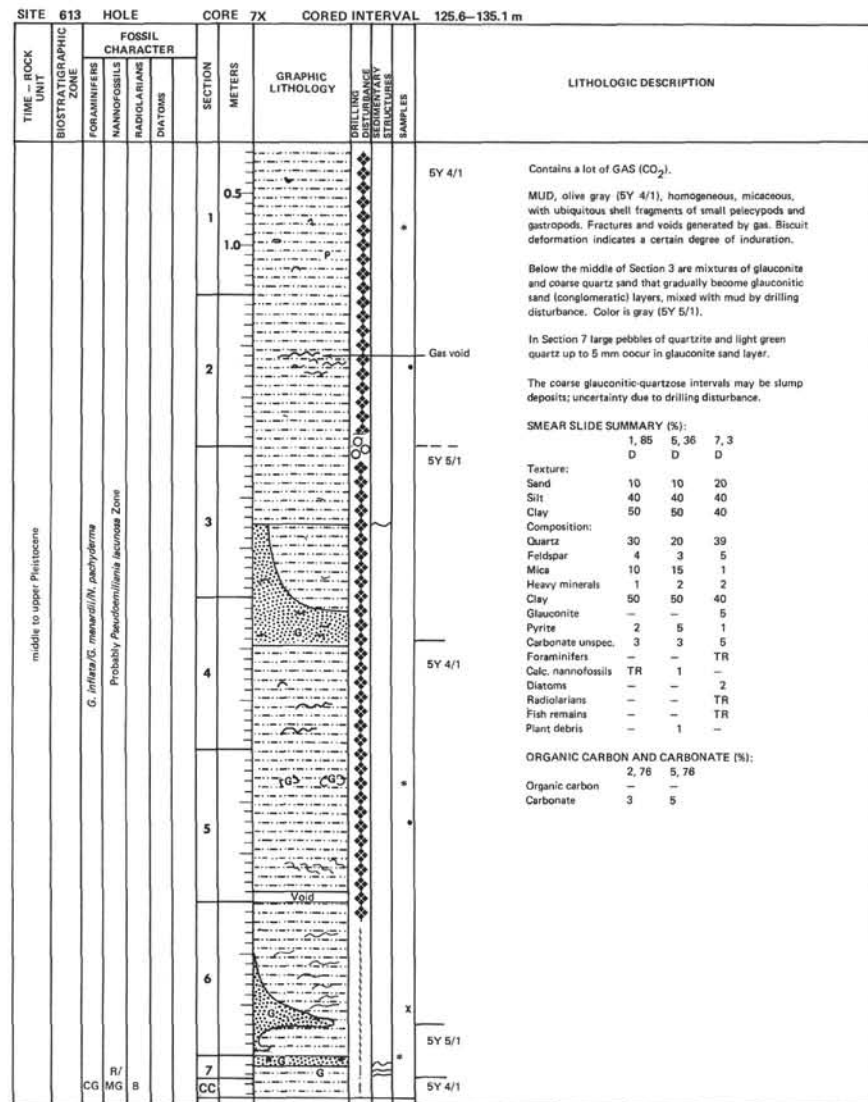
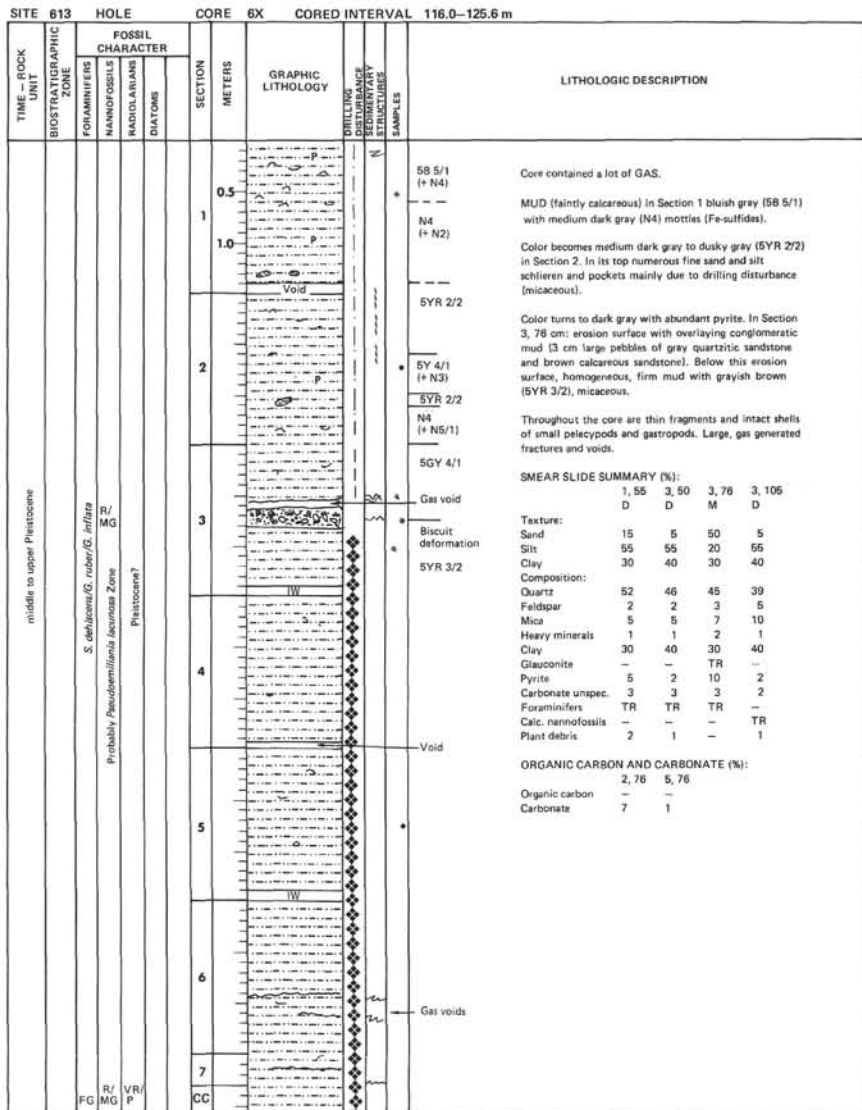


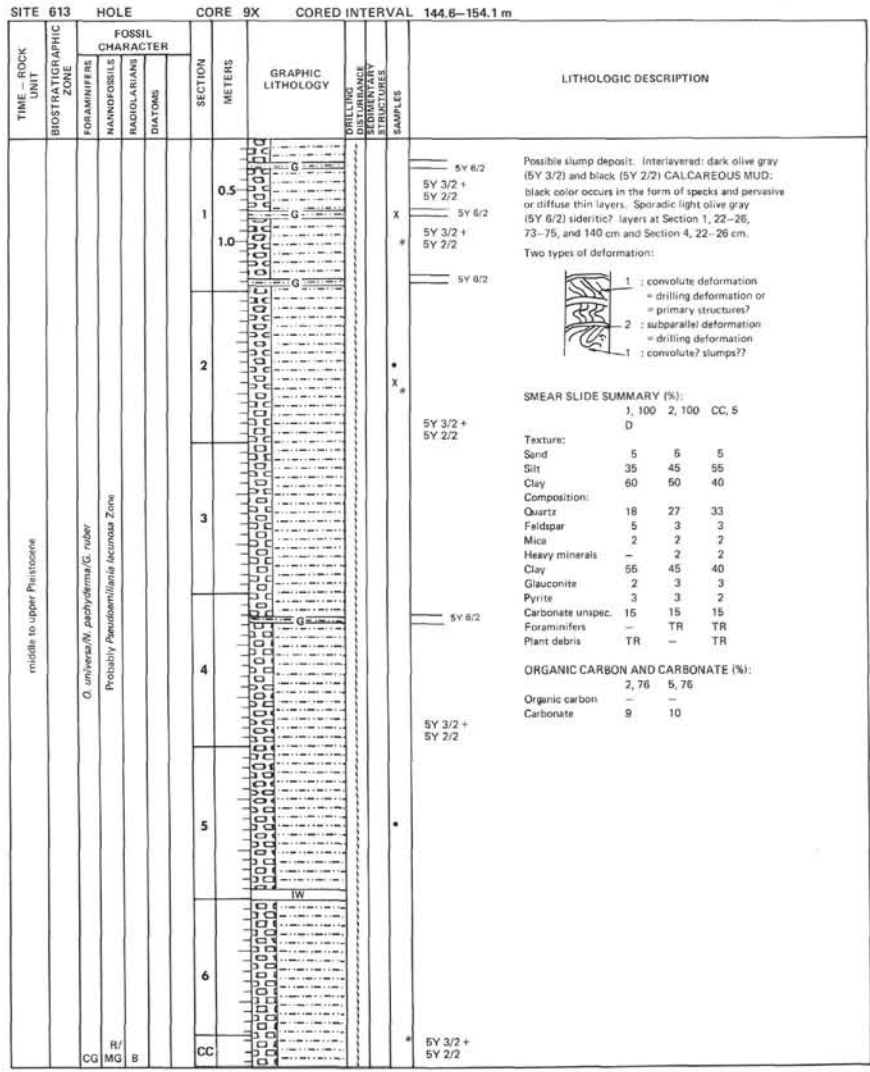
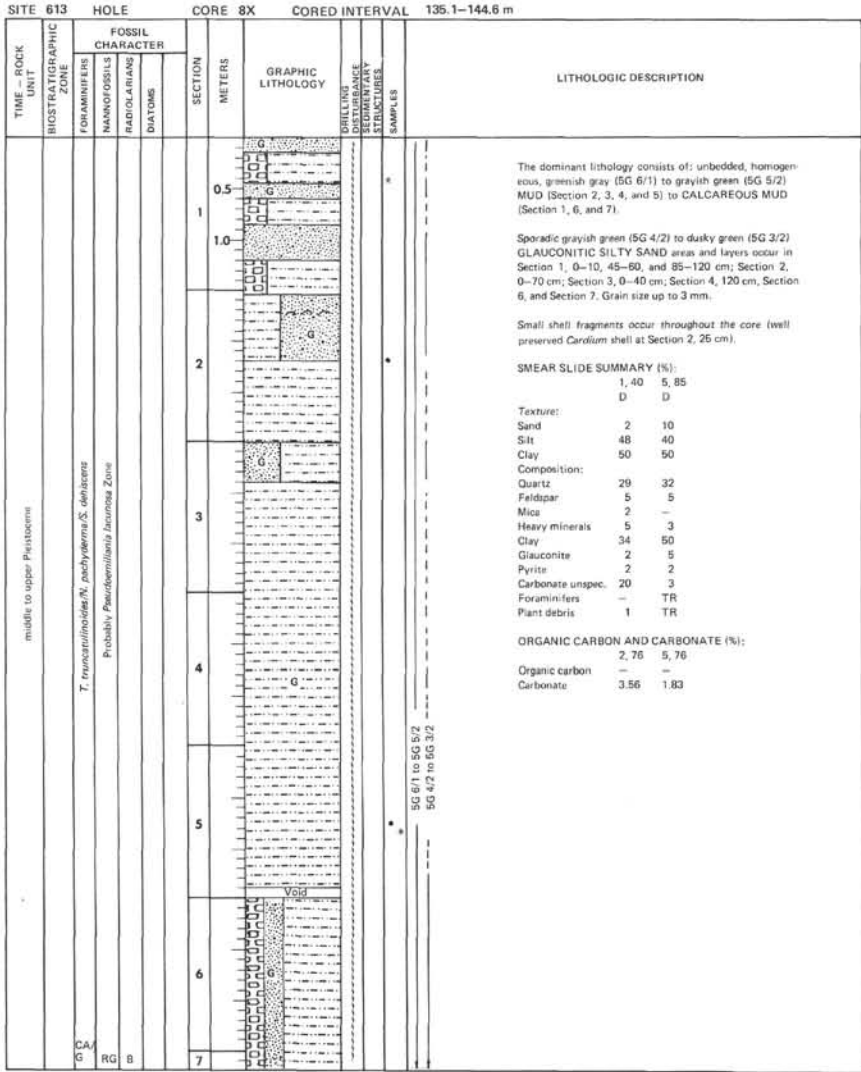
0.5 mm

Plate 1. Porcellanitic nannofossil limestone, Unit III (Sample 613-41-4, 10-12 cm). Radiolarian opaline tests are dissolved; open spaces in radiolarian and planktonic foraminifer tests are filled with sparry calcite and opal-CT. Clayey limestone matrix is cemented by opal-CT and calcite. Partially crossed nicols.

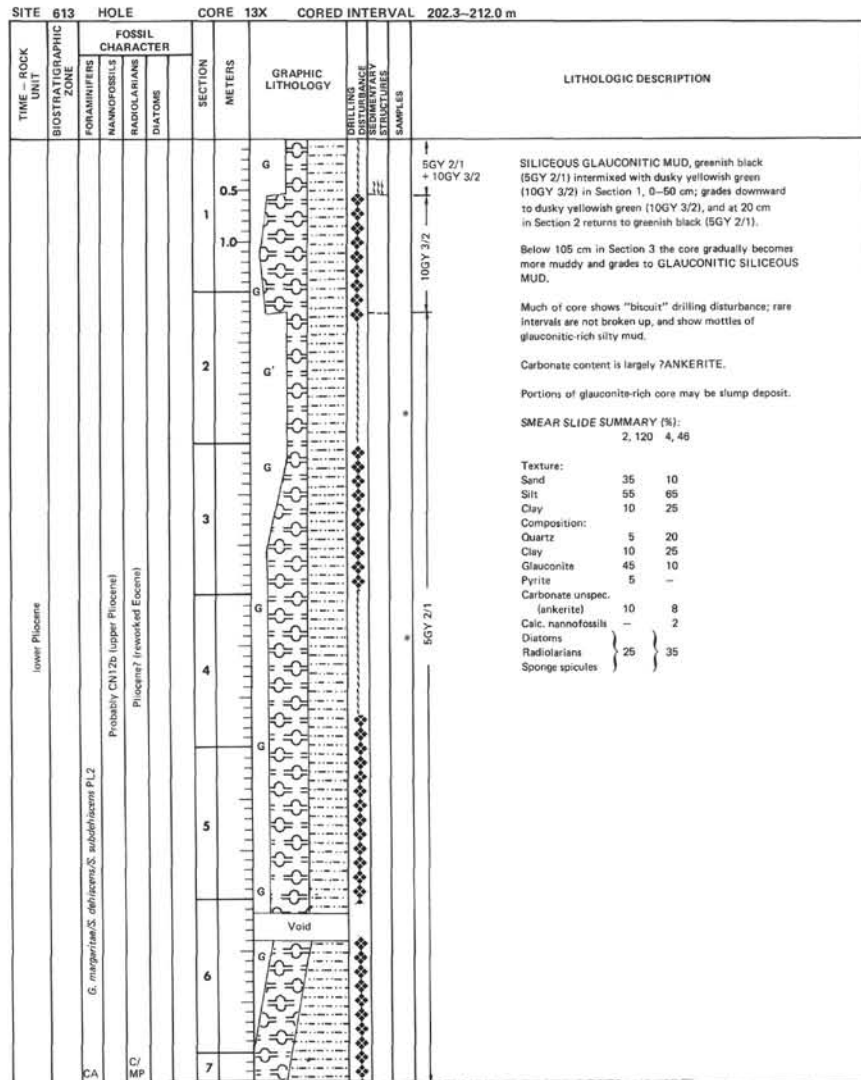
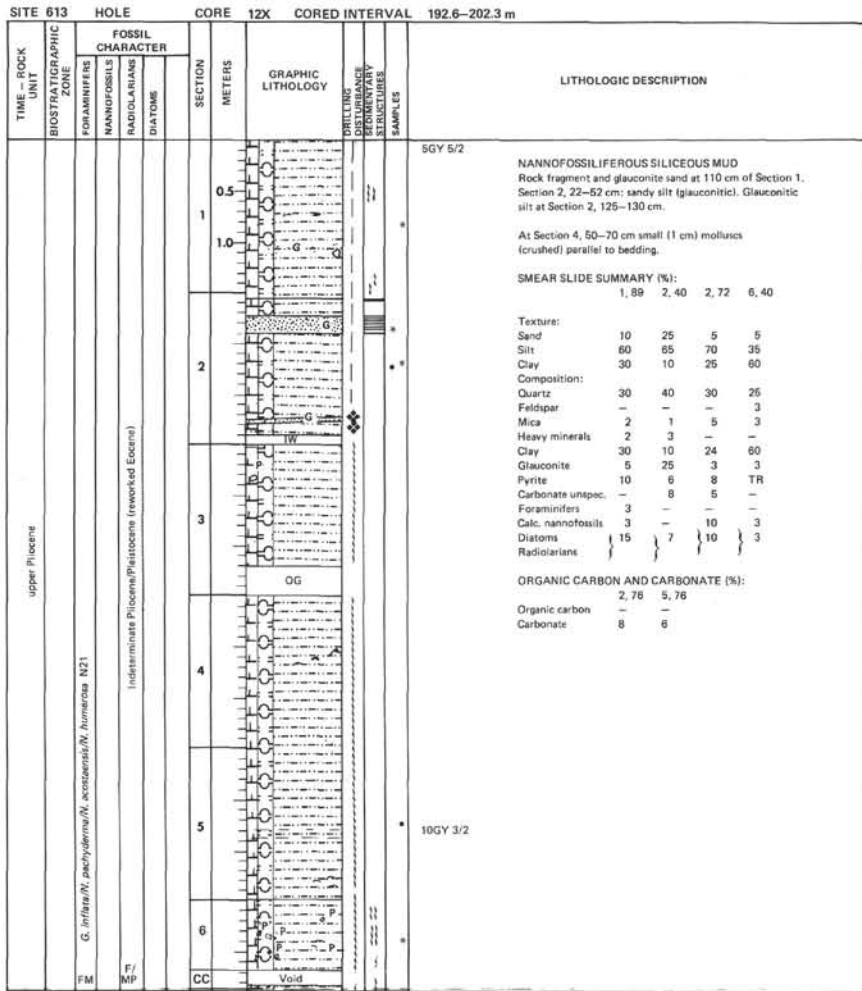












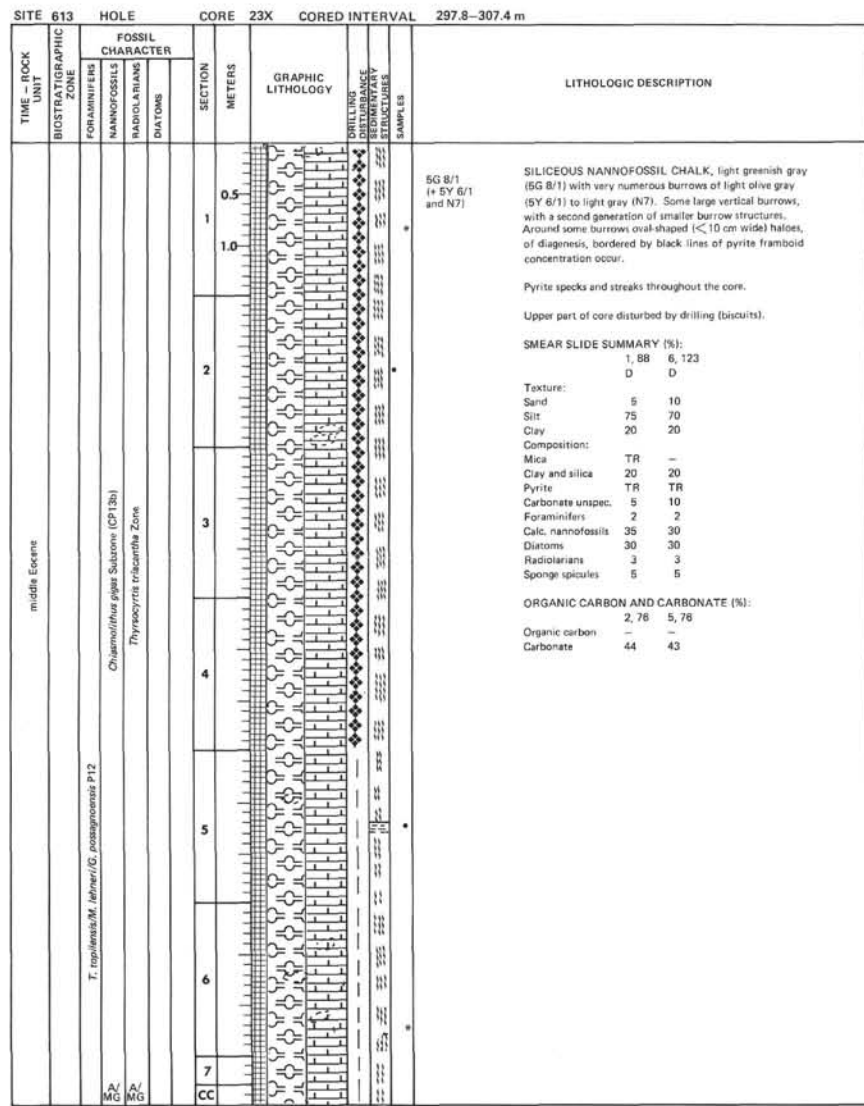
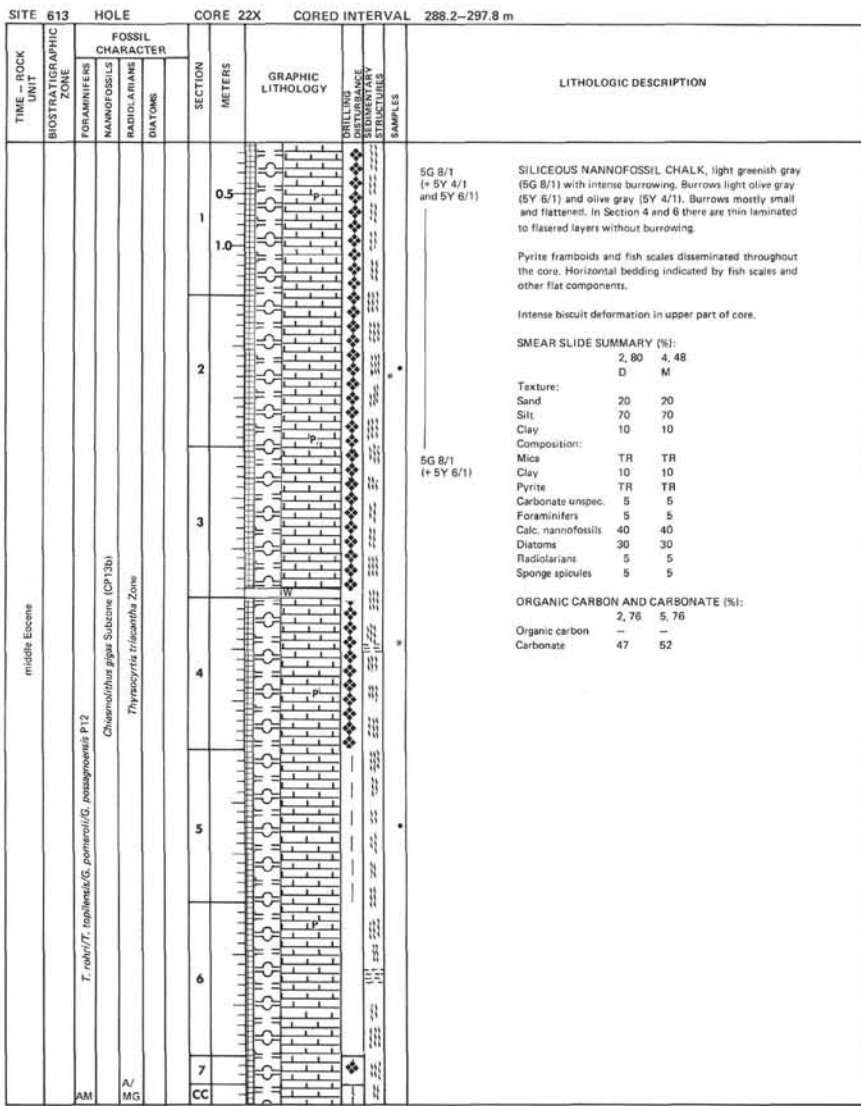


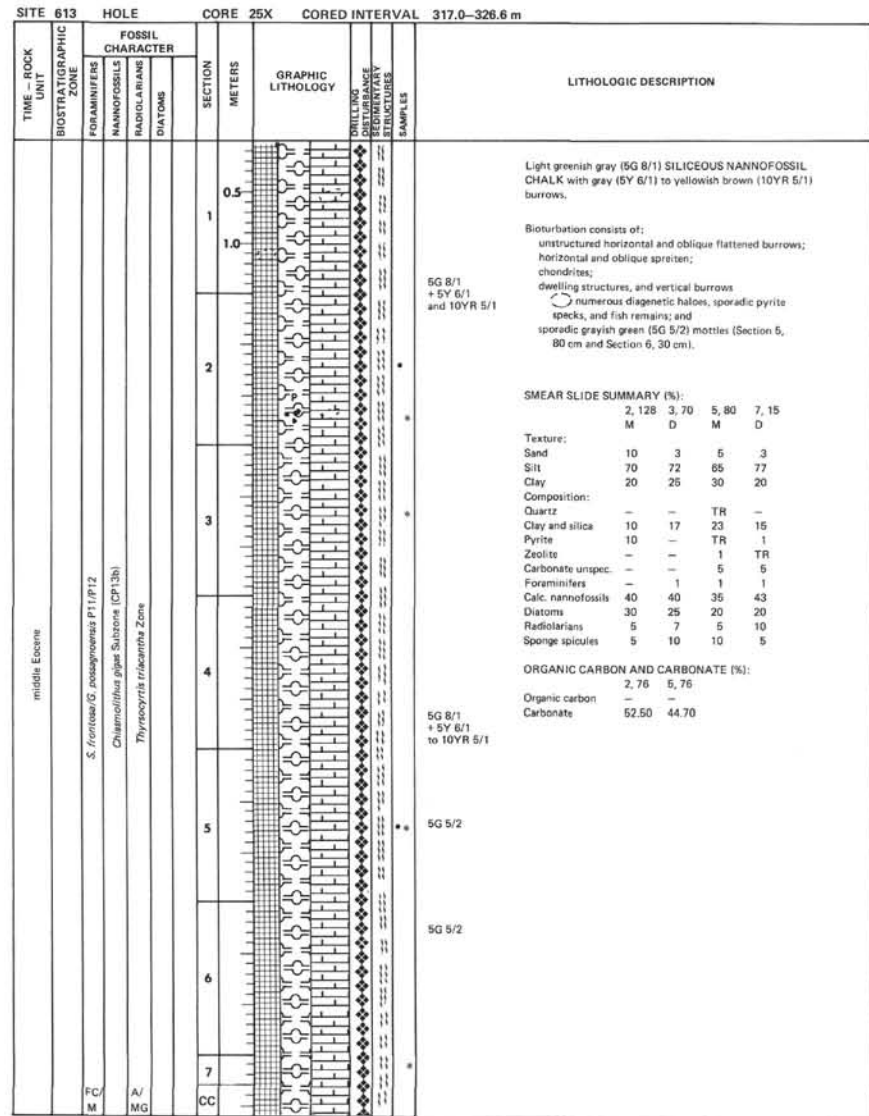
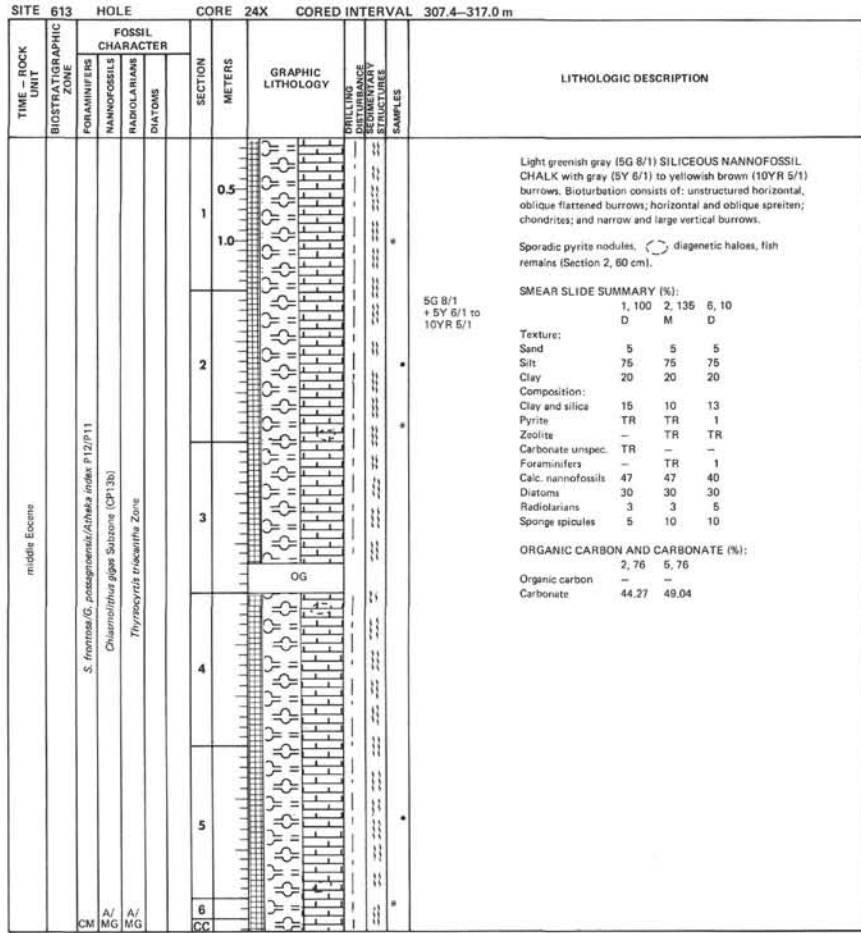


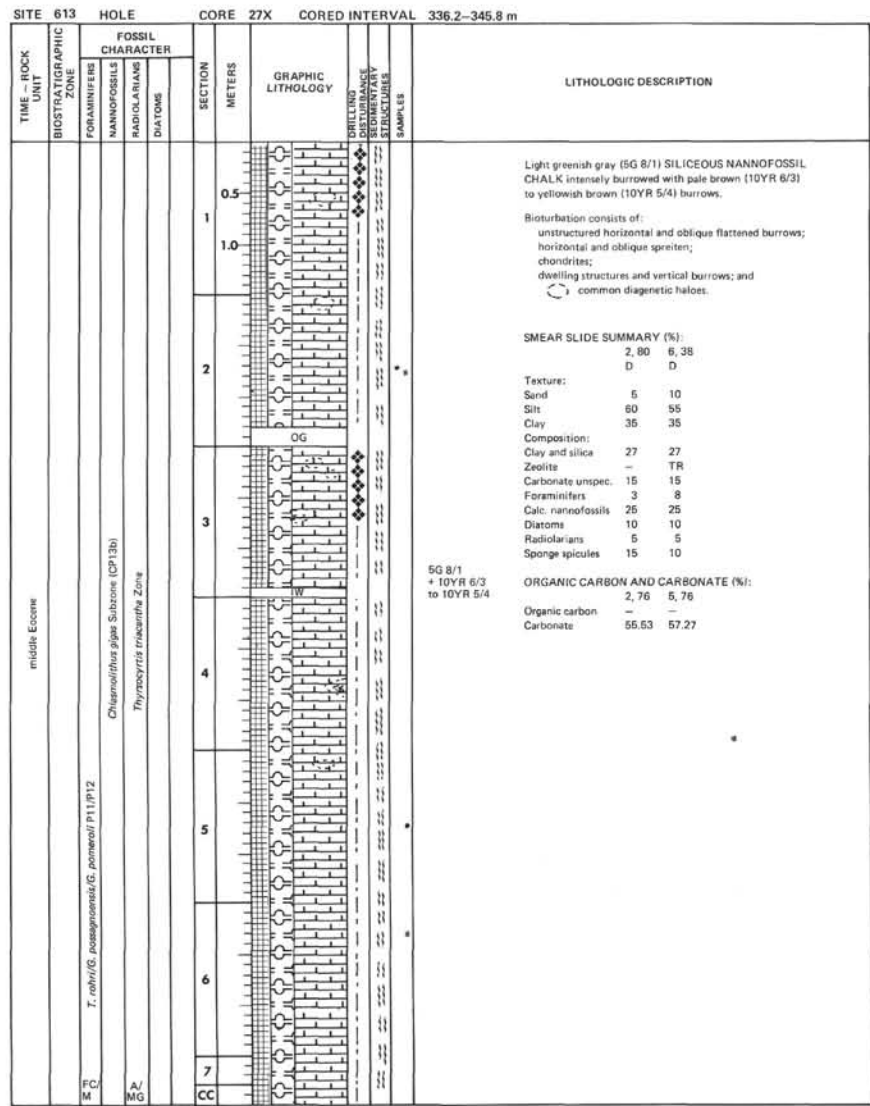
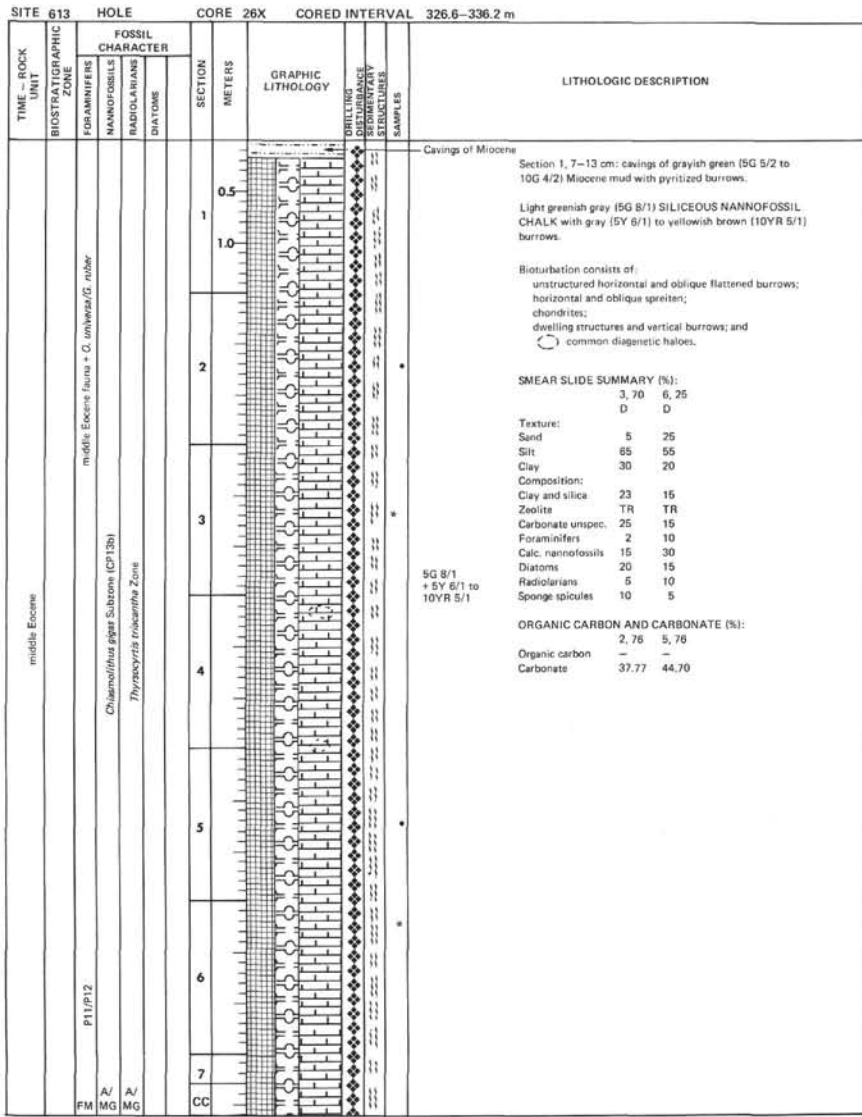


SITE 613 HOLE		CORE 20X		CORED INTERVAL 269.0-278.6 m					
TIME - ROCK UNIT	BIOSTRATIGRAPHIC ZONE	FOSSIL CHARACTER			SECTION METERS	LITHOLOGIC DESCRIPTION			
		FORAMINIFERS	NANNOFOSSILS	RADIOLARIANS			DIATOMS		
middle Eocene	CG AM	<i>T. rohrli/M. spinulosum/T. topilensis/M. lehneri</i> P12	Chamaethururgles Subzone (CP13b)		CC	5GY 7/2 (+ 5Y 6/1)			
			Thyrocypris triacantha Zone						
<p>SILICEOUS NANNOFOSSIL CHALK, grayish yellow green (5GY 7/2), intensely burrowed. Burrow structures filled with light olive gray (5Y 6/1) to greenish gray (5GY 6/1) siliceous chalk. Burrows slightly flattened.</p> <p>The clay-size fraction of this core and all of those down to Core 37 of Site 613 contains an undetermined amount of biogenic opal-A, and is identified by IIIII in the graphic lithology column.</p> <p><b>SMEAR SLIDE SUMMARY (%):</b></p> <table border="1"> <tr><td>CC</td><td>7</td></tr> <tr><td>D</td><td></td></tr> </table> <p>Texture:</p> <p>Sand 5 Silt 75 Clay 20</p> <p>Composition:</p> <p>Quartz 1 Clay and silica 20 Volcanic glass TR Zeolite TR Foraminifers TR Calc. nannofossils 66 Diatoms 10 Radiolarians 1 Sponge spicules 2 Plant debris TR</p>						CC	7	D	
CC	7								
D									

SITE 613 HOLE		CORE 21X		CORED INTERVAL 278.6-288.2 m													
TIME - ROCK UNIT	BIOSTRATIGRAPHIC ZONE	FOSSIL CHARACTER			SECTION METERS	LITHOLOGIC DESCRIPTION											
		FORAMINIFERS	NANNOFOSSILS	RADIOLARIANS			DIATOMS										
middle Eocene	CM AM	<i>T. topilensis/G. potapovensis/M. cf. lehneri</i> P12	Chamaethururgles Subzone (CP13b)		CC	5GY 8/1 (+ 10YR 5/2 and 5Y 6/1)											
			Thyrocypris triacantha Zone														
<p>SILICEOUS NANNOFOSSIL CHALK, light greenish gray (5GY 8/1) with numerous burrows of grayish brown (10YR 5/2) to light olive gray (5Y 6/1). Matrix color grades at bottom to light gray (N7) with burrows greenish gray (5G 6/1) and olive gray. Pyrite occurs as framboids throughout the core, rare nodules. Burrows more or less flattened. Main types: horizontal and diagonal "spreiten"/planolites/large diagonal to vertical pear-shaped dwellings/rare chondrites (see Site 612). Intense biscuit deformation in top of core.</p> <p><b>SMEAR SLIDE SUMMARY (%):</b></p> <table border="1"> <tr><td>1, 64</td><td>1, 102</td><td>6, 120</td></tr> <tr><td>M</td><td>D</td><td>D</td></tr> </table> <p>Texture:</p> <p>Sand 20 20 20 Silt 70 70 70 Clay 10 10 10</p> <p>Composition:</p> <p>Mica TR TR TR Clay and silica 10 10 10 Pyrite TR TR TR Carbonate unsp. 5 5 5 Foraminifers 5 5 5 Calc. nannofossils 40 40 40 Diatoms 35 35 30 Radiolarians - - 5 Sponge spicules 5 5 5 Fish remains TR - -</p> <p><b>ORGANIC CARBON AND CARBONATE (%):</b></p> <table border="1"> <tr><td>2, 76</td><td>5, 76</td></tr> <tr><td>Organic carbon</td><td>-</td></tr> <tr><td>Carbonate</td><td>39 40</td></tr> </table>						1, 64	1, 102	6, 120	M	D	D	2, 76	5, 76	Organic carbon	-	Carbonate	39 40
1, 64	1, 102	6, 120															
M	D	D															
2, 76	5, 76																
Organic carbon	-																
Carbonate	39 40																

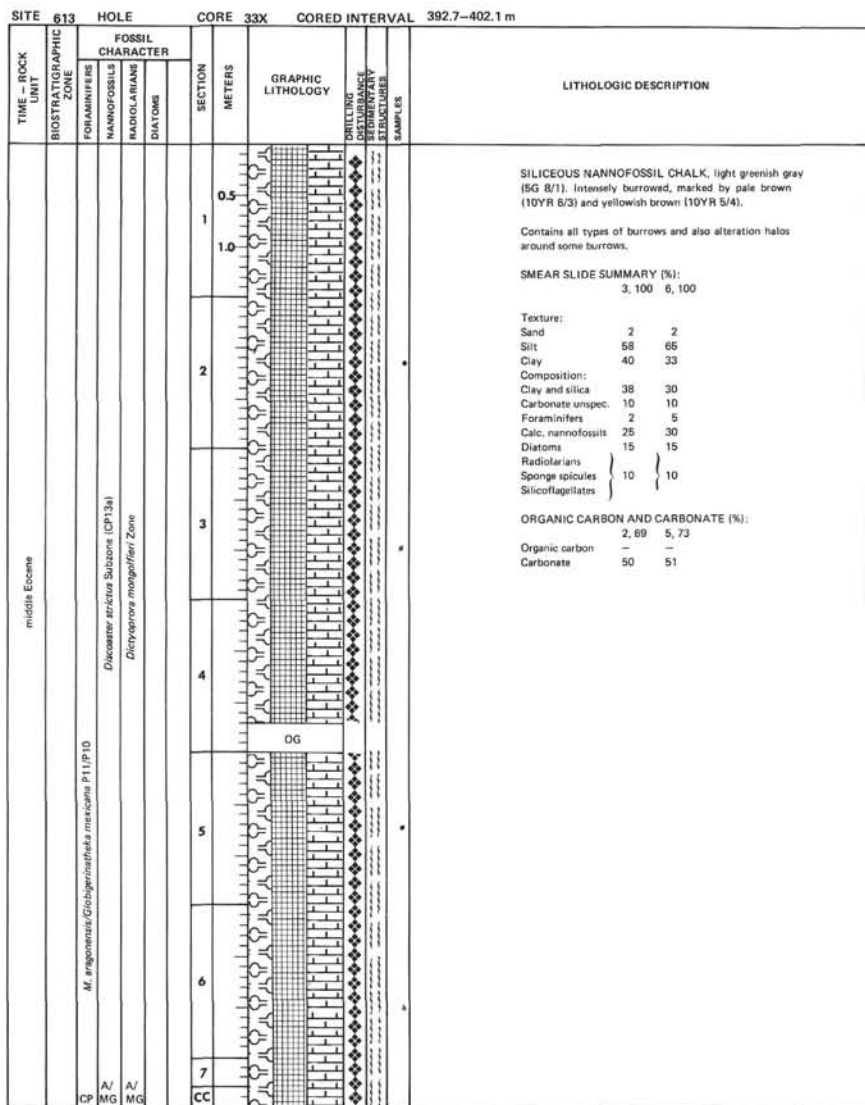
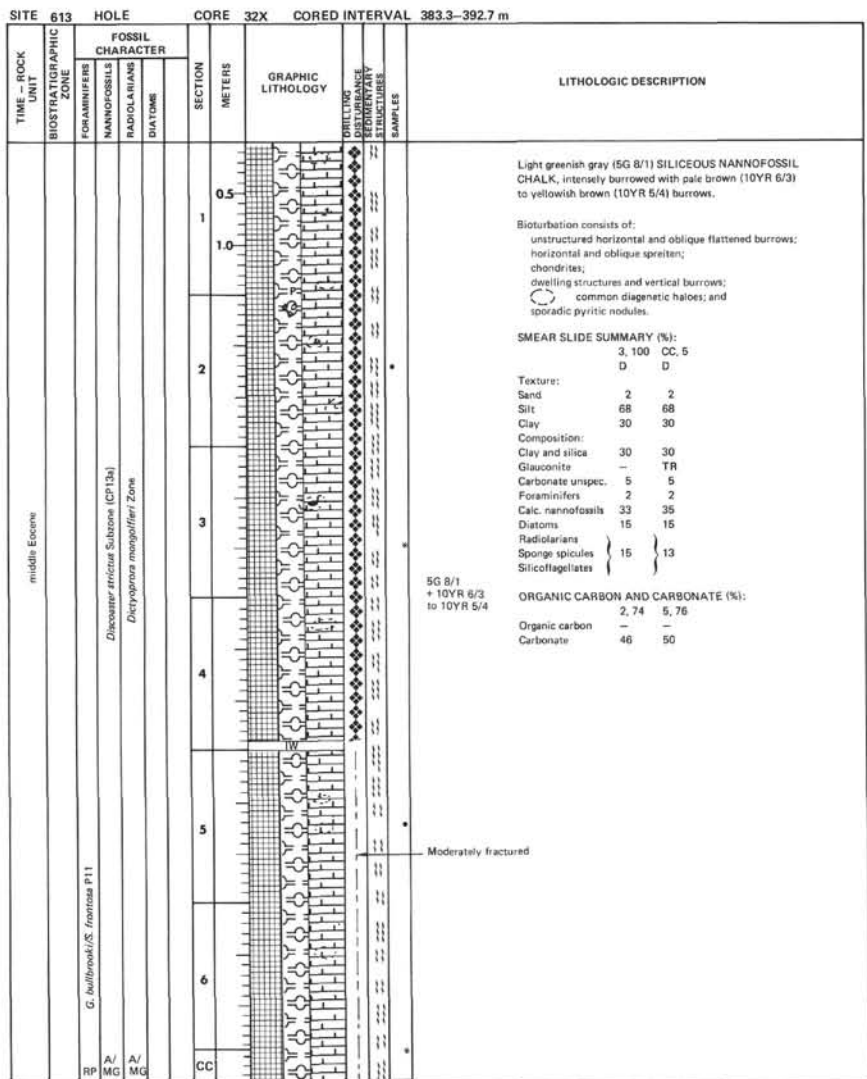


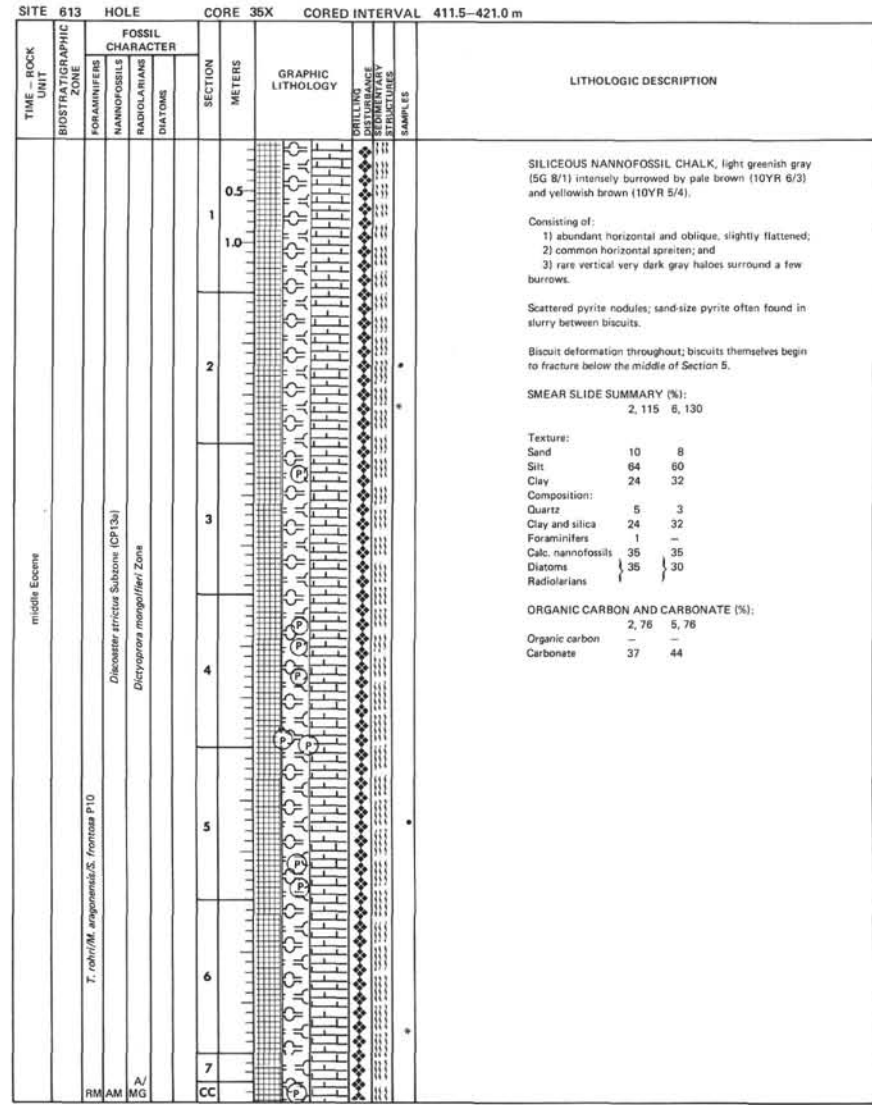
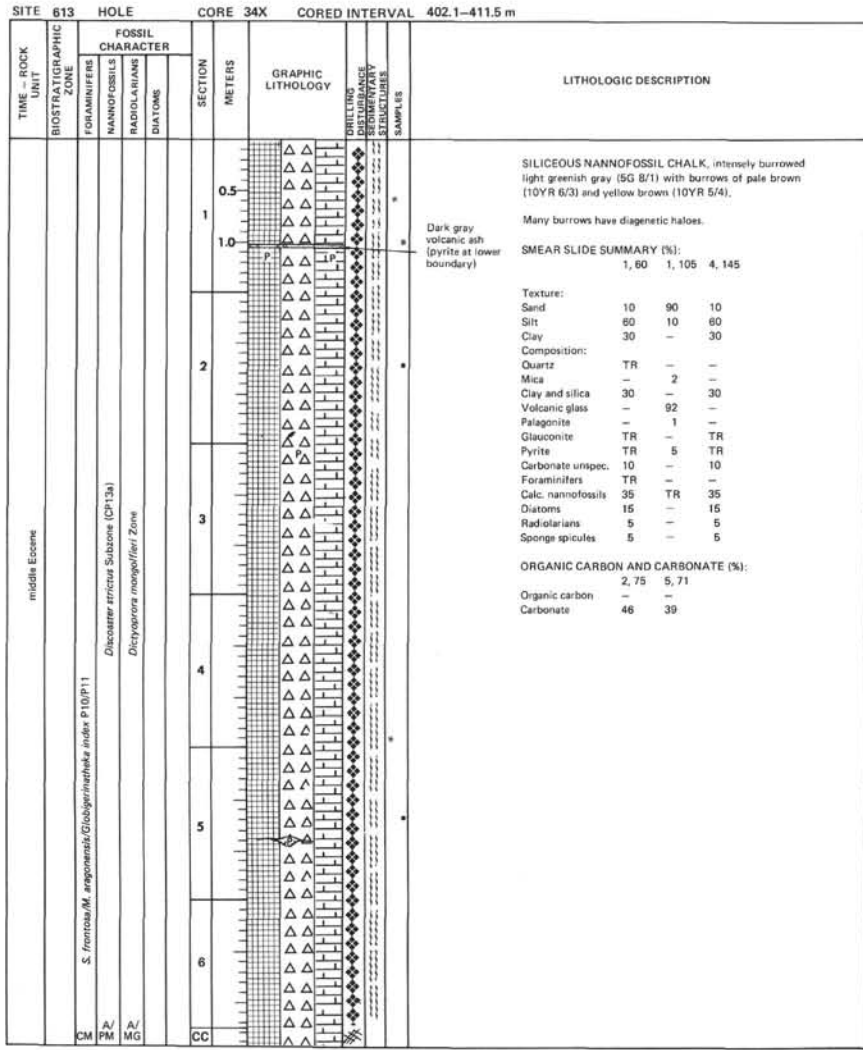


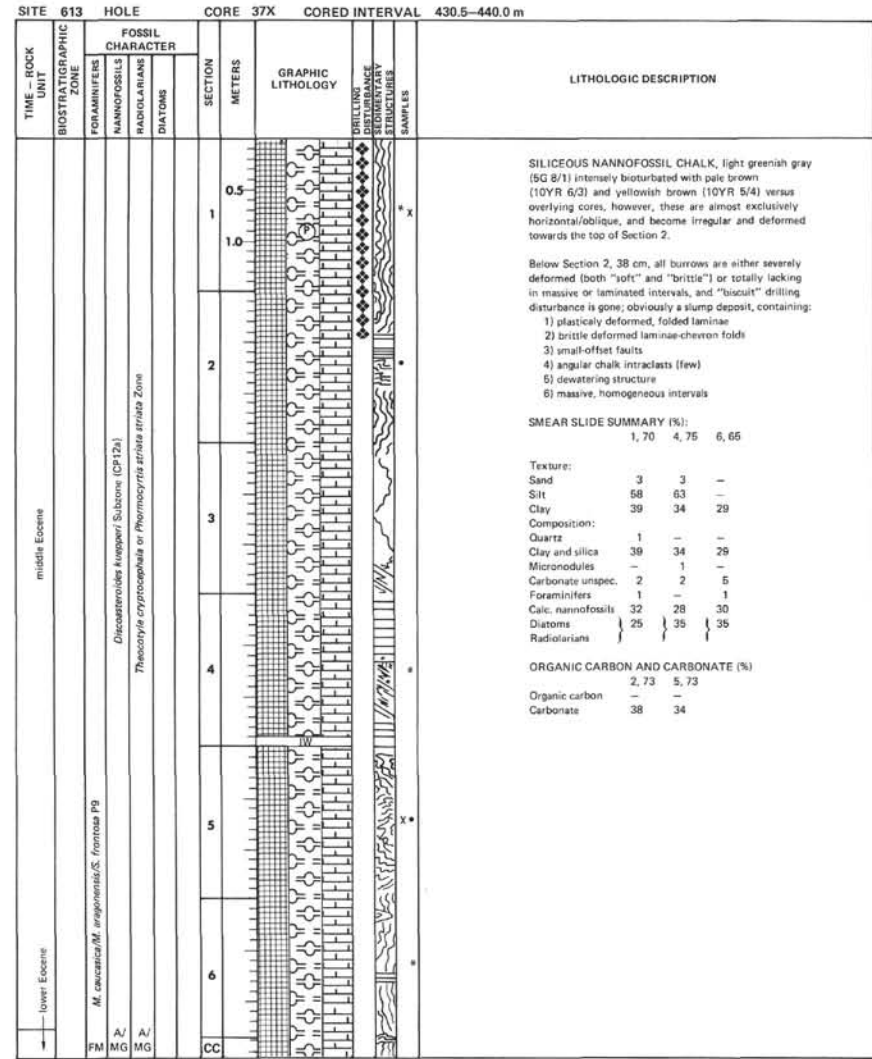
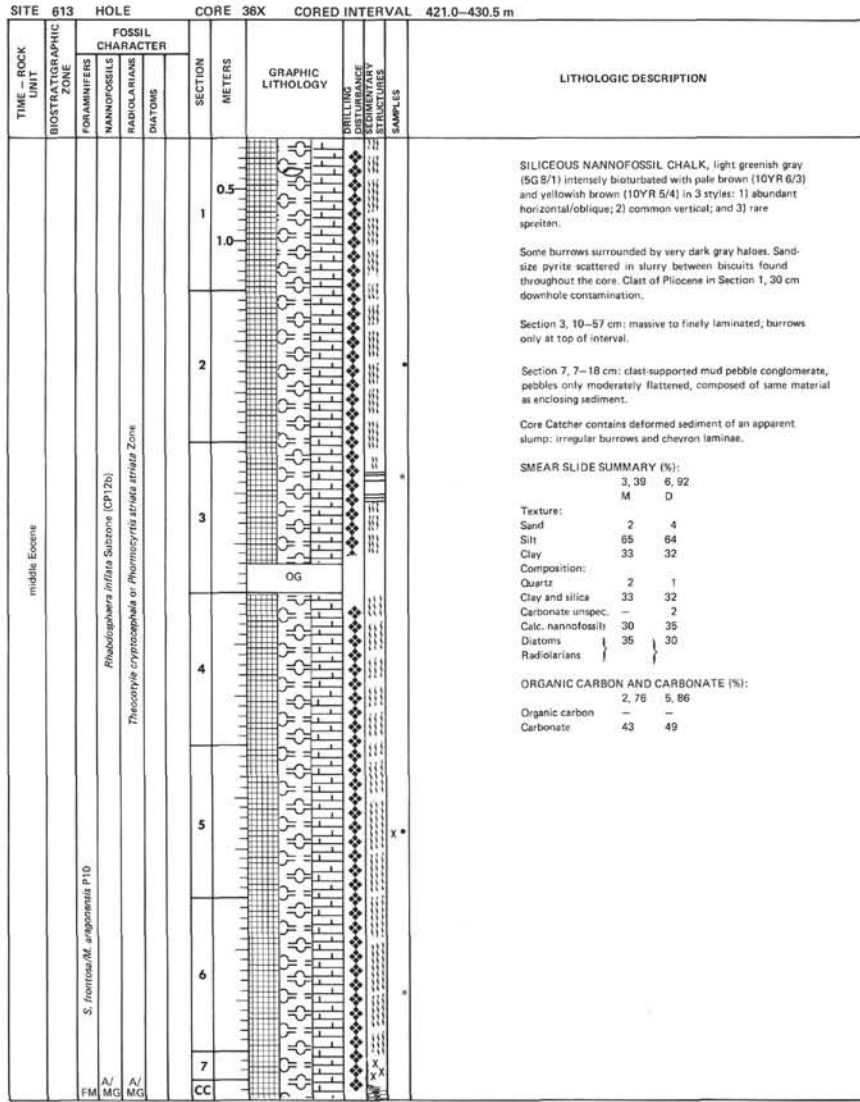


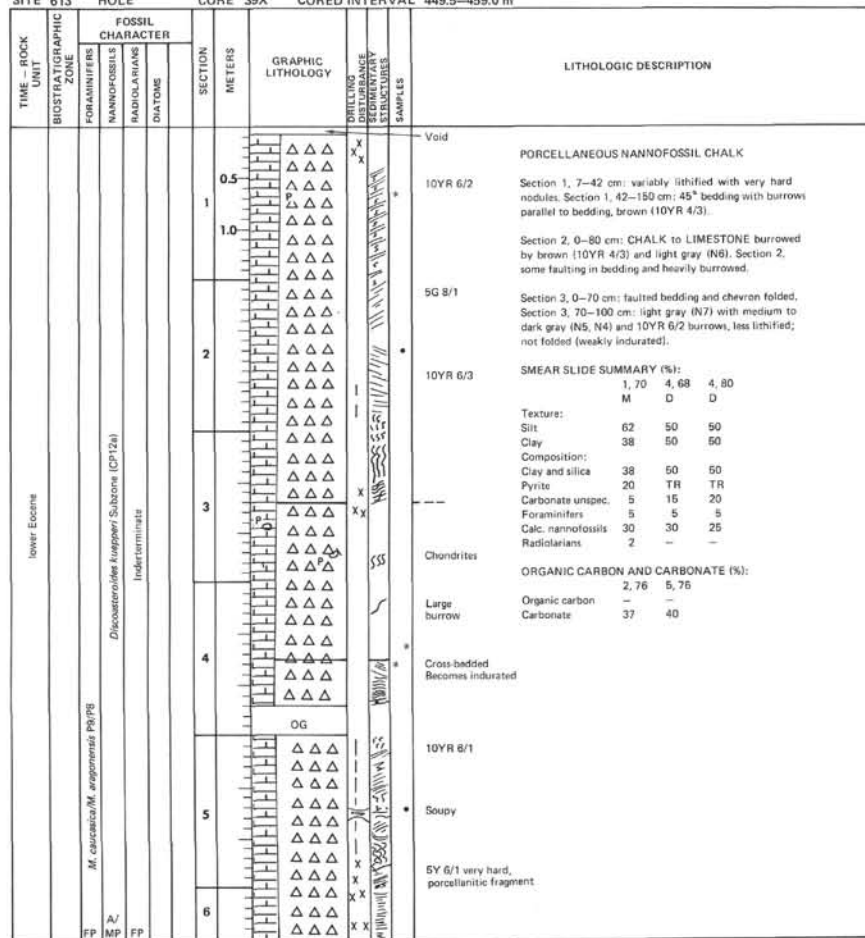
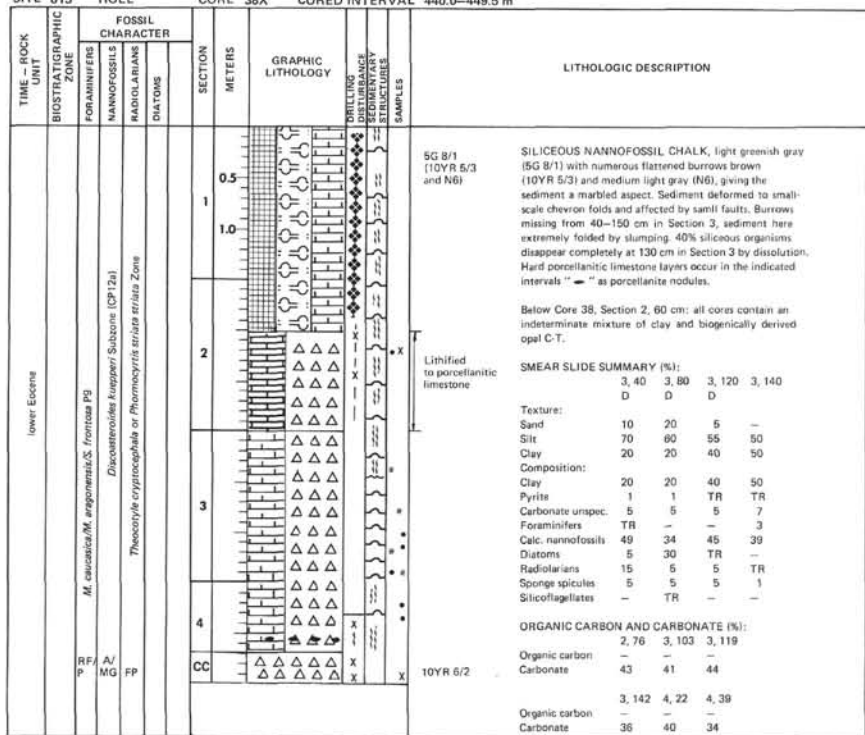








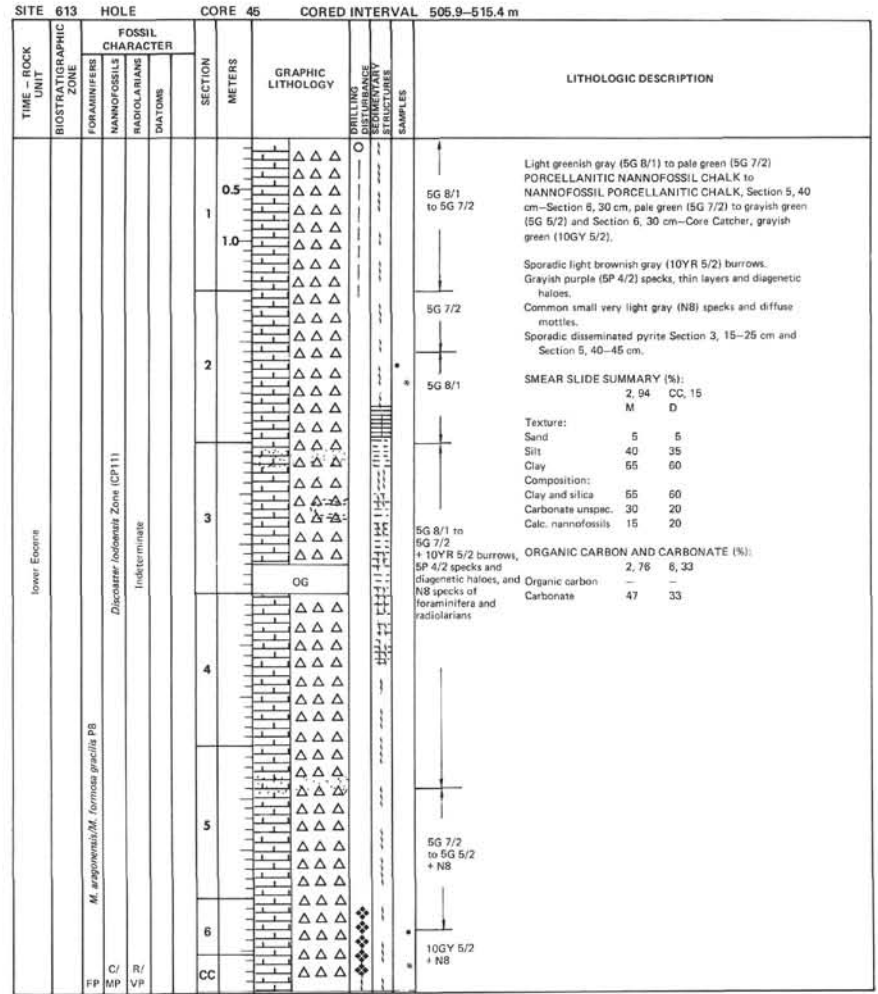
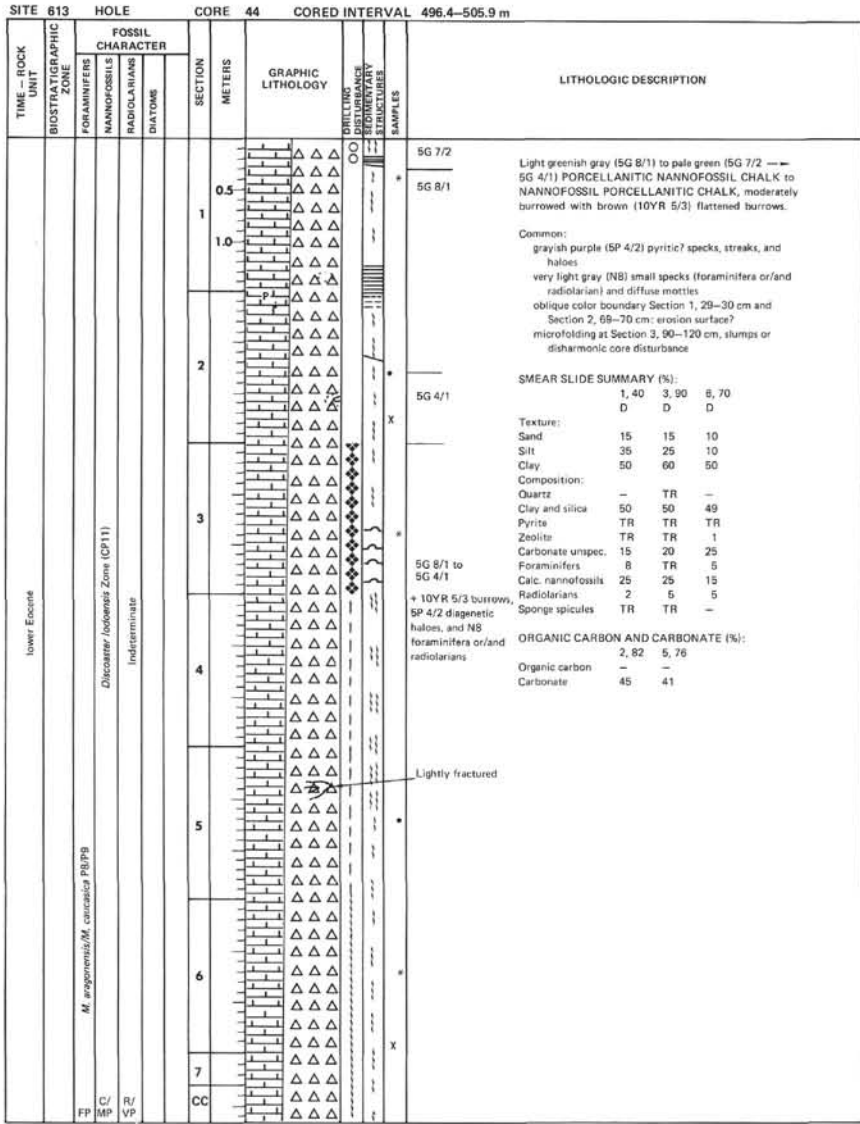




SITE 613		HOLE		CORE 40X		CORED INTERVAL 459.0-468.5 m	
TIME - ROCK UNIT	BIOSTRATIGRAPHIC ZONE	FOSSIL CHARACTER			SECTION METERS	GRAPHIC LITHOLOGY	LITHOLOGIC DESCRIPTION
		FORAMINIFERS	NANNOFOSSILS	RADIOLARIANS			
lower Eocene	PR/PB	FC	FC	VR	1		N7 + 10YR 5/3 N7 (10YR 5/3)  PORCELLANITIC NANNOFOSSIL LIMESTONE, light gray (N7) with burrows of brown (10YR 5/3). Medium gray specks and streaks with pyrite framboids.  SMEAR SLIDE SUMMARY (%): CC, 18  Texture: Sand 5 Silt 55 Clay 40 Composition: Clay and silica 40 Carbonate unspec. 10 Calc. nannofossils 30 Diatoms 10 Radiolarians 5 Sponge spicules 5
		FC	FC	VR			

SITE 613		HOLE		CORE 41X		CORED INTERVAL 468.5-477.8 m	
TIME - ROCK UNIT	BIOSTRATIGRAPHIC ZONE	FOSSIL CHARACTER			SECTION METERS	GRAPHIC LITHOLOGY	LITHOLOGIC DESCRIPTION
		FORAMINIFERS	NANNOFOSSILS	RADIOLARIANS			
lower Eocene	RM	M. caucasicola/M. angipennata	PR/PB	Indeterminate	7		N7 + 10YR 5/3 N7 (10YR 5/3)  PORCELLANITIC NANNOFOSSIL LIMESTONE, light greenish gray (5G 5/1) and light gray (N7 to 10YR 5/1) intensely burrowed. Burrows brown (10YR 4/3). Burrows often surrounded by large bleached haloes with black outer rim of pyrite framboids.  About 10% of sand-sized foraminifera enriched in layers throughout the core.  Many dark gray (N4) specks and thin streaks of pyrite framboids.  SMEAR SLIDE SUMMARY (%): 1, 15 6, 80 D D  Texture: Silt 50 50 Clay 50 50 Composition: Clay and silica 50 50 Pyrite TR TR Carbonate unspec. 10 10 Foraminifera 10 5 Calc. nannofossils 30 34 Radiolarians TR 1  ORGANIC CARBON AND CARBONATE (%): Organic carbon - - Carbonate 30 35



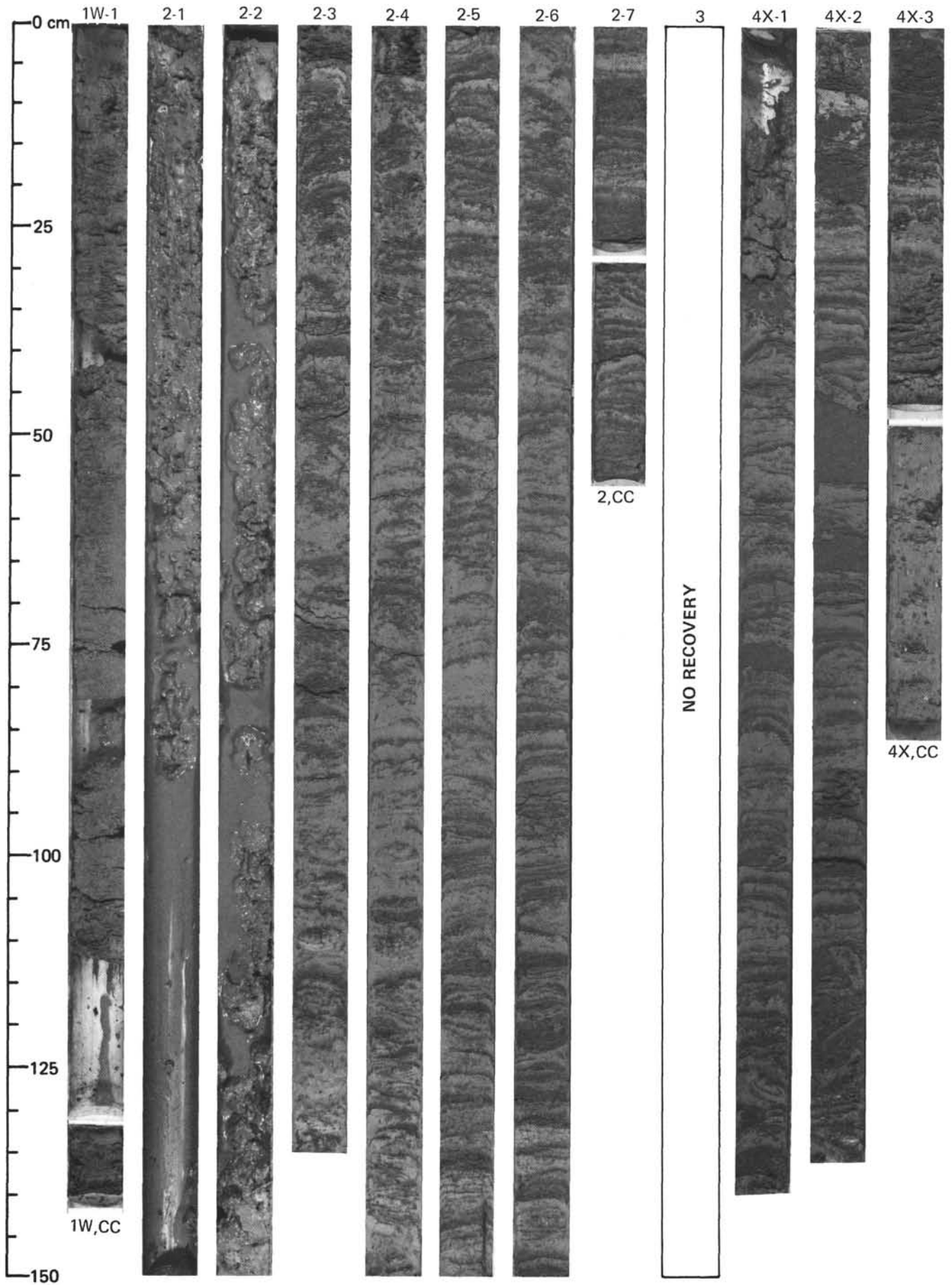


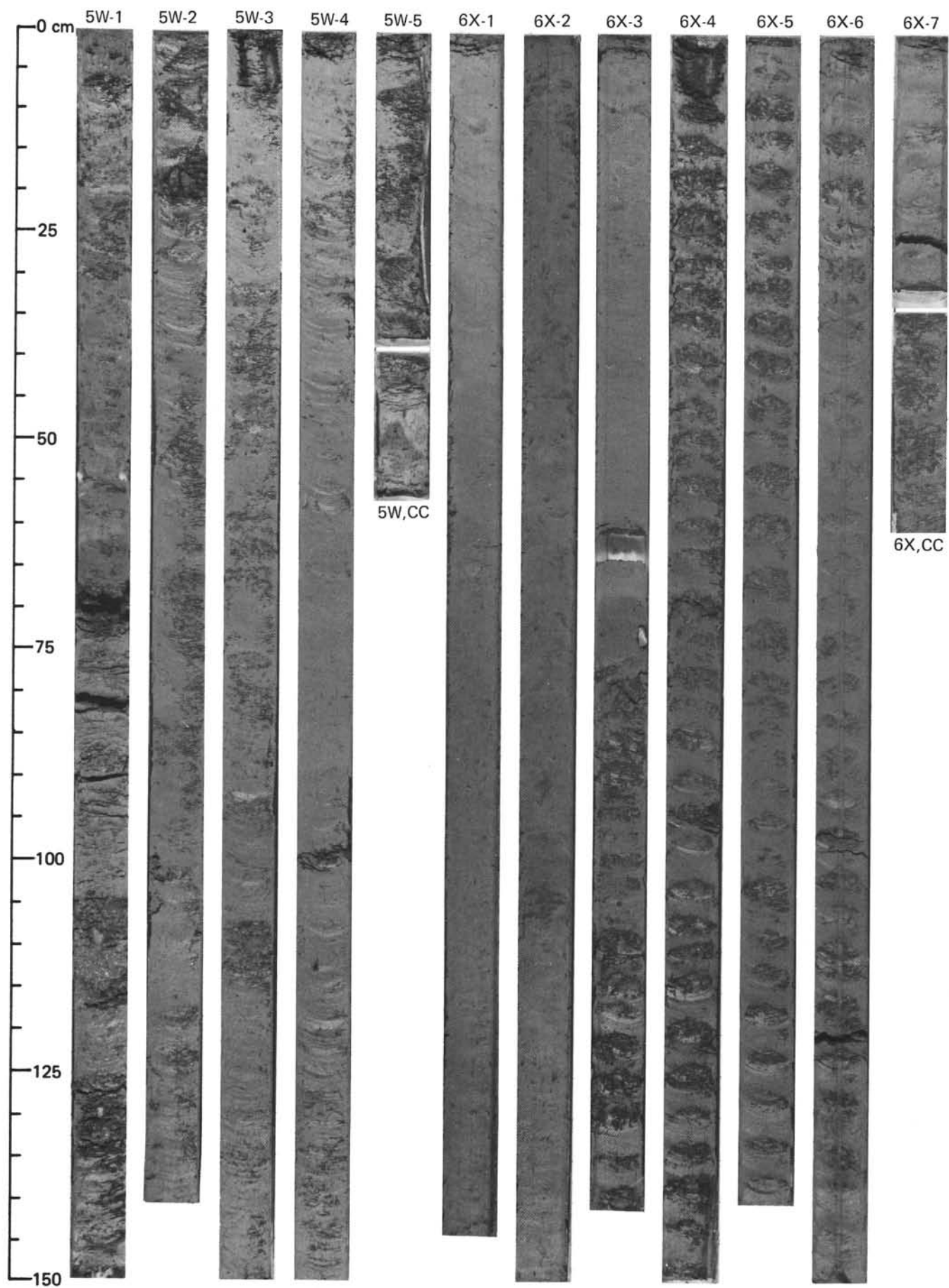




SITE 613		HOLE		CORE 51X		CORED INTERVAL 562.9-572.4 m	
TIME - ROCK UNIT	BIOSTRATIGRAPHIC ZONE	FOSSIL CHARACTER			SECTION METERS	GRAPHIC LITHOLOGY	LITHOLOGIC DESCRIPTION
		FORAMINIFERS	NANNOFOSSILS	RADIOLARIANS			
lower Eocene	M. magnumensis/M. magnumensis Zone (CP9b)	Dicoelaster binodiosus Zone (CP9b)	Bekoma bidertensis Zone		0.5	△△△	10G 6/2
					1	△△△	10GY 7/2
					1.0	△△△	10GY 7/2 + SG 4/1, 5YR 4/1, and EP 2/2
					2	△△△	Large parts of core show crenulated fissile structures, probably due to in situ creep (or to drilling activity?). In Section 5 chondritus-type burrows.
					3	△△△	SMEAR SLIDE SUMMARY (%): 3, 60 6, 95 D D Texture: Sand 10 10 Silt 20 20 Clay 70 70 Composition: Quartz - TR Mica - TR Clay and silica 60 60 Pyrite TR TR Carbonate unsp. 19 19 Calc. nannofossils 11 11 Other 10 <sup>a</sup> 10 <sup>a</sup>  <sup>a</sup> Fragments of organisms. Foraminifera or calcified radiolarians.
					4	△△△	ORGANIC CARBON AND CARBONATE (%): 3, 76 Organic carbon - Carbonate 40
					5	△△△	10G 6/2
6	△△△	10GY 7/2					
7	△△△	5G 7/2					
CC	△△△	10G 6/2					

SITE 613		HOLE		CORE 52		CORED INTERVAL 572.4-581.9 m	
TIME - ROCK UNIT	BIOSTRATIGRAPHIC ZONE	FOSSIL CHARACTER			SECTION METERS	GRAPHIC LITHOLOGY	LITHOLOGIC DESCRIPTION
		FORAMINIFERS	NANNOFOSSILS	RADIOLARIANS			
lower Eocene	S. inaperta/M. magnumensis/M. formosa gracilis P1/PB	Dicoelaster binodiosus Zone (CP9b)	Bekoma bidertensis Zone		0.5	△△△	10G 6/2
					1	△△△	NANNOFOSSIL to NANNOFOSSIL-FORAMINIFERA PORCELLANITIC CHALK, pale green (10G 6/2) to pale yellowish green (10GY 7/2) with burrows of brownish gray (5YR 4/1), dark greenish gray (5GY 4/1) and purplish (5P 2/2).
					1.0	△△△	Upper part of core mainly irregularly parallel bedded, bottom shows crenulated fissile structures due to in situ sediment creep (or to drilling activity?).
					2	△△△	Section 2, 25-80 cm is affected by slump movement and shows elegant folds.
					3	△△△	SMEAR SLIDE SUMMARY (%): 2, 60 3, 135 CC, 25 D D D Texture: Sand - - 1 Silt 30 40 49 Clay 70 60 50 Composition: Quartz - 5 5 Clay and silica 70 55 50 Glauconite TR 1 - Carbonate unsp. 15 14 15 Foraminifera 5 15 15 Calc. nannofossils 10 10 15 Other <sup>a</sup> TR TR -
					4	△△△	ORGANIC CARBON AND CARBONATE (%): 4, 76 Organic carbon - Carbonate 33
					CC	△△△	10GY 7/2





5W-1

5W-2

5W-3

5W-4

5W-5

6X-1

6X-2

6X-3

6X-4

6X-5

6X-6

6X-7

5W,CC

6X,CC

